SECTION I

RESEARCH IN PROGRESS

NUCLEAR REACTIONS -- EXPERIMENTAL

COINCIDENCE STUDIES OF INTERMEDIATE MASS FRAGMENTS PRODUCED IN ^{32}S-INDUCED REACTIONS ON SILVER AT E/A=22.5 MEV

D.J. Fields, W.G. Lynch, T.K. Nayak, M.B. Tsang, C.B. Chitwood, C.K. Gelbke, R. Morse[a], J. Wilczynski[b], T.C. Awes[c], R.L. Ferguson[c], F. Plasil[c], F.E. Obenshain[c] and G.R. Young[c]

The emission of low energy intermediate mass fragments, $4<A_f\leq 40$, in processes distinct from fission is recognized to be a phenomenon characteristic of energetic proton-nucleus and nucleus-nucleus collisions. At present, there is no consensus concerning the origin of these fragments. A variety of models have been proposed and have been compared principally with single particle inclusive data, and each of them has achieved a certain degree of success in these comparisons. Critical judgements or improvements on the various models can be expected only in light of more restrictive measurements. In this report, we describe the statistical and dynamical aspects of ^{32}S induced reactions on Ag at E/A=22.5 MeV observed by investigating the emission of intermediate mass fragments in coincidence with non-equilibrium light particles and heavy reaction residues. In addition, we present single particle inclusive cross sections.

The experiment was performed at the Holifield Heavy-Ion Research Facility at Oak Ridge National Laboratory. Alpha particles and intermediate mass fragments, $3\leq Z_f\leq 24$, were detected with three ΔE-ΔE-E detector telescopes located at an azimuthal angle of $\phi=0°$ with respect to the beam axis. The velocities of coincident heavy reaction residues were measured with a position sensitive parallel plate detector located at an azimuthal angle of $\phi=180°$ and covering a total angular range, $5°\leq\theta\leq 23°$, in the reaction plane defined by the beam axis and the three intermediate mass fragment telescopes. Light particles, p,d,t, and α, were detected by five silicon-NaI(Tl) ΔE-E telescopes; three were placed at an azimuthal angle of $\phi=90°$ and two telescopes were positioned at $\phi=180°$.

The measured single particle inclusive cross sections for $3\leq Z\leq 8$ are shown in Fig. 1. Both light particle and intermediate mass fragment inclusive cross sections are forward peaked in the laboratory and center-of-mass rest frames, indicating the onset of emission prior to the establishment of thermal equilibrium in the composite system. We fit our cross sections with a parametrization modeling both a fusion-like and a non-equilibrium source, each emitting isotropically with a Maxwellian energy distribution in its respective rest frame. The parametrization includes momentum conservation and integrates the cross sections over a range of Coulomb barriers. The fusion-like source is assumed to move with a velocity consistent with the systematics for linear momentum transfer observed in measurements on fissile targets[1]. The temperature parameter of the fusion-like source was fixed at T_{eq}= 7 MeV. This leaves the normalizations, the velocity and temperature of the non-equilibrium source, and the mean Coulomb barrier as free parameters.

The resulting fits, shown as the solid lines in Fig. 1, suggest that the non-equilibrium source contributes significantly to the total cross section for the lighter fragments, and continue to contribute even to Z=13. The velocity of this source decreases with increasing fragment mass, suggesting that heavier fragments originate from more equilibrated sources.

The shapes of the energy spectra of light particles detected in coincidence with intermediate mass fragments are very similar to the single particle inclusive cross sections. However, there are sizable anisotropies in the angular correlations between light particles and intermediate mass fragments. The most

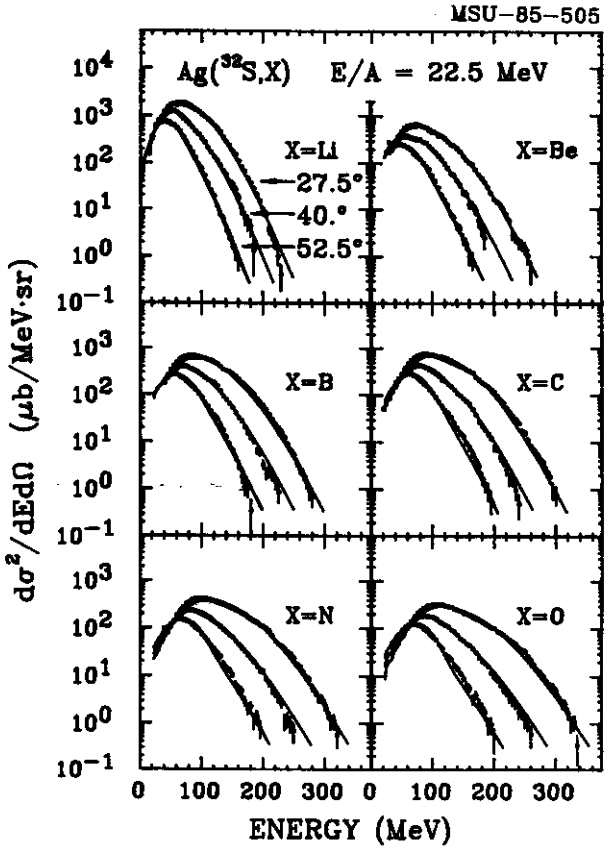

Fig. 1 Differential cross sections for Li, Be, B, C, N, and O nuclei measured at 27.5°, 40°, and 52.5°. The solid curves correspond to fits with the parametrization described in the text.

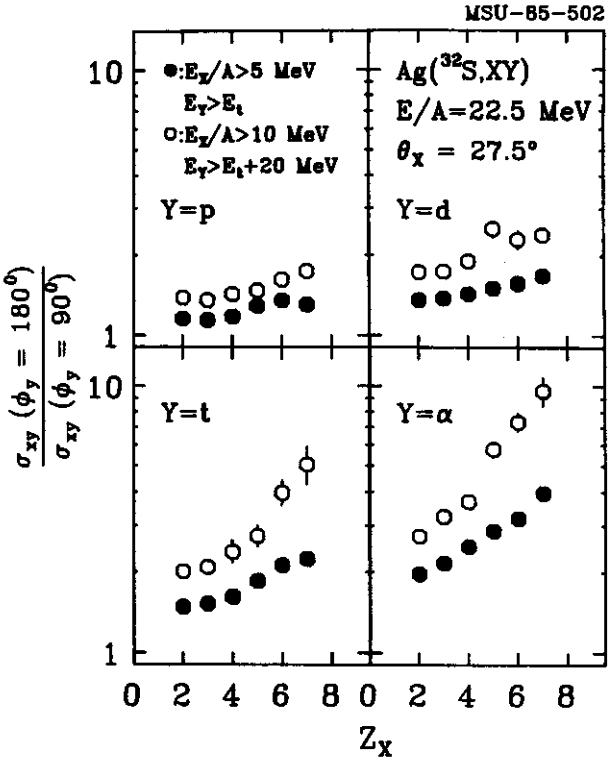

Fig. 2 Azimuthal asymmetries, defined in Eq.(5), for protons, deuterons, tritons and alpha particles detected in coincidence with intermediate mass fragments of element number Z_x. Light particles are emitted at the angles θ_y=40° and ϕ_y=180° or 90°; intermediate mass fragments are detected at θ_x=27.5°, ϕ_x=0°. The energy thresholds are given in the text; open points represent higher energy thresholds.

remarkable aspect of these correlations is their dependence on relative azimuthal angle. Fig. 2 depicts the ratios of the intermediate mass fragment-light particle coincidence cross sections at a relative azimuthal angle of ϕ=180° to the cross sections measured out of the reaction plane at ϕ=90°. These ratios are shown for light particles, p,d,t, and α, detected with fragments of charge 2-7. The energy thresholds used to produce the solid points were E_t= 15, 20, 20, and 40 MeV for protons, deuterons, tritons and alpha particles, respectively, and E_x/A_x>5 MeV for intermediate mass fragment. The open points show the azimuthal asymmetries for fragments and light particles of higher energy, E_x/A_x>10 MeV and E_y> E_t+ 20 MeV. The azimuthal asymmetries increase with increasing mass of the coincident particles and become more pronounced with increasing particle energy. For correlations between high energy nitrogen ions and alpha particles, the in-plane to out-of-plane ratio is nearly 10.

We find that the production of intermediate mass fragments, $3 \leq Z_x \leq 7$, is accompanied by the emission of approximately 10 nucleons in non-equilibrium light particles. The multiplicity of intermediate mass fragments, as deduced from coincidence data with both light particles and other intermediate mass fragments, is of the order of 1, with approximately 12 nucleons being emitted in this form, ruling out multifragmentation as the dominant production mechanism of intermediate mass fragments.

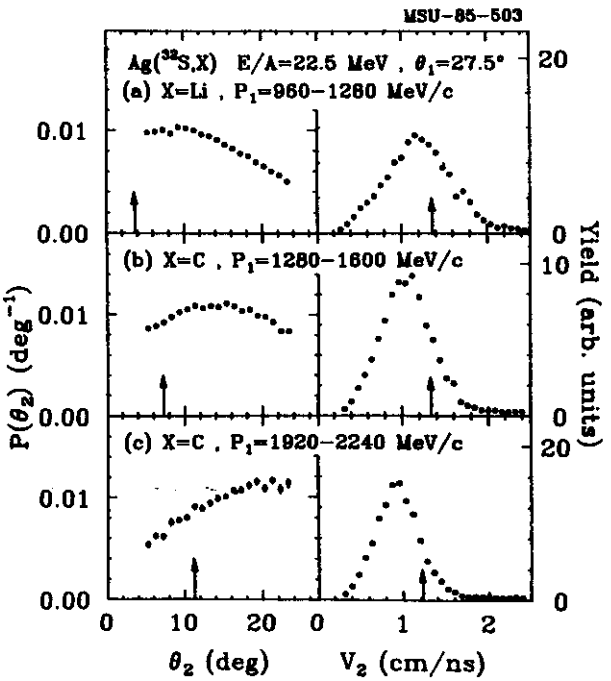

Fig. 3 Velocity distributions for heavy recoil nuclei detected in coincidence with intermediate mass fragments emitted at θ_1=27.5°. The left hand side shows the distribution as a function of the polar angle, θ_2, of the projection of the recoil velocity onto the reaction plane. The right hand side shows the measured distributions of $|\vec{v}_2|$. The arrows show the values expected for binary reactions.

Angular distributions for target-like residues detected in coincidence with lithium and carbon nuclei emitted at θ_1=27.5° are shown on the left hand side of Fig. 3. These spectra are normalized to represent the probability distributions for the detection of target-like residues in coincidence with Li and C nuclei in the momentum ranges P_{Li}=960-1280 MeV/c , P_C=1280-1600 MeV/c, and P_C=1920-2249 MeV/c. The distributions are shown as a function of θ_2, the polar angle of the projection of $\vec{v}_2$ onto the reaction plane, where $\vec{v}_2$ denotes the velocity of the coincident heavy residue. They exhibit broad maxima the widths of which are comparable to the angular acceptance of our experiment. The peak positions expected for complete fusion followed by binary decay are indicated by arrows. The observed maxima are located at angles larger than expected for such fusion-fission processes, indicating that the two particles do not carry away the entire projectile momentum. In fact, the peaks in the angular distributions of the recoiling residues never occur at the angles expected for complete fusion followed by binary decay. This includes reactions producing fragments with masses comparable to the mass of the projectile.

The location of the maximum, θ_2^{max}, is a function of both P_1 and M_1, the momentum and mass of the intermediate mass fragment. For energies above the exit channel Coulomb barrier, θ_2^{max} increases with increasing values of P_1, qualitatively consistent with momentum conservation. However, as P_1 decreases below the Coulomb barrier, θ_2^{max} increases again; θ_2^{max} is smallest for emission at the Coulomb barrier. The increase of θ_2^{max} at momenta below the Coulomb barrier may be caused by sequential decay processes for which the laboratory velocities of the parent nuclei are, on the average, larger than those of the detected daughter nuclei. They are in qualitative agreement with the trends measured[2] for ^{14}N induced reactions on Ag at E/A=35 MeV.

If we assume that the probability distribution is a Gaussian function of angle and that the width both in- and out-of-plane are the same, then for the typical case of carbon nuclei detected at θ=27.5° with momenta between 1280 and 1600 MeV/c the extrapolated probability that a coincident heavy residue exits is approximately one, consistent with the existence of a single target-like residue remaining after fragment emission.

Velocity distributions of coincident heavy residues are shown on the right hand side of Fig. 3. They, too, are inconsistent with fusion-fission processes (The velocities expected for purely binary reactions are indicated by arrows.)

A kinematic analysis of the residue velocity distributions indicates that an energy

between 200 and 400 MeV is deposited into internal excitations of the residual nucleus and emitted fragments. The missing momentum is directed close to the beam axis. The velocity of the missing mass is less than or equal to the beam velocity. A value of about half the beam velocity, characteristic of pre-equilibrium light particle emission, is consistent with the emission of 15-20 nucleons at the early stages of the reaction. This number is consistent with our estimates of the associated particle multiplicities. The magnitude of the missing momentum of the order of 20% of the projectile momentum.

In summary, the single particle inclusive cross sections of light particles and intermediate mass fragments provide evidence for a gradual transition from predominantly non-equilibrium emission of lighter particles to predominantly equilibrium emission for the heaviest nuclei. Intermediate mass fragments and non-equilibrium light particles are preferentially emitted in a plane which contains the beam axis, probably corresponding to the plane perpendicular to the entrance channel orbital angular momentum[3]. This implies that fragment production results from collisions with a large range of impact parameters and is not restricted to central collisions. The fragment multiplicities are low, of the order of one. For the present reaction, there is no evidence that violent multifragmentation processes dominate the emission of intermediate mass fragments, as implied by some models[4,5]. Instead, it appears that fragments are emitted with modest probabilities from a class of reactions representing 60-70% of the total reaction cross section. Intermediate mass fragments are emitted in highly inelastic collisions in which a large part of the kinetic energy of the incident projectile is converted into excitations of internal degrees of freedom. However, the dissipated energy is never completely thermalized in the composite system. Significant parts of the incident momentum and energy are carried away by particles emitted in non-equilibrium processes.

Some of these observations are qualitatively consistent with the expectations from a variety of statistical calculations[5,6]. However, present model calculations of intermediate mass fragment emission do not incorporate important dynamical effects which might give rise to the observed angular correlations and non-equilibrium emission.

---

a. Massachusetts Institute of Technology, Cambridge MA.
b. Institute for Nuclear Studies, Warsaw, Poland.
c. Oak Ridge National Laboratory, Oak Ridge, TN.

References

1. M. Fatyga, K. Kwiatkowski, V.E. Viola, C.B. Chitwood, D.J. Fields, C.K. Gelbke, W.G. Lynch, J. Pochodzalla, M.B. Tsang, and M. Blann, Phys. Rev. Lett. 55,1376(1985).
2. R. Bougault, D. Horn, C.B. Chitwood, D.J. Fields, C.K. Gelbke, D.R. Klesch, W.G. Lynch, M.B. Tsang, and K. Kwiatkowski, submitted to Phys. Lett.
3. M.B. Tsang, C.B. Chitwood, D.J. Fields, C.K. Gelbke, D.R. Klesch, W.G. Lynch, K. Kwiatkowski, and V.E. Viola, Phys. Rev. Lett. 52,1967(1984).
4. A.S. Hirsch, A. Bujak, J.E. Finn, L.J. Gutay, R.W. Minich, N.T. Porile, R.P. Scharenberg, B.C. Stringfellow, and F. Turkot, Phys. Rev. C29,508(1984).
5. D.J. Fields, W.G. Lynch, C.B. Chitwood, C.K. Gelbke, M.B. Tsang, H. Utsunomiya, and J. Aichelin, Phys. Rev. C30,1912(1984).
6. L.G. Sobotka, M.L. Padgett, G.J. Wozniak, G. Guarino, A.J. Pacheco, L.G. Moretto, Y. Chan, R.G. Stokstad, I. Tserruya, and S. Wald, Phys. Rev. Lett. 51,2187(1983).

LINEAR MOMENTUM TRANSFER LIMITATIONS FOR ^{6}Li, ^{12}C AND ^{14}N INDUCED REACTIONS

M. Fatyga[a], K. Kwiatkowski[a], V.E. Viola[a],
C.B. Chitwood, D.J. Fields, C.K. Gelbke, W.G. Lynch[b], J. Pochodzalla, and M.B. Tsang
M. Blann

We investigate the energy dependence of linear-momentum-transfer distributions which characterize collisions between light complex projectiles (^{6}Li, ^{12}C, and ^{14}N) and a heavy target nucleus (^{238}U). Linear-momentum-transfer distributions were determined by measurement of the angular correlation between coincident fission fragments.[1] Experiments were performed at the National Superconducting Cyclotron Laboratory at Michigan State University with ^{14}N beams of E/A=30, 35, 40, and 45 MeV, ^{12}C beams of E/A=20, 25, 30, and 35 MeV, and ^{6}Li beams of E/A=30 and 35 MeV.

Coincident fission fragments emitted from a 300-$\mu g/cm^2$ ^{238}U strip target were measured with two position-sensitive parallel-plate avalanche detectors.[2] For the data reported here a gate was placed on a region of one detector which spanned ±4° both in and out of the reaction plane, centered at 90° with respect to the beam axis. The second detector was placed 15 cm from the target with its center at an angle of -65°. This permitted 100% coincidence efficiency for fragments detected in the gated region of the defining detector.

Figure 1 shows the folding-angle distributions, $d^2\sigma/d\Omega_A d\theta_{AB}$, for the $^{14}N+^{238}U$ system. Previous results at lower energies[2,3] are included in the figure to demonstrate the evolution of the folding-angle distributions over the energy range from E/A=7 to 45 MeV. for each energy we have indicated the ratio $\Delta p/p_{beam}$, where Δp and p_{beam} denote the linear momentum transfer to the fissioning nucleus and the beam momentum, respectively. Qualitatively similar results are obtained for ^{6}Li and ^{12}C projectiles.

At beam energies above 8 MeV/A two distinct components are observed, one associated with large momentum transfers (or peripheral processes) and the other is associated with small momentum transfers (central collision

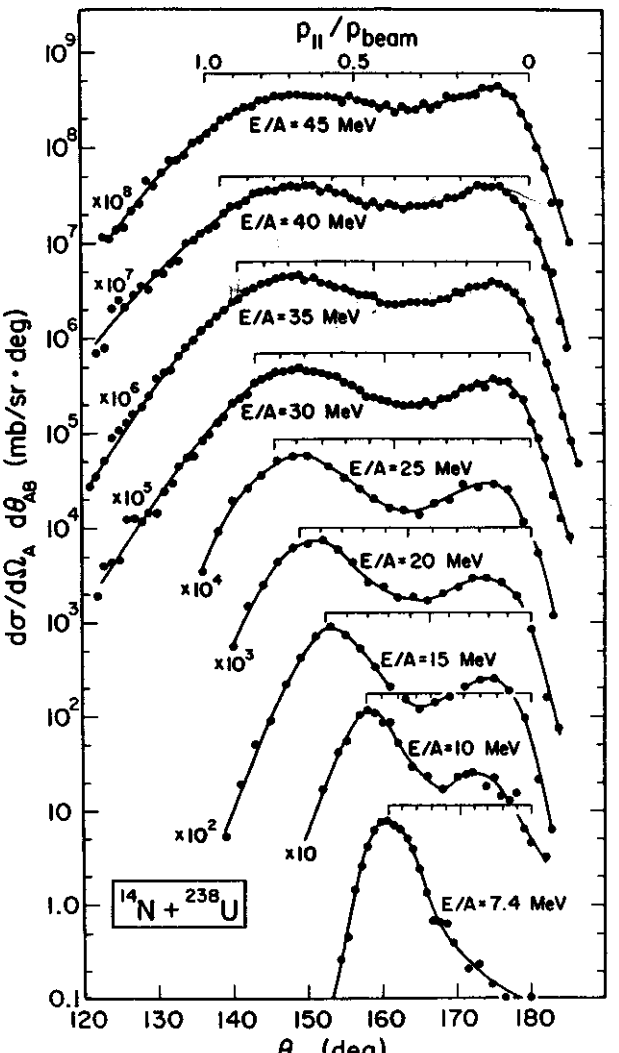

Fig. 1 Fission-fragment folding-angle distributions for the $^{14}N+^{238}U$ reaction. Data at E/A=30, 35, 40 and 45 MeV are from this work; data at E/A=7.4 and 10.4 MeV are from Ref. 3, and data at E/A=15, 20, 25 MeV are from Ref. 2. For each Measurement a linear-momentum-transfer scale, Wp/p, is shown immediately above the data.

process). For energies above E/A≈20 MeV, the most probable folding angle of the large-momentum-transfer component remains essentially constant near θ_{AB}≈149° for ^{14}N, corresponding to a limiting value of the maximum linear momentum transfer of Δp^{max}≈2800 MeV/c. (For ^{6}Li- and ^{12}C-induced reactions these limiting values are Δp^{max}≈1200 MeV/c and Δp^{max}≈2400 MeV/c, respectively.) For all three cases the maximum linear momentum transfer per projectile nucleon is limited to 200 MeV/c. At higher energies the folding-angle distributions become rather structure-less, corresponding to a broad continuum of linear momentum transfers and deposition energies in the residual system.

The peak angle of the low-momentum-transfer component does not exhibit pronounced energy dependence. However, the relative importance of these peripheral processes increases strongly with bombarding energy and beyond E/A≈40 MeV, the fission cross section becomes dominated by peripheral interactions.[4] Qualitatively similar observations have been made for ^{40}Ar-induced reactions between E/A≈27 and 44 MeV.[5]

Figure 2 shows the average values of the linear momentum transfer per projectile nucleon, Δp/A (bottom part) and Δp/p (top part) as a function of the beam velocity parameter, $[(E-V)/A]^{1/2}$, where E and V are laboratory values of the beam energy and of the Columb barrier and the ratio of linear momentum transfer to the beam momentum. The departure of the results from full linear momentum transfer (solid line in bottom part) becomes more pronounced with increasing beam energy. For ^{12}C and ^{14}N projectiles the average linear momentum transfer per nucleon exhibit a maximum near E/A≈35 MeV; for ^{6}Li (not shown in Fig. 2) this maximum occurs nearer E/A≈30 MeV. Similar limitations have previously been observed in

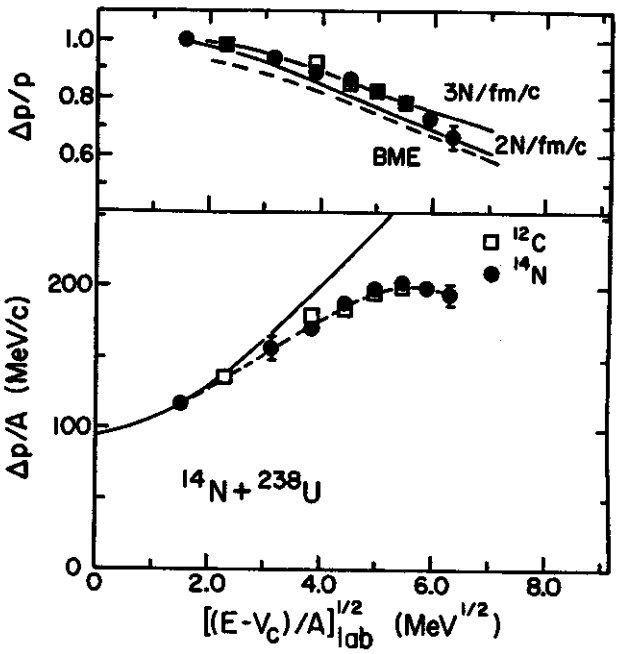

Fig. 2 Longitudinal momentum transfer per projectile nucleon (bottom part) and the ratio of average momentum transfer (top part) as a function of laboratory beam velocity parameter $[(E-V)/A]^{1/2}$. Squares and circles correspond to the ^{12}C- and ^{14}N-induced reaction on ^{238}U, respectively.

light-ion-induced reactions,[6] where the maxima occur at higher values of E/A.

Upper bounds for Δp/A are now established for a variety of light complex projectiles up to ^{40}Ar. It appears that the most probable values of the linear momentum transfer for all ions with $6 \leq A \leq 40$ are limited to values less than 200 MeV/c per projectile nucleon.

Incomplete momentum transfer in the fission channel must be associated with processes which account for the missing momentum; e.g., precompound particle emission, absorptive breakup of the projectile, or fragmentation of the target nucleus. Previous experimental studies have indicated the importance of particle emission prior to the attainment of full statistical equilibrium as an important mechanism for incomplete momentum transfer in central collisions.[7] In order to investigate

the connection between precompound particle emission and incomplete linear momentum transfer, we have performed two model calculations for the $^{14}N+^{238}U$ system which estimate the average linear momentum carried away by precompound particle emission in central collisions.[8,9] The dashed line in Fig. 3(a) shows the results obtained with a Boltzmann master-equation approach which includes emission of H and He precompound particles.[8] These calculations tend to over-estimate the amount of energy carried away by precompound particles at lower beam energies, but with increasing energy they yield increasingly better agreement with the data.

The solid lines in upper part of Fig. 2 show the results of calculations which assume emission of particles with A=1-10 from a localized region of excitation which is in the process of equilibrating with the remainder of the composite system.[9] An accretion rate of 2-3 nucleons per fm/c reproduces the energy dependence of the linear momentum transfer reasonably well. This value also provides a reasonable description of light-particle and intermediate-mass fragment emission ($Z \leq 10$) for ^{12}C induced reactions on gold at E/A=30 MeV.[8]

---

a. Indiana University, Bloomington, Indiana
b. Lawrence Livermore National Laboratory, Livermore, California

References

1. V.E. Viola et al., Phys. Rev. C26, (1982)
2. M.B. Tsang et al., Phys. Lett. 134B, 169 (1984).
3. T. Sikkeland et al., Phys. Rev. 125, 1350 (1962).
4. A.I. Warwick et al., Phys. Rev. C 27, 1083 (1983).
5. D. Jacquet et al., Phys. Rev. Lett. 53, 226 (1984).
6. F. Saint-Laurent et al., Nucl. Phys. A422, 307 (1984).
7. T.C. Awes et al., Phys. Rev. C24, 89(1981).
8. M. Blann, Phys. Rev. C31, 1245 (1985).
9. D.J. Fields et al., Phys. Rev. C30, 1912 (1984).

DEFLECTION OF NON-EQUILIBRIUM LIGHT PARTICLES BY THE NUCLEAR MEAN FIELD

M.B. Tsang, R.M. Ronningen, G. Bertsch, Z. Chen, C.B. Chitwood, D.J. Fields[a], C.K. Gelbke, W.G. Lynch, T. Nayak, J. Pochodzalla, and T. Shea, W. Trautmann[a]

In intermediate energy nucleus-nucleus collisions, non-equilibrium light particles are observed to be emitted preferentially in the entrance channel scattering plane,[2] indicating a collective motion in this plane and transverse to the beam axis.[2,3] Microscopic calculations with the Boltzmann-Uehling-Uhlenbeck equation interpret this effect in terms of the deflection to negative emission angles by the attractive nuclear mean field.[1,4] Since the collective motion in the nuclear mean field is damped by individual nucleon-nucleon collisions, the relative importance of positive and negative emission angles is sensitive to the interplay between mean field dynamics and two-body dissipation.

We have addressed these issues experimentally by determining the sign of the average emission angle of non-equilibrium light particles from the circular polarization of associated γ-rays emitted by the residual nucleus for ^{14}N induced reactions on ^{154}Sm at E/A = 20 MeV and E/A = 35 MeV. For these mass-asymmetric systems, the light particle spectra are dominated by non-equilibrium processes.[3,5-7]

The experiment was performed at the National Superconducting Cyclotron Laboratory at Michigan State University. A metallic self-supporting ^{154}Sm target of 11 mg/cm^2 areal density was bombarded with ^{14}N ions of 280 and 490 MeV energy. Light particles were detected with four ΔE-E telescopes arranged in a doubly symmetric geometry[8] at polar angles of θ=30° and 60° and azimuthal angles of φ=0° and 180° with respect to the beam axis. The circular polarization of coincident γ-rays was measured with two forward scattering polarimeters[8] positioned at θ=90°, φ=90° and θ=90°, φ=270°.

The measured light particle energy spectra and γ-ray polarizations are shown in Figures 1 and 2. The cross sections are forward peaked and the energy spectra exhibit nearly

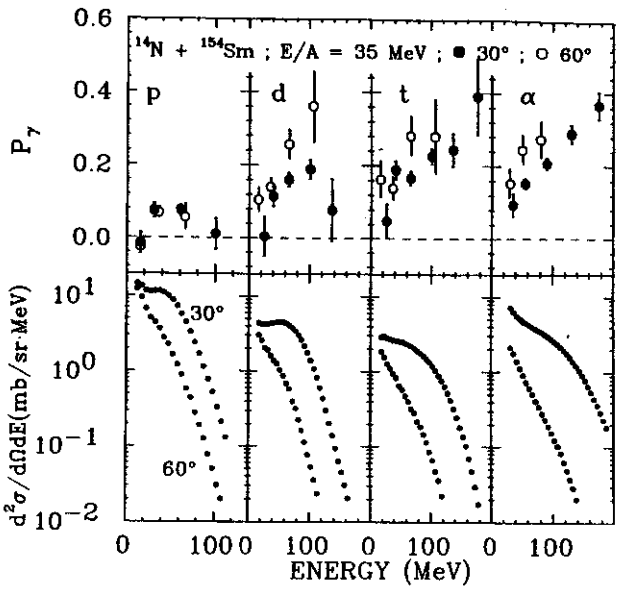

Fig. 1 Circular γ-ray polarizations plotted as a function of particle energies for p, d, t, and α (upper part) for E/A = 35 MeV. Closed and open circles correspond to measurements in coincidence with light particles detected at 30° and 60°, respectively. The lower part shows the inclusive energy spectra for the corresponding light particles.

exponential slopes in agreement with the trends established previously for non-equilibrium light particle emission.[6,7] Positive polarizations are observed at both energies and emission angles. The magnitude of the measured polarization increases with increasing energy and mass of the coincident light particles. No significant dependence on beam energy is observed. For a given particle and energy, the polarization is slightly larger at θ=60° than at θ=30°. In our sign convention,[8] the quantization axis $\vec{n}$ is defined by: $\vec{n}=\vec{k}_i \times \vec{k}_f / |\vec{k}_i \times \vec{k}_f|$ where $\vec{k}_i$ and $\vec{k}_f$ are the momentum

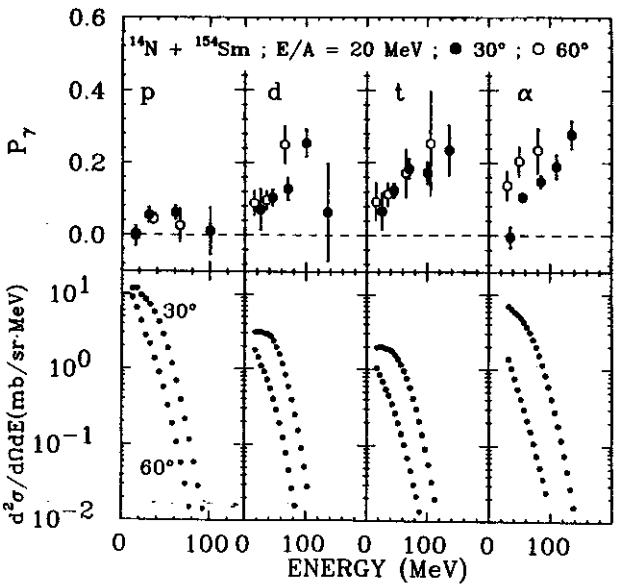

Fig. 2 Circular γ-ray polarizations plotted as a function of particle energies for p, d, t, and α (upper part) for E/A = 20 MeV. Closed and open circles correspond to measurements in coincidence with light particles detected at 30° and 60°, respectively. The lower part shows the inclusive energy spectra for the corresponding light particles.

vectors of the beam and the detected particle respectively; positive circular γ-ray polarizations correspond to negative deflection angles and vice versa. Our experiment clearly establishes the preferential emission of non-equilibrium light particles to negative emission angles, consistent with an attractive nuclear mean field and with measurements at lower energies.[9,10] The sign is opposite to what is expected if only shadowing by the residual nucleus would affect the particle emission.[3] For light particle energies of E/A ≈ 35 MeV, P_γ increases approximately linearly with A as would be expected in a coalescence model of light particle production.

Considerable progress has been made recently in treating the dynamics of the nucleon-nucleon collisions in the presence of the mean field generated by the participating nuclei.[1,4,13] We have performed numerical calculations with the Boltzmann-Uehling-Uhlenbeck (BUU) equation[4,13] for ^{14}N+^{154}Sm collisions at E/A=35 MeV with impact parameters between b=1 to 10 fm. The calculations predict the preferential emission of nucleons to negative angles, in qualitative agreement with the experimental observations.

To allow a more quantitative comparison with the data, we have calculated the circular polarization predicted by the BUU model. The angular momentum, $\vec{J}(b)$, of the residual nucleus (assumed to correspond to nucleons within a radius of 7.5 fm at the collision time of 200 fm/c) was determined for each impact parameter. For simplicity, the residual nucleus was assumed to decay via stretched E2 transitions, corresponding to a γ-ray multiplicity of $M_\gamma = J(b)/2$. The polarization is integrated over the geometry of the polarimeters[8], and averaging over impact parameters b, the azimuthal angles of the emitted nucleons and over energies greater than 30 MeV. At the angles of 30° and 60°, the predicted polarizations are 0.18±0.03 and 0.25±0.03, respectively. The values should be reduced by about 20% if one accounts for non-stretched transitions.[11,12] In comparison, the calculated polarizations are larger than the experimentally observed proton polarizations of 0.07 both at θ=30° and θ=60°. However, the present calculations do not include emission of composite particles which have larger measured polarizations. In accordance with the coalescence picture, one may assess the effects of complex particle emission by evaluating an "effective nucleon polarization" according to the definition:

$$P_{eff}(\theta) = \frac{\sum_i \sum_j A_i \sigma_i(\theta,E_j) P_i(\theta,E_j)}{\sum_i \sum_j A_i \sigma_i(\theta,E_j)} \quad , \quad (2)$$

where A_i, $P_i(\theta,E_j)$ and $\sigma(\theta,E_j)$ denote mass, experimentally measured polarization and cross section for particle i and i=p,d,t,α. For particle energies E/A≥30 MeV, the effective polarizations are $P_{eff}(30°) = 0.17\pm0.03$ and

$P_{eff}(60°)=0.12\pm0.03$. Considering the experimental uncertainties of the absolute calibrations of the analysing power and the theoretical uncertainties in the relative weights for the composite particles, $P_{eff}(\theta)$ and the calculated polarizations $\langle P_y(\theta)\rangle$ are in good agreement.

In order to illustrate the dependence of the predicted polarizations on the nucleon-nucleon collision dynamics, we have varied the strength of the residual interaction. For simplicity, calculations were only performed for one impact parameter, b=6.5 fm. This impact parameter contributes the largest weight to the polarization integral of equation 1. For σ_{NN}= 41 mb, the polarization is reduced by over a factor of three below the value calculated with the mean field alone. Thus the magnitude of the impact parameter averaged polarizations calculated with equation 2 reflect the balance between deflection by the mean field and randomization of the particle velocities by nucleon-nucleon collisions.

---

a. Brookhaven National Laboratory, Upton, NY 11973

References

1. J.J. Molitoris, D. Hahn and H. Stocker, Nucl. Phys. A447, 13c (1985)
2. M.B. Tsang, et al., Phys. Rev. Lett. 52, 1967 (1984)
3. M.B. Tsang, et al., Phys. Lett. 148B, 265 (1984)
4. J. Aichelin and G. Bertsch, Phys. Rev. C31, 1730 (1985) and private communication
5. T.C. Awes, et al., Phys. Rev. C24, 89 (1981)
6. T.C. Awes, et al., Phys. Rev. C25, 2361 (1982)
7. G.D. Westfall, et al., Phys. Lett. 116B, 118 (1982)
8. W. Trautmann, et al., Nucl. Instr. and Meth. 184, 449 (1981)
9. W. Trautmann, et al., Phys. Rev. Lett. 53, 1630 (1984)
10. T. Fukuda et al, 6th International Symposium on Polarization Phenomena in Nuclear Physics. Osaka (Japan) 26-30 Aug, 1985 Pg. 116
11. W. Trautmann et al., Nucl. Phys. A422, 418 (1984).
12. D.G. Sarantites et al., Phys. Rev. C18, 774 (1978)
13. G. Bertsch, H. Kruse and S. Das Gupta, Phys. Rev. C29, 673 (1984)

TWO-PARTICLE CORRELATION FUNCTIONS AT SMALL RELATIVE MOMENTA FOR ^{14}N INDUCED REACTIONS ON ^{197}Au AT E/A=35 MeV

J. Pochodzalla, C.B. Chitwood, D.J. Fields[a], C.K. Gelbke, W.G. Lynch, M.B. Tsang, D.H. Boal, and J.C. Shillcock[a]

Models of intermediate energy nucleus-nucleus collisions often use the assumption of statistical particle emission from highly excited subsets of the composite system. Because of sensitivities to final-state interactions[1,2] and quantum statistics,[3-5] two-particle correlation functions at small relative momenta contain information about the space-time characteristics of these subsets. Particles with different reaction cross sections may be expected to decouple from the emitting system at different average densities or source radii.[6] Therefore, the investigation of two-particle correlation functions for <u>different</u> particle pairs, emitted in the same reaction, may provide detailed information about the breakup of highly excited nuclear systems.[2,6] Furthermore, particles of different energies may be emitted at different stages of the reaction.[7,8] The energy dependence of the correlation functions can, therefore, provide useful additional information about the space-time characteristics of the equilibration process. We have investigated the energy dependence of two-particle correlation functions for several different combinations of coincident light particles emitted in collisions between ^{14}N and ^{197}Au at E/A=35 MeV.

The experiment was performed at the National Superconducting Cyclotron Laboratory of Michigan State University. A gold target of 19 mg/cm^2 areal density was irradiated by ^{14}N ions with an incident energy of 490 MeV. Light particles ($Z \leq 2$) were detected by a close-packed hexagonal array of 13 ΔE-E telescopes, each consisting of a 400 μm thick Si detector and a 10 cm thick NaI detector. Each telescope subtended a solid angle of 0.94 msr; the angular separation between adjacent telescopes was 6.1°. The center of the hodoscope was positioned at laboratory angles of Θ_{av}=35° and 50°. The energy calibrations of individual detectors are accurate to within 3%. In the off-line analysis, low-energy thresholds of 12, 15, 18 and 40 MeV were placed by software on the energy spectra of protons, deuterons, tritons and alpha particles, respectively.

We present our data in terms of the two-particle correlation function, R(q), which is defined in terms of the singles yields, $Y_1(\vec{p}_1)$ and $Y_2(\vec{p}_2)$, and the coincidence yield, $Y_{12}(\vec{p}_1,\vec{p}_2)$, of particles 1 and 2:

$$\sum Y_{12}(\vec{p}_1,\vec{p}_2) = C_{12}\cdot(1+R(q))\cdot\sum Y_1(\vec{p}_1)Y_2(\vec{p}_2). \quad (1)$$

Here, $\vec{p}_1$ and $\vec{p}_2$ are the laboratory momenta of particles 1 and 2, and q is the momentum of relative motion. For each particle pair, the normalization constant C_{12} was chosen such that R(q)=0 at sufficiently large relative momenta, where correlations due to final state interactions should vanish. The correlation functions were evaluated for different constraints on the sum energy, E_1+E_2, of the two coincident particles. For each constraint, the summation was performed over all energies and angles corresponding to a given value of q; C_{12} was chosen to be independent of these energy constraints.

Two-particle correlation functions measured at Θ_{av}=35° are shown in Figures 1 and 2; very similar correlations were measured at Θ_{av}=50°. The correlations for pairs of identical hydrogen isotopes are presented in Figure 1. For the two-proton correlation function, the attractive singlet S-wave interaction gives rise to a maximum at q=20 MeV/c. The two-deuteron and two-triton correlation functions, on the other

hand, do not exhibit maxima since the interactions between these pairs of particles are not resonant at low relative momenta.[2,9,10] The p-α correlation functions, shown in Figure 2, exhibit broad maxima near q≈50 MeV/c which are due to the decay of the ground state of ^{5}Li ($J^{\pi}=\frac{3}{2}^{-}$, Γ=1.5 MeV) in the Coulomb field of the heavy residue.[11] The rise of the correlation function at small relative momenta, q≲25 MeV/c, is caused[11] by the decay of $^{9}B \rightarrow 2\alpha+p$.

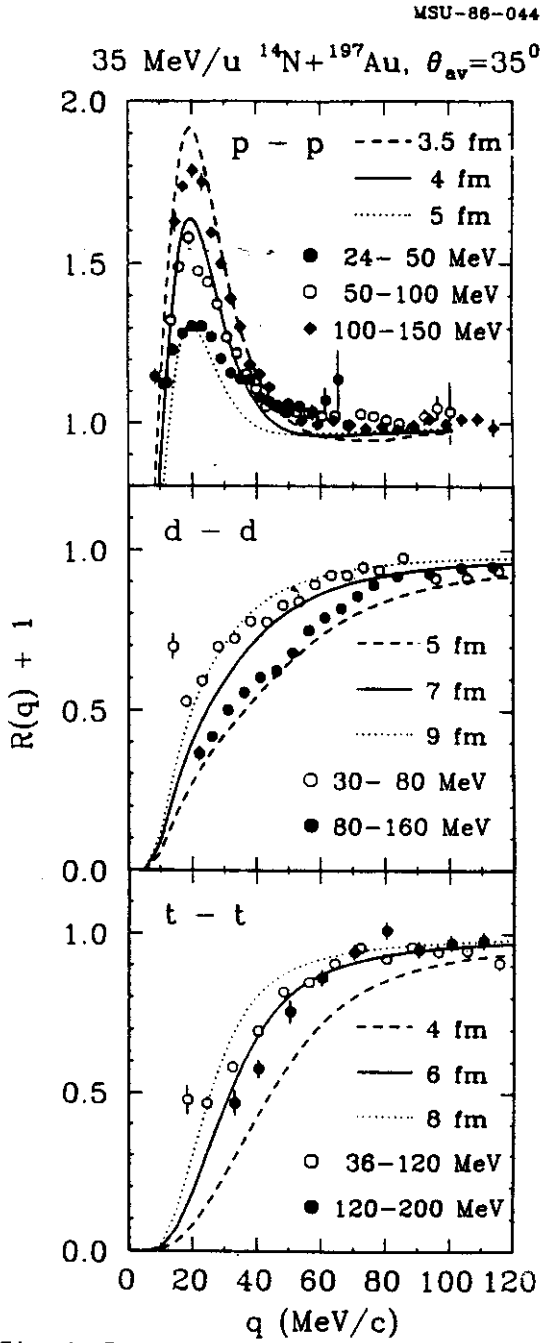

Fig. 1 Two-particle correlation functions for protons (p-p), deuterons (d-d), and tritons (t-t) emitted at θ_{av}=35° in ^{14}N induced reactions on ^{197}Au at E/A=35 MeV.

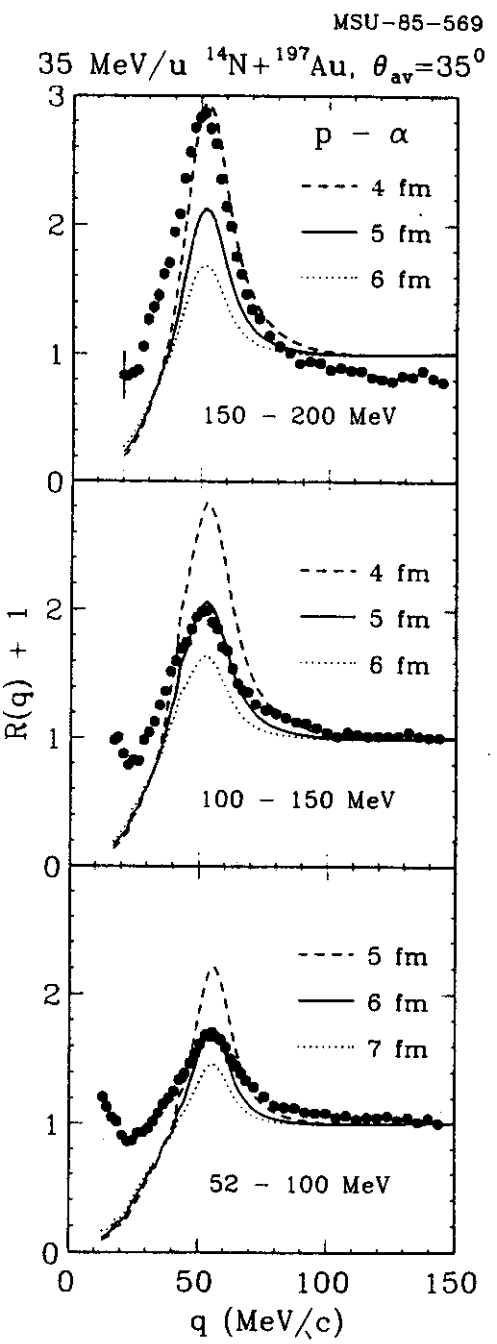

Fig. 2 Correlation functions between coincident protons and alpha particles emitted at θ_{av}=35° in ^{14}N induced reactions on ^{197}Au at E/A=35 MeV.

The solid, dashed and dotted curves shown in the figures represent theoretical correlation functions predicted by an extension of the final-state interaction model of ref. 1 to particles heavier than protons. Finite lifetime effects were neglected. In this approximation, the model becomes equivalent with the thermal model.[12] Since the inclusion of the temporal evolution of the emitting system is expected to reduce the calculated two-particle correlations,[1,6] our source radii represent upper limits for the spatial extent of the emitting system.

For all cases investigated, the measured correlations become more pronounced with increasing energy of the two coincident particles indicating that more energetic light particles are emitted from sources which are more localized in space-time. This feature is quantified by the estimated source radii summarized in Table 1. Also included in the table are source radii extracted from the measurements at Θ_{av}=50° and those extracted from a previous analysis[8] of the α+d correlation functions. No significant dependence of the correlation functions on angle is established. The observation of considerable correlations at angles significantly larger than the grazing angle (Θ_{gr}≈10°) renders interpretations[13] in terms of the sequential decay of projectile fragments unlikely.

The source sizes extracted for the emission of energetic p-p and α-d pairs are smaller than the size of the target nucleus [$r_0(Au) = \sqrt{2/3}\cdot r_{rms}(Au) \approx 4.3$ fm]. For the other particle pairs, larger source dimensions are obtained. The extracted source radii may be ordered approximately as follows: $r_0(\alpha+d) \lesssim r_0(p+p) \lesssim r_0(\alpha+p) \lesssim r_0(t+t), r_0(d+d)$. For an interpretation of these results, several questions should be addressed: (i) Different reaction products may have different impact parameter weightings; protons may have larger contributions from larger impact parameters than composite particles.[14] (ii) The problem of sequential feeding from highly excited primary reaction products may alter the two-particle correlation functions. (iii) Different particle species may go out of equilibrium at different densities, depending on their interaction cross sections.[6] A consistent treatment of the temporal evolution of the emitting source is not yet available. (iv) The calculation of the theoretical correlation functions involve several uncertainties. The effects of the Coulomb interaction with the residual nuclear matter have not yet been treated reliably. In addition, there are still uncertainties in the low energy phase shifts (particularly for the t+t system).

Table 1:

Source radii, r_o, for a source of negligible lifetime and Gaussian density, $\rho(r)=\rho_o \cdot \exp(-r^2/r_o^2)$, extracted from two-particle correlation functions; the corresponding rms radii are given by: $r_{rms}=\sqrt{3/2}\cdot r_o$; equivalent sharp sphere radii are given by: $R=\sqrt{5/2}\cdot r_o$. The errors include normalization uncertainties for the different energy gates.

1+2	E_1+E_2 [MeV]	$r_o(35°)$ [fm]	$r_o(50°)$ [fm]
p+p	24 - 50	4.9 ± 0.5	5.2 ± 0.5
	50 - 75	4.3 ± 0.3	4.0 ± 0.3
	75 - 100	3.8 ± 0.2	3.6 ± 0.2
d+d	30 - 80	8 ± 2	-
	80 - 160	5.5 ± 1	-
t+t†	36 - 120	6.5 ± 1	-
	120 - 200	5.5 ± 1	-
p+α	52 - 100	6 ± 0.5	6 ± 0.5
	100 - 150	5 ± 0.5	4.8 ± 0.3
	150 - 200	4 ± 0.5	3.7 ± 0.3
d+α††	55 - 100	3.8 ± 0.2	3.9 ± 0.2
	100 - 150	3.0 ± 0.2	2.8 ± 0.2
	150 - 220	3.0 ± 0.2	2.7 ± 0.2

† The calculations include a nuclear potential only for the $\ell=0$ partial wave; see text.

†† From ref. 8; source radii were extracted from the sharp peak at q≈42 MeV/c; radii extracted from the broad peak at q≈85 MeV/c are larger by about 0.5 fm.

a. Department of Physics, Simon Fraser University, Burnaby, B.C. V5A 1S6, Canada

References:

1. S.E. Koonin, Phys. Lett. 70B (1977) 43
2. C.B. Chitwood, et al, Phys. Rev. Lett. 54 (1985) 302
3. G.I. Kopylov and M.I. Podgoretskii, Yad. Fiz. 18 (1973) 656 [Sov. J. Nucl. Phys. 18 (1974) 336]
4. G.I. Kopylov, Phys. Lett. 50B (1974) 472
5. F.B. Yano and S.E. Koonin, Phys. Lett. 78B (1978) 556
6. D.H. Boal and J.C. Shillcock, Phys. Rev. C33 (1986) 549
7. W.G. Lynch, et al., Phys. Rev. Lett. 51 (1983) 1850
8. C.B. Chitwood, et al., Phys. Lett. B (in press)
9. G.M. Hale and B.C. Dodder, Few-Body Problems in Physics, edited by B. Zeidnitz (Elsevier, Amsterdam, 1984), Vol. 2, p. 433
10. G.M. Hale, private communication
11. J. Pochodzalla, et al., Phys. Lett. 161B (1985) 256
12. B.K. Jennings, D.H. Boal and J.C. Shillcock, Phys. Rev. C (in press)
13. P.D Bond and R.J. de Meijer, Phys. Rev. Lett. 52 (1984) 2301
14. G.E. Beauvais and D.H. Boal, University of Illinois preprint, 1986, and to be published

ENERGY DEPENDENCE OF SOURCE RADII AND EMISSION TEMPERATURES FOR ^{14}N INDUCED REACTIONS AT E/A=35 MeV.

C.B. Chitwood, C.K. Gelbke, J. Pochodzalla, Z. Chen, D.J. Fields[a], W.G. Lynch, R. Morse, M.B. Tsang, D.H. Boal[a] and J.C. Shillcock[a]

The emission of complex particles prior to the attainment of full statistical equilibrium of the composite system is clearly established for intermediate energy nucleus-nucleus collisions.[1,2] In the absence of a complete dynamical treatment, recourse is often taken to models based on the assumption of statistical particle emission from subsets of nucleons[1-5] characterised by their average velocity, space-time extent, and excitation energy or "temperature". The experimental determination of the detailed characteristics of these subsets from single particle inclusive cross sections[6] can be uncertain due to sensitivities to collective motion[7] and the temporal evolution of the emitting system.[2,8-10]

If one assumes thermal equilibrium for a system contained within a sphere of volume V, one can approximate the correlation function as[11]

$$R(q) = \frac{2\pi}{(2s_1+1)(2s_2+1)Vq^2} \sum_{J,\ell} (2J+1) \frac{\partial \delta_{J,\ell}}{\partial q} , \quad (1)$$

Here, s_1 and s_2 denote the spins of the two coincident particles and $\delta_{J,\ell}$ denotes the scattering phase shift (assumed to be diagonal in ℓ and J). To first order within the thermal model, the correlation function depends on the volume of the emitting source but not its temperature.[11]

Correlation functions, $Y_{\alpha d}(\vec{p}_\alpha,\vec{p}_d) = C \cdot Y_\alpha(\vec{p}_\alpha) Y_d(\vec{p}_d)[1+R(q)]$, for coincident deuterons and alpha particles, measured for ^{14}N induced reactions on ^{197}Au at E/A=35 MeV are shown in Figure 1. The upper and lower parts of the figure show measurements at 35° and 50°, respectively. The α-d correlation functions exhibit two maxima corresponding to the T=0

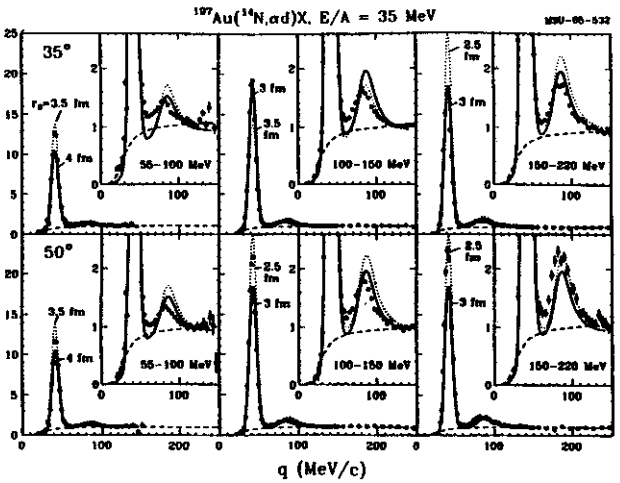

Fig.1 Correlation functions measured for coincident deuterons and alpha particles for ^{14}N induced reactions on ^{197}Au at E/A=35 MeV. A detailed discussion of the figure is given in the text.

state in ^6Li at 2.186 MeV ($J^\pi=3^+$, Γ=24 keV, $\Gamma_\alpha/\Gamma_{tot}$=1.00) and the overlapping T=0 states at 4.31 MeV ($J^\pi=2^+$, Γ=1.3 MeV, $\Gamma_\alpha/\Gamma_{tot}$=0.97) and at 5.65 MeV ($J^\pi=1^+$, Γ=1.9 MeV, $\Gamma_\alpha/\Gamma_{tot}$=0.74).

Instead of using eq. 1 directly, we have performed calculations of the α-d correlation function which correspond to a generalization of the final-state interaction model of ref. 12. For these calculations, a source of Gaussian spatial density, $\rho(r)=\rho_0 \cdot e^{-r^2/r_0^2}$, was assumed and finite lifetime effects were neglected. In this approximation, the model becomes equivalent with the thermal model.[11] Technical details are given in ref. 13.

The calculations are shown by the solid and dotted lines in Figure 1. The measured correlations do not exhibit a strong dependence on angle, but become more pronounced with increasing kinetic energies, $E_\alpha+E_d$, indicating that more energetic particles may originate from subsets of nucleons which are more localised in

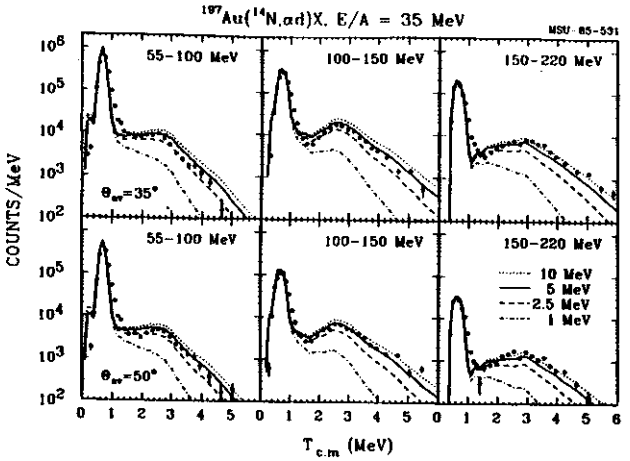

Fig. 2 Energy spectra resulting from the decay $^6Li^* \rightarrow \alpha+d$. A detailed discussion of the figure is given in the text.

space-time. This feature is quantified by the estimated source radii summarized in Table 1.

Emission temperatures were obtained by comparing the experimental yields of particle unstable ^6Li nuclei with thermal calculations. The experimental yield of particle unstable decays $^6Li^* \rightarrow \alpha+d$, Y_c, was assumed to be given by $Y_c = Y_{\alpha d} - C \cdot Y_\alpha Y_d [1+R_b(q)]$, where $R_b(q)$ denotes the "background correlation function"[14] shown by the dashed lines in Figure 1. The resulting yields are shown in Figure 2 as a function of the kinetic energy, $T_{c.m.}$, in the ^6Li rest frame.

Calculations based on the thermal model are shown in Figure 2 for emission temperatures of T = 1, 2.5, 5, and 10 MeV. Extracted emission temperatures are summarized in Table 1. Higher emission temperatures are extracted for higher kinetic energies, $E_\alpha + E_d$, of the emitted particles.

The temperatures extracted from the α-d coincidence yields can have considerable systematic errors due to uncertainties in the α-d background correlation function and due to the saturation of the coincidence yields at higher temperatures; statistical uncertainties are negligible. At T = 5 MeV, the temperatures are believed to be accurate within 25%; at higher temperatures the uncertainties can be larger. Uncertainties of the absolute temperature scale may be caused by feeding from higher lying states. Quantum statistical calculations[15] for infinite nuclear systems suggest that sequential decay corrections could result in temperatures 10-50% higher, depending on breakup density.

The temperatures determined in the present experiment are about an order of magnitude larger than the ones reported in refs. 16 and 17. This discrepancy is probably caused by feeding of the ground state by sequential decay.

Table 1:

Emission temperatures and source radii extracted from the decay $^6Li^* \rightarrow \alpha+d$.

constraint on $E_1 + E_2$	θ = 35° T(MeV)	θ = 35° r_0(fm)	θ = 50° T(MeV)	θ = 50° r_0(fm)
55 - 220 MeV	4	3.4	4	3.6
55 - 100 MeV	4	3.8	3	3.9
100 - 150 MeV	4	3.0	5	2.8
150 - 220 MeV	7	3.0	9	2.7

a. Simon Fraser University, Burnaby, B.C., Canada

References:

1. B.V. Jacak, et al., Phys. Rev. Lett. 51 (1983) 1846
2. D.J. Fields, et al., Phys. Rev. C30 (1984) 1912
3. G.D. Westfall, et al., Phys. Rev. Lett. 37 (1976) 1202
4. J. Gosset, et al., Phys. Rev. C18 (1978) 844
5. J. Knoll, Phys. Rev. C20 (1979) 773
6. G.D. Westfall, et al., Phys. Lett. 116B (1982) 118
7. P.J. Siemens and J.O. Rasmussen, Phys. Rev. Lett. 42 (1979) 880
8. H. Stöcker, et al., Z. Phys. A303 (1981) 259
9. W.A. Friedman and W.G. Lynch, Phys. Rev. C28 (1983) 16
10. D.H. Boal, Phys. Rev. C30 (1984) 749
11. B.K. Jennings, D.H. Boal, and J.C.

Shillcock, Phys. Rev. C (in press)
12. S.E. Koonin, Phys. Lett. 70B (1977) 43
13. D.H. Boal and J.C. Shillcock, Phys. Rev. C33 (1986) 549
14. J. Pochodzalla, et al., Phys. Rev. Lett. 55 (1985) 177
15. D. Hahn and H. Stöcker, private communication and to be published
16. D.J. Morrissey, et al., Phys. Lett. B148 (1984) 423
17. D.J. Morrissey, et el., Phys. Rev. C32 (1985) 877

EMISSION TEMPERATURES IN INTERMEDIATE ENERGY NUCLEAR COLLISIONS FROM THE RELATIVE POPULATIONS OF WIDELY SEPARATED STATES IN ^{5}Li and ^{8}Be

J. Pochodzalla[a], W.A. Friedman[b], C.K. Gelbke, W.G. Lynch, M. Maier, D. Ardouin[c], H. Delagrange[c], H. Doubre[c], C. Grégoire[c], A. Kyanowski[c], W. Mittig[c], A. Péghaire[c], J. Péter[c], F. Saint-Laurent[c], Y.P. Viyogi[c,d], B. Zwieglinski[c,e], G. Bizard[f], F. Lefèbvres[f], B. Tamain[f], J. Québert[g]

Statistical models have successfully described the emission of complex particles in intermediate and high energy nucleus-nucleus collisions[1-5]. In several of these models, the concept of temperature plays a central role. Most attempts to extract temperatures are based on analyses of the kinetic energy spectra of the emitted particles[6]. The interpretation of such spectra may, however, be complicated by additional sensitivities to the collective motion[7] and the temporal evolution of the emitting system[4,5,8].

An alternative determination of the "emission temperature", i.e. the temperature at the point at which the particles leave the equilibrated subsystem, is based on the relative population of states. First particle-γ coincidence measurements[9,10] of the population of excited states in Li and Be nuclei were performed for ^{14}N induced reactions on ^{197}Au at E/A=35 MeV. These measurements investigated the population of states at rather low excitation energy; they were interpreted in terms of surprisingly low emission temperatures, T ≤ 1 MeV. However, feeding from higher lying particle unstable states and neutron induced deexcitations may make this temperature determination inaccurate[9-12].

More accurate determinations of the emission temperature can be made by measuring the relative populations of states separated by significantly larger energy intervals. We have measured the population of particle unstable states in ^{5}Li and ^{8}Be for ^{40}Ar induced reactions on ^{197}Au at E/A=60 MeV. These states are separated by 16.7 and 14.6 MeV, respectively.

The experiment was performed at the Laboratoire GANIL at Caen. A gold target of 10 mg/cm^2 areal density was irradiated by a beam of ^{40}Ar of E/A=60 MeV incident energy. Light particles (Z≤3) were detected by a close packed hexagonal array of 13 ΔE-E telescopes. The center of the hodoscope was positioned at a laboratory angle of 30°; the angular separation between adjacent telescopes was 4.2°.

We present our data in terms of the correlation function, R(q), which is defined in terms of the singles and the coincidence yields:

$$Y_{12}(\vec{p}_1,\vec{p}_2) = C_{12}\cdot Y_1(\vec{p}_1)Y_2(\vec{p}_2)[1+R(q)] \quad \text{(Eq. 1)}$$

Here, $\vec{p}_1$ and $\vec{p}_2$ are the laboratory momenta for particles 1 and 2; q is the momentum of relative motion between the two coincident particles; C_{12} is a normalisation constant which was determined by requiring R(q)=0 for large relative momenta.

Figs. 1 and 2 show the measured p-α, d-^{3}He, α-α, and p-^{7}Li correlation functions, respectively. The p-α correlation function, Fig. 1a, exhibits two peaks which have been identified as due to the decay of the particle unstable ground states of ^{9}B and ^{5}Li. The ground state of ^{5}Li was used in our analysis. The most pronounced peak in the d-^{3}He correlation function, Fig. 1b, corresponds to the decay of the 16.66 MeV state in ^{5}Li. The α-α correlation function, Fig. 2a, shows the tail of the peak resulting from the decay of the particle unstable ground state of ^{8}Be. The structure at q≈50 MeV/c is caused by the decay of ^{9}Be$^{*}_{2.43}$, the structure at q≈105 MeV/c is caused by the decay of the 3.04 MeV state in ^{8}Be; this peak was used in our analysis. The p-^{7}Li correlation function, Fig. 2b, exhibits several sharp structures resulting from the decay of high lying states in ^{8}Be. For our

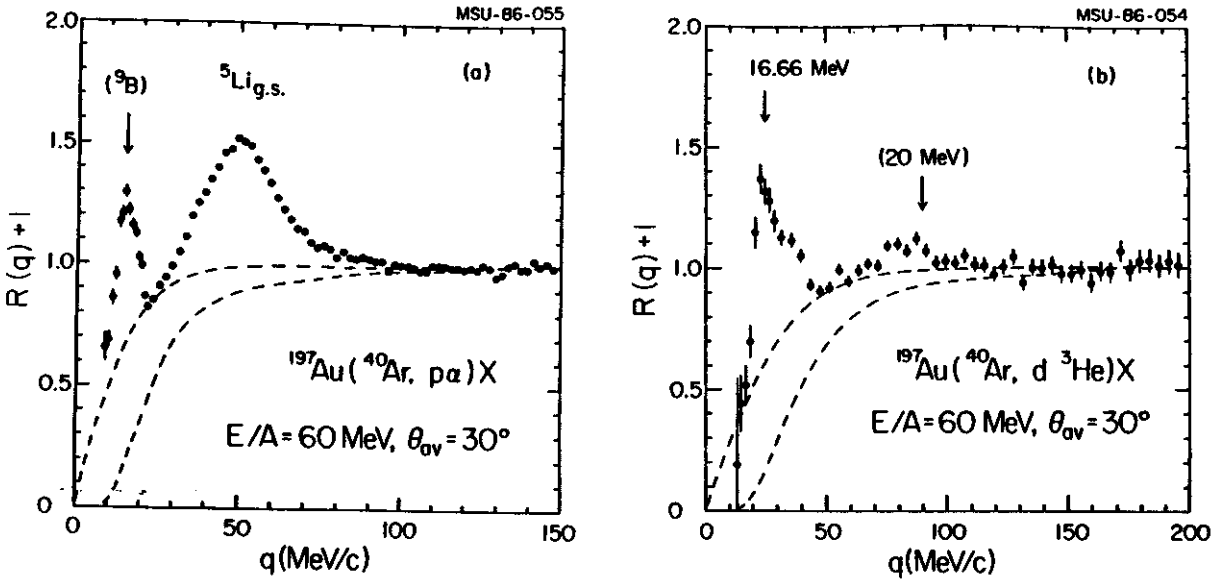

Fig. 1 Correlation functions for coincident protons and alpha particles (part a) and coincident deuterons and ^{3}He nuclei (part b) measured for ^{40}Ar induced reactions on ^{197}Au at E/A=60 MeV.

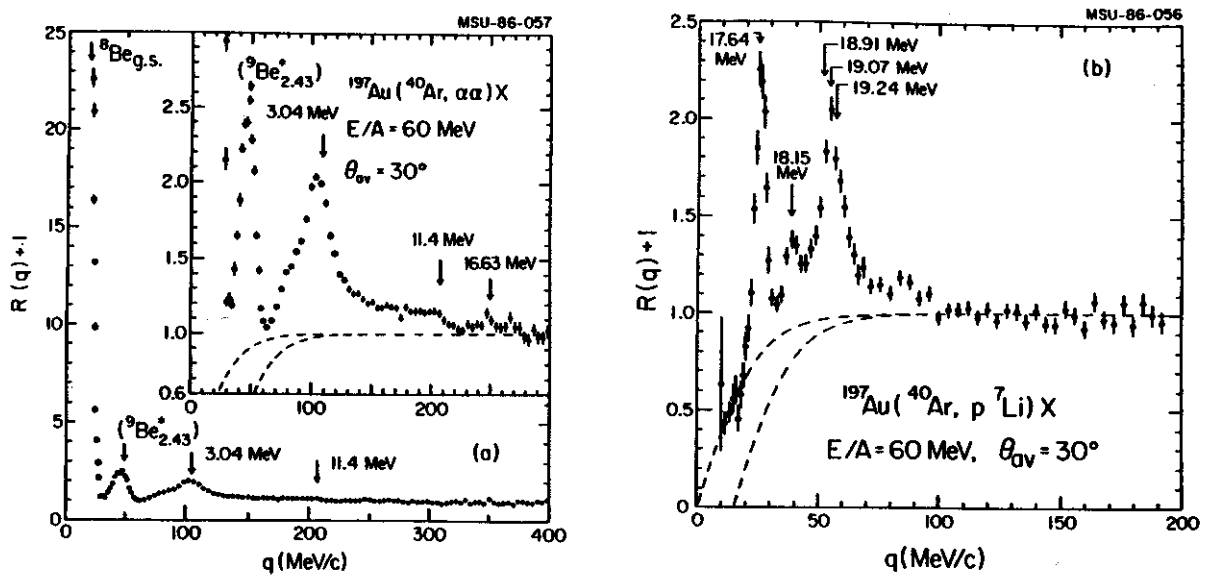

Fig. 2 Correlation functions for coincident alpha particles (part a) and coincident protons and ^{7}Li nuclei (part b).

analysis we will use the first peak which corresponds to the decay of the 17.64 MeV state in ^{8}Be.

The coincidence yield, Y_c, corresponding to the decay of a given particle unstable isotope was extracted by assuming that the total coincidence yield, Y_{12}, is given by: $Y_{12}=Y_c+Y_b$, where Y_b denotes the "background" yield. In our analysis, we have described this background yield in terms of a background correlation function $R_b(q)$: $Y_b(q)=C_{12}\cdot Y_1(\vec{p}_1)Y_2(\vec{p}_2)[1+R_b(q)]$. The background correlation functions were assumed to lie within the extremes indicated by the dashed lines in Figs. 1 and 2.

The decay coincidence yields Y_c were calculated for each decay channel according to the equation:

$$Y_c(E^*,T) = \int dE \left(\varepsilon_c(E^*,E)\cdot\rho_c(E)\cdot e^{-E/T}\right) \qquad \text{(Eq. 2)}$$

where E and E^* denote the actual and measured excitation energies of the decaying parent nucleus, respectively; T is the emission temperature, $\varepsilon_c(E^*,E)$ is the efficiency function of the hodoscope for the detection of the specific decay channel, and

$$\rho_c(E) = \sum_i \frac{(2J_i+1)\cdot\Gamma_i/2\pi}{(E-E_i)^2+\Gamma_i^2/4}\cdot\frac{\Gamma_{c,i}}{\Gamma_i} \quad . \qquad \text{(Eq. 3)}$$

The sum in Eq. 3 includes the relevant resonances characterised[13] by the excitation energies E_i, the widths Γ_i, and the branching ratios $\Gamma_{c,i}/\Gamma_i$. The efficiency functions, $\varepsilon_c(E^*,E)$, were calculated for the precise geometry, detection thresholds and energy resolution of the experiment. In these calculations, each resonance was assumed to decay isotropically in its center-of-mass frame. The laboratory energy spectra and angular distributions of the parent states were parameterised with simple analytic functions which describe the measured energy spectra and angular distributions of particle stable ^{6}Li and ^{7}Li nuclei[12].

To determine the relative populations of the four particle unstable resonances, $^{5}Li_{0.0}\rightarrow \alpha+p$, $^{5}Li_{16.7}\rightarrow d+^{3}He$, $^{8}Be_{3.04}\rightarrow 2\alpha$, $^{8}Be_{17.6}\rightarrow p+^{7}Li$, the calculated decay yields were integrated over the range of excitation energy for which the coincidence yields were dominated by these respective decays. The corresponding integrals were performed for the experimental decay yields. The integrals over the two states at low and high excitation energies for a given particle unstable nucleus are denoted by $N_L(T)$ and $N_H(T)$, respectively. The functional dependence of the calculated yield ratios N_L/N_H for particle unstable ^{5}Li and ^{8}Be nuclei is shown by the solid lines in Fig. 3. The hatched

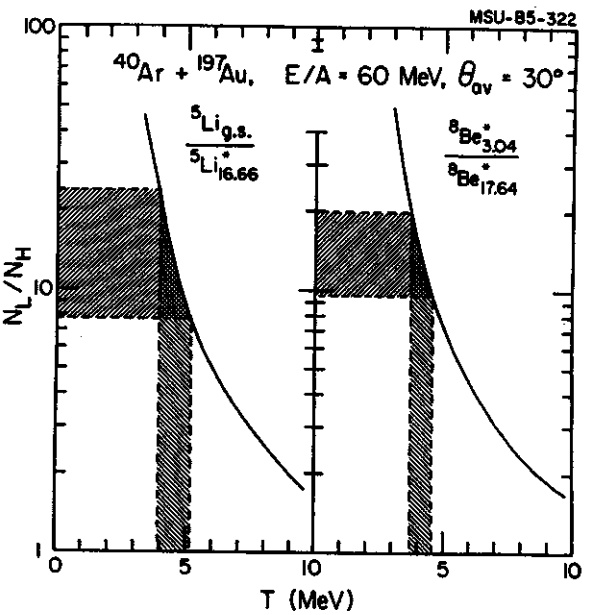

Fig. 3 Yield ratios N_L/N_H corresponding to the decays of ^{5}Li and ^{8}Be nuclei. The solid curves show the calculated ratios as a function of the emission temperature and the hatched regions indicate the range of values consistent with our assumptions for the background coincidence cross sections.

regions in the figure indicate the range of yield ratios and emission temperatures which are consistent with the extreme background assumptions shown in Figs. 1 and 2. The

relative populations of states in ^{5}Li and ^{8}Be correspond to emission temperatures of T = 4.6 ± 0.7 MeV and T = 4.2 ± 0.5 MeV, respectively. These temperatures are consistent with the results (T ≈ 5 MeV) of our recent analysis of the α-d coincidence spectrum[12]. However, the large energy spacing between the states at low and high excitation energy ensures that the extracted temperatures are relatively insensitive to the effects of sequential decay. Thus both significantly higher and lower emission temperatures are precluded. The extracted emission temperatures are considerably lower than the temperature parameters of about 20 MeV which characterise the kinetic energy spectra of the emitted particles. Future theoretical treatment of the disintegration of highly excited nuclear matter will be required to quantitatively explain this low emission temperature.

---

a. fellow of DFG, West Germany

b. University of Wisconsin, Madison, WI

c. GANIL, France

d. BARC Calcutta, India

e. Institute for Nucl. Science, Warsaw, Poland

f. Université de Caen, France

g. CEN Bordeaux, France

References

1. G.D. Westfall, et al., Phys. Rev. Lett. 37,1202(1976)
2. J. Gosset, et al., Phys. Rev. C18,844(1978)
3. J. Knoll, Phys. Rev. C20,773(1979)
4. W.A. Friedman and W.G. Lynch, Phys. Rev. C28,16(1983)
5. D.J. Fields, et al., Phys. Rev. C30,1912(1984)
6. G.D. Westfall, et al., Phys. Lett. 116B,118(1982)
7. P.J. Siemens and J.O. Rasmussen, Phys. Rev. Lett. 42,880(1979)
8. H. Stöcker, et al., Z. Phys. A303,259(1981)
9. D.J. Morrissey, et al., Phys. Lett. B148,423(1984)
10. D.J. Morrissey, et al., Phys. Rev. C32,877(1985)
11. D.H. Boal, Phys. Rev. C30,749(1984)
12. J. Pochodzalla, et al., Phys. Rev. Lett. 55,177(1985)
13. F. Ajzenberg-Selove, Nucl. Phys, A413,302(1985)

THREE - PARTICLE EFFECTS OBSERVED IN TWO - PARTICLE CORRELATION MEASUREMENTS

J. Pochodzalla[a], W.A. Friedman[b], C.K. Gelbke, W.G. Lynch, M. Maier, D. Ardouin[c], H. Delagrange[c], H. Doubre[c], C. Grégoire[c], A. Kyanowski[c], W. Mittig[c], A. Péghaire[c], J. Péter[c], F. Saint-Laurent[c], Y.P. Viyogi[c,d], B. Zwieglinski[c,e], G. Bizard[f], F. Lefèbvres[f], B. Tamain[f], J. Québert[g]

Small angle correlations between coincident alpha particles and protons were measured for ^{40}Ar induced reactions on ^{197}Au, at E/A=60 MeV. The correlation function exhibits two pronounced maxima located at values of the relative momentum near 15 and 50 MeV/c. The peak near 15 MeV/c is totally unexpected from properties of the mass 5 system. A peak near 50 MeV/c is expected from the free decay of ^{5}Li; however, the precise location of this peak was observed to depend on the relative magnitude of the proton and alpha particle velocities. Both of these surprising features can be explained in terms of simple three-body effects.

The experiment was performed at the Laboratoire GANIL at Caen. A gold target of 10 mg/cm^2 areal density was irradiated by a beam of ^{40}Ar of E/A=60 MeV incident energy. Light particles (Z≤3) were detected by a close-packed hexagonal array of 13 ΔE-E telescopes, each consisting of a 400 μm thick Si detector and a 10 cm thick NaI detector. The center of the hodoscope was positioned at a laboratory angle of 30°. Each telescope subtended a solid angle of 0.46 msr; the angular separation between adjacent telescopes was 4.2°.

We present our data in terms of the α-p correlation function, R(q), which is defined in terms of the singles yields, $Y_\alpha(\vec{p}_\alpha)$ and $Y_p(\vec{p}_p)$, and the coincidence yield, $Y_{\alpha p}(\vec{p}_\alpha,\vec{p}_p)$:

$$Y_{\alpha p}(\vec{p}_\alpha,\vec{p}_p) = C \cdot Y_\alpha(\vec{p}_\alpha) Y_p(\vec{p}_p)[1+R(q)] \quad . \qquad \text{(Eq.1)}$$

Here, $\vec{p}_\alpha$ and $\vec{p}_p$ are the laboratory momenta for alpha particles and protons, respectively; $\vec{q}$ is the proton momentum in the center-of-momentum frame of the α-p system; C is a normalisation constant which was determined by requiring R(q)=0 for q=100-150 MeV/c for the experimental correlation function shown in the upper part of Fig. 1. The experimental correlation functions were obtained by summing both sides of eq. 1 over all energies and angles corresponding to a given value of $q=|\vec{q}|$. For the correlation functions shown in the lower part of Fig. 1, the summation was performed with the constraints $v_\alpha < v_p$ (open points) and $v_\alpha > v_p$ (solid points),

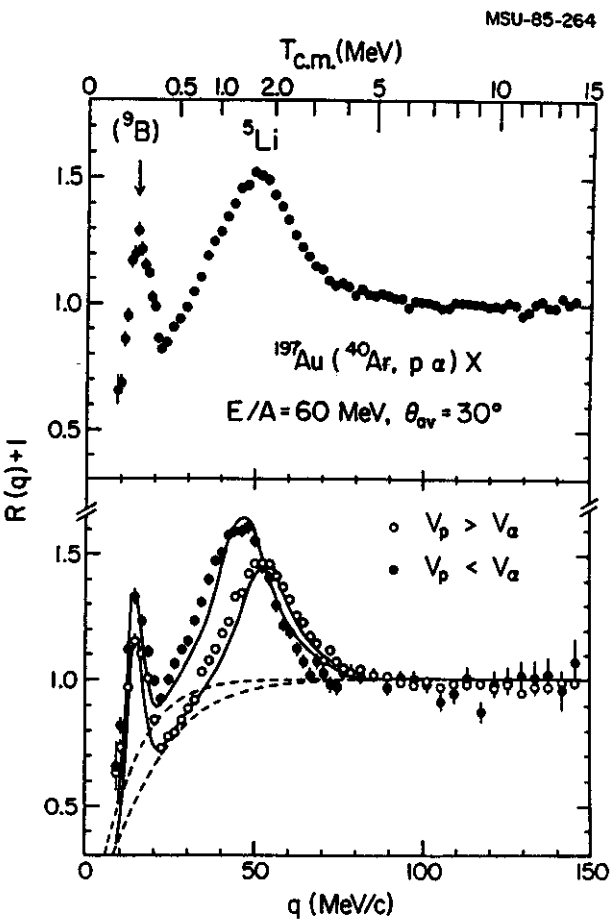

Fig.1 p-α correlation function for ^{40}Ar induced reactions on ^{197}Au at E/A=60 MeV. The upper part of the figure shows the correlation function corresponding to the sum over all particle velocities. The lower part shows the correlation functions corresponding to $v_\alpha < v_p$ (open points) and $v_\alpha > v_p$ (full points).

where v_α and v_p denote the laboratory velocities of alpha particles and protons, respectively. The experimental correlation functions exhibit two pronounced maxima located at q ≈ 15 and 50 MeV/c. While the location of the first maximum (q≈15 MeV/c) is the same for both branches, the location of the second maximum (q≈50 MeV/c) is not.

The peak near q≈15 MeV/c is not related to resonances in the mass five system. However, its position and width are consistent with the detection of two of the three fragments from the two stage decay of ^9B: $^9B_{gs} \rightarrow p + ^8Be_{gs} \rightarrow p + (\alpha+\alpha)$. Qualitatively, the occurrence of a sharp peak can be understood to result from the small decay energies and the narrow widths of the ground states of ^9B and ^8Be.

The peak near q≈50 MeV/c is clearly related to the unbound ground state of ^5Li. This state has a width of about 1.5 MeV and consequently has the short mean life of about τ=130 fm/c. For short lived states, the Coulomb interaction with the target residue can be important[1,2]. Since the charge-to-mass ratio of protons is greater than that of alpha particles the former will experience a greater acceleration from the reaction residue. Qualitatively, the velocity difference between protons and alpha particles should be decreased if $v_p < v_\alpha$ at the time of decay, while the difference should be increased if $v_p > v_\alpha$. If the life time were long, as is the case of the the decay of the ^9B, this effect would be negligible.

Detailed calculations were performed to test these hypotheses. The calculations took into account the measurement efficiency by including the exact detector geometries and detection thresholds. The decays of ^9B (and ^8Be) and ^5Li were assumed to be isotropic in the rest frames of the corresponding parent nuclei. For the case of ^5Li decay, the Coulomb interaction with the reaction residue was treated classically. Each ^5Li nucleus was assumed to decay at the time t=τ=130 fm/c, where t=0 denotes the instant of emission of the ^5Li parent nucleus. The energy gain in the Coulomb field of the residue was found to have a major effect on the peak position; angular deflections were found to be of minor importance. The energy gain was approximated as

$$E_{\alpha,p} = E^\circ_{\alpha,p} + e^2 Z_{eff} \cdot Z_{\alpha,p} / (R_\circ + \beta \cdot \tau) \ , \qquad \text{(Eq.2)}$$

where E° and E denote the kinetic energy at the point of decay and the asymptotic kinetic energy; β is the velocity of the ^5Li nucleus and Z_{eff} is the charge number characterising the Coulomb field of the residual matter. We have set Z_{eff}=80, $R_\circ$=8 fm. The line shape of ^5Li was approximated as[3]

$$dN/dE \propto \sin^2\delta_R \ / P_1 \ , \qquad \text{(Eq.3)}$$

where δ_R is the resonant phase shift[4] and P_1 is the l=1 penetration factor, $k/(F_1(k,a)^2 + G_1(k,a)^2)$; k is the wave number; F and G are the Coulomb wave functions evaluated at the radius a= 3 fm. The results of our calculations are shown by the solid lines in Fig. 1. The agreement with the experimental correlation function is good.

According to Eq. 2, the line shape distortion caused by the Coulomb interaction with the reaction residue should become less important at higher energies $E_\alpha + E_p$, i.e. higher velocities β. This effect is illustrated in Fig. 2, where the energy dependence of the peak location is shown for the two kinematic branches of the correlation function. The calculations are shown by the solid and dashed histograms; they reproduce the observed trend in each branch rather satisfactorily.

In addition, we have examined the angular distribution for the decay of ^5Li nuclei. Fig. 3 shows the angular distribution of the experimental yield, dY/dΨ, integrated over the range dominated by the second peak in the correlation function, 25 MeV/c ≤ q ≤ 100 MeV/c.

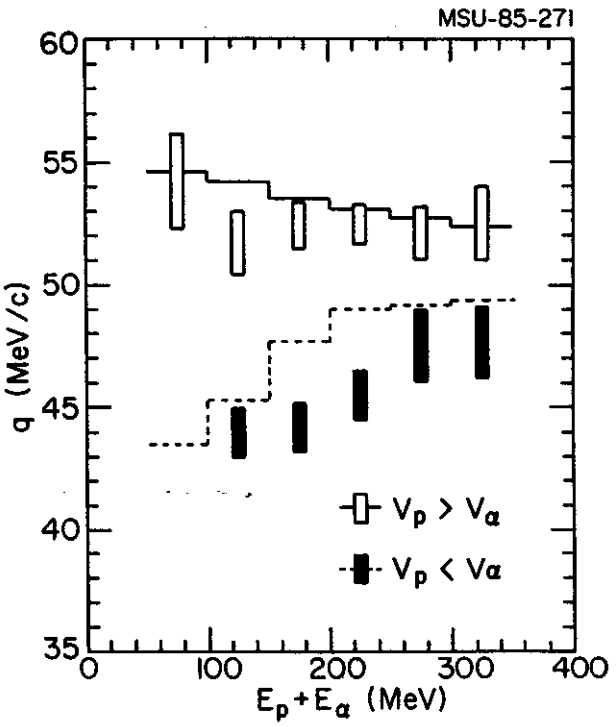

Fig.2 Location of the maximum of the experimental and theoretical correlation functions corresponding to $v_\alpha < v_p$ (open points, solid histogram) and $v_\alpha > v_p$ (full points, dashed histogram) as a function of the summed energy $E_\alpha+E_p$.

The angle Ψ denotes the angle between the vectors $\vec{q}$ and $(\vec{p}_\alpha+\vec{p}_p)$. The size of the vertical bars corresponds to the uncertainties associated with the background, which was assumed to lie within the boundaries shown by the dashed lines in Fig. 1. The yields calculated for the case of isotropic emission are shown by the solid histogram. Considering the uncertainties which have to be attributed to the background, the data are consistent with the assumption of isotropic decay. The angular distribution for data in the vicinity of the peak at q≈15 MeV/c was also studied and found to be consistent with

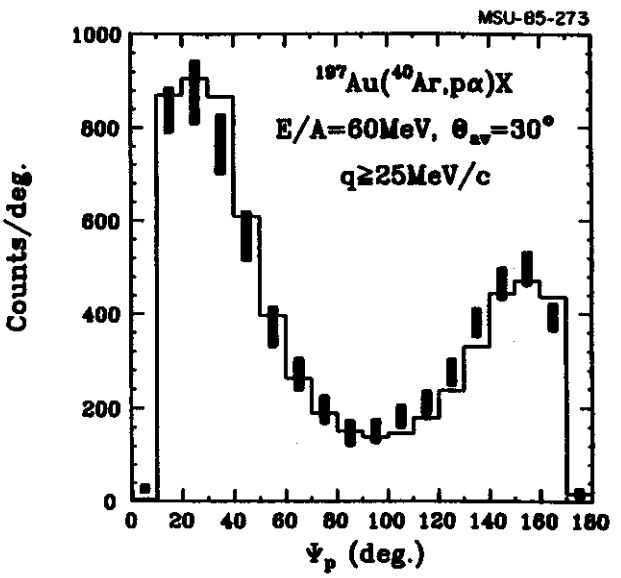

Fig.3 Dependence of the experimental yield above background on the angle Ψ between $\vec{q}$ and $(\vec{p}_\alpha+\vec{p}_p)$. The histogram corresponds to the yield calculated for the isotropic decay of ^{5}Li.

the isotropic distribution expected for the two stage decay of ^{9}B.

---

a. fellow of DFG, West Germany
b. University of Wisconsin, Madison, WI
c. GANIL, France
d. BARC Calcutta, India
e. Institute for Nucl. Science, Warsaw, Poland
f. University of Caen, France
g. CEN Bordeaux, France

References

1. M.A. Bernstein and W.A. Friedman, Phys. Rev. C31,843(1985)
2. D.R. Brown, et al., Nucl. Phys. A313,157(1979)
3. F.C. Barker and P.B. Treacy, Nucl. Phys. 38,33(1962)
4. Th. Stammbach and R.L. Walter, Nucl. Phys. A180,225(1972)

NUCLEAR TEMPERATURES AND THE POPULATION OF PARTICLE UNSTABLE STATES OF ^{6}Li IN ^{40}Ar INDUCED REACTIONS ON ^{197}Au AT E/A=60 MeV.

J. Pochodzalla, W.A. Friedman, C.K. Gelbke, W.G. Lynch, M. Maier, D. Ardouin,[a] H. Delagrange,[a] H. Doubre,[a] C. Grégoire,[a] A. Kyanowski,[a] W. Mittig,[a] A. Péghaire,[a] J. Péter,[a] F. Saint-Laurent,[a] Y.P. Viyogi,[a] B. Zwieglinski,[a] G. Bizard,[b] F. Lefèbvres,[b] B. Tamain,[b] and J. Québert[c]

Complex particle emission in intermediate and high energy nucleus-nucleus collisions presents a problem of such complexity that recourse to statistical methods seems appropriate. Statistical model calculations are often based on the assumption of particle emission from equilibrated subsets of nucleons.[1-4] In specifying the phase space of decay configurations, in-medium corrections are nearly always neglected and the asymptotic nuclear states (bound and unbound) are used. Such calculations make specific predictions about the relative populations of ground and excited states of the emitted fragments. Indeed, in each model a unique relation exists between the relative population of states and the temperature at the point at which the particles leave the equilibrated sub-system. In principle, this "emission temperature" can be deduced from the relative population of excited states.

We have measured the population of particle unbound states of ^{6}Li for ^{40}Ar induced reactions on ^{197}Au at E/A=60 MeV. The experiment was performed at the Laboratoire GANIL at Caen. A gold target of 10 mg/cm^2 areal density was irradiated by a beam of ^{40}Ar of E/A=60 MeV incident energy. Light particles (Z≤3) were detected by a close-packed hexagonal array of 13 ΔE-E telescopes, each consisting of a 400 μm thick Si detector and a 10 cm thick NaI detector. The center of the hodoscope was positioned at a laboratory angle of 30°.

Figure 1 shows the measured α-d correlation function, R(q), defined by

$$\sigma_{\alpha d}(\vec{p}_\alpha,\vec{p}_d) = C\cdot\sigma_\alpha(\vec{p}_\alpha)\sigma_d(\vec{p}_d)[1+R(q)] \quad . \qquad (1)$$

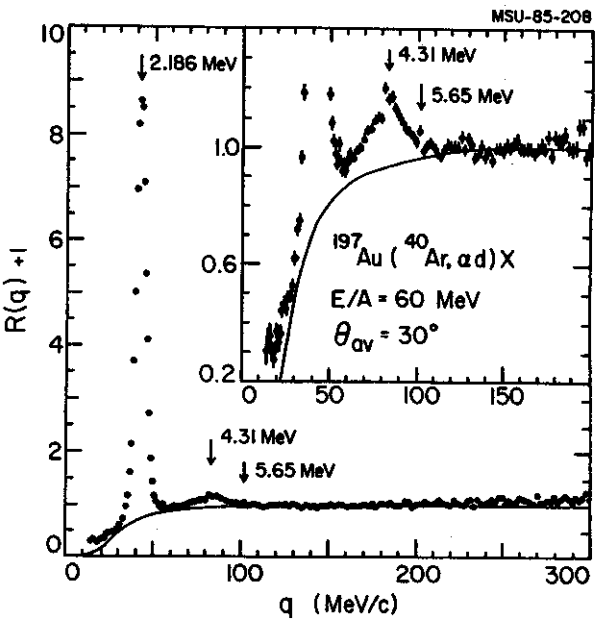

Fig. 1 Correlation function for coincident deuterons and alpha particles for ^{40}Ar induced reactions on ^{197}Au at E/A=60 MeV. The curve is explained in the text.

Here, $\sigma_{\alpha d}$ and σ_α, σ_d denote the two-particle and single-particle inclusive cross sections for alpha-particles and deuterons, respectively; $\vec{p}_\alpha$ and $\vec{p}_d$ are the laboratory momenta; q is the momentum of relative motion; and C is a normalisation constant which is determined by requiring R(q)=0 for q=160-200 MeV/c. The measured correlation function exhibits two maxima corresponding to the T=0, $J^\pi=3^+$ state in ^{6}Li at 2.186 MeV (Γ=24 keV, $\Gamma_\alpha/\Gamma_{tot}$=1.00) and the overlapping T=0 states at 4.31 MeV ($J^\pi=2^+$, Γ=1.3 MeV, $\Gamma_\alpha/\Gamma_{tot}$=0.97) and at 5.65 MeV ($J^\pi=1^-$, Γ=1.9 MeV, $\Gamma_\alpha/\Gamma_{tot}$=0.74).

The coincidence yield resulting from the decay of excited ^{6}Li nuclei was obtained by assuming that the α-d coincidence yield is given by $Y_{\alpha d} = Y_{^6Li} + Y_b$, where $Y_{^6Li}$ denotes the yield from decaying ^{6}Li nuclei and Y_b denotes the "background" yield. The background yield was assumed to be given by $Y_b = C \cdot Y_\alpha Y_d [1+R_b(q)]$, where Y_d and Y_α are the singles yields and $R_b(q)$ corresponds to the "background correlation function" shown by the solid curves in Figure 1. The yield, $Y_{^6Li}(E^*)$, of particle unstable excited ^{6}Li nuclei is shown in Figure 2. It is related to the energy spectrum, dn(E)/dE, in the ^{6}Li center-of-mass frame by the equation

$$Y_{^6Li}(E^*) = \int \varepsilon(E^*,E) \cdot \frac{dn(E)}{dE} \cdot dE \quad . \qquad (2)$$

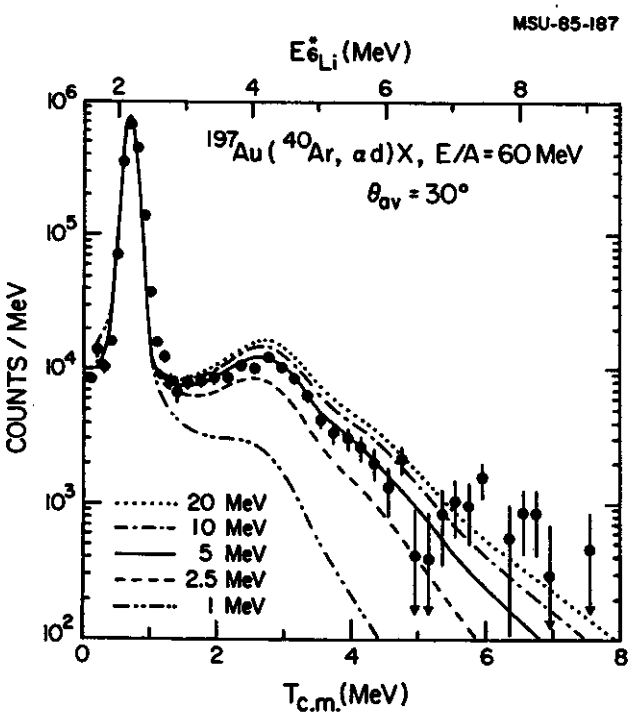

Fig. 2 Energy spectrum resulting from the decay of particle unbound states in ^{6}Li. The curves correspond to thermal distributions, T= 1, 2.5, 5, 10, and 20 MeV in eq. 2, taking the response of the hodoscope into account.

Here, $\varepsilon(E^*,E)$ is the efficiency function for the response of the hodoscope to α-d pairs arising from the decay of excited ^{6}Li nuclei; E and E^* denote the actual and measured excitation energies, respectively.

The efficiency function for our hodoscope was calculated for the precise geometry, light particle detection thresholds and detector energy resolution. In these calculations, the parent nucleus, ^{6}Li*, was assumed to decay isotropically in its rest frame. The laboratory energy spectra and angular distributions of excited ^{6}Li nuclei were constrained to be identical those of particle-stable ^{6}Li nuclei.

The excitation energy spectrum, dn/dE for thermally emitted ^{6}Li nuclei is given by

$$\frac{dn(E)}{dE} = N \cdot e^{-E/T} \cdot \sum_i \frac{(2J_i+1)\cdot\Gamma_i/2\pi}{(E-E_i)^2 + \Gamma_i^2/4} \cdot \frac{\Gamma_{\alpha,i}}{\Gamma_i} \quad , \qquad (3)$$

where N is a normalisation constant and the sum includes the three T=0 excited states of ^{6}Li below 10 MeV excitation energy. Calculations based on eqs. 2 and 3 are shown in Figure 2 for a variety of emission temperatures. The calculations were normalised to reproduce the experimental yield over the energy range of $T_{c.m.}$ = 0.3-1.2 MeV. The spectral shapes are sensitive to emission temperatures smaller than the level separation; higher emission temperatures are more difficult to distinguish. The experimental yields are consistent with an emission temperature of T ≈ 5 MeV. This value is lower than the temperature parameter T ≈ 20 MeV which characterises[5] the energy spectra of complex nuclei emitted at intermediate rapidity.

---

a. Laboratoire G.A.N.I.L., Caen Cedex, France
b. Universite de Caen, Caen Cedex, France
c. Centre d' Etudes Nucléaires de Bordeaux, Gradignan Cedex, France

References:

1. G.D. Westfall, et al., Phys. Rev. Lett. 37, 1202 (1976)
2. J. Gosset, et al., Phys. Rev. C18, 844 (1978)
3. J. Knoll, Phys. Rev. C20, 773 (1979)
4. D.J. Fields, et al., Phys. Rev. C30, 1912 (1984)
5. B.V. Jacak, et al., Phys. Rev. Lett. 51, 1846 (1983)

EFFECT OF ^{8}BE-DECAY ON NUCLEAR TEMPERATURE MEASUREMENTS

C. Bloch, W. Benenson, E. Kashy, D.J. Morrissey, R.A. Blue, R.M. Ronningen, and H. Utsunomiya[a]

In our recent measurements of the production of excited states of ^{7}Li and ^{7}Be nuclei emitted at large angles from the reaction of ^{14}N+Ag at E/A=35 MeV[1,2] we observed a large discrepancy between the temperature calculated from the excited state populations (about 0.5 MeV) and the temperature extracted from the shape of the particle kinetic energy spectra (about 12 MeV). Additionally, there was a much smaller discrepancy (about 2 standard deviations) between the temperatures determined from the excited state populations of ^{7}Li and ^{7}Be. We have examined the effects of ^{8}Be-decay and explain the latter discrepancy.

In most cases, the identification of an isotope in a ΔE-E silicon telescope is unambiguous. However, when both of the alpha particles from the decay of a ^{8}Be fragment pass through a silicon detector, they produce a signal indistinguishable from that of a ^{7}Li fragment. The observed ^{7}Li spectrum is then the sum of the true spectrum plus a solid angle dependent spectrum of α-pairs, which reduces the apparent fraction of ^{7}Li fragments in their excited state, and hence the inferred temperature. Our measurements of the solid angle dependence of the fragment yields in the reaction of E/A=35 MeV ^{14}N+Ag enabled us to determine the extent of the contamination of the ^{7}Li spectrum by ^{8}Be-decay and thereby correct our previous measurements. The new values show excellent agreement between the temperatures extracted from ^{7}Li and ^{7}Be.

In addition, we extended the measurements of excited state production in this system to beam energies of E/A=20 and E/A=25 MeV. We estimated the α-pair contamination of the ^{7}Li particle identification in these latter two cases from the results we obtained at E/A=35 MeV. This correction again produced consistent results between the temperatures obtained from the ^{7}Li and ^{7}Be excited state populations.

Lithium and beryllium nuclei were produced by the interaction of nitrogen ions with a silver target. Beams of 490 MeV $^{14}N^{5+}$, 280 MeV $^{14}N^{4+}$ and 350 MeV $^{14}N^{5+}$ ions were provided by the K500 cyclotron. The target was a self-supporting foil of natural silver, 1.8 mg/cm^2 thick. Inclusive energy spectra for lithium, beryllium, and boron isotopes were obtained from silicon ΔE-E telescopes, each with a 300 mm^2 area. The ΔE detectors were either 50 or 100 μm thick, while the E detectors were all 1000 μm thick. As in ref. 2, we employed eight 7.6 by 7.6 cm NaI(Tl) detectors to obtain the γ-ray energy spectrum in coincidence with each fragment mentioned above.

The first goal was to determine what portion of the particles identified as ^{7}Li was actually α-pairs from ^{8}Be-decays in order to correct the previous determination of excited state production. We can determine the extent of such a contamination by varying the solid angle of the silicon detectors because the yield of ^{7}Li fragments detected is linearly proportional to the solid angle while the yield of α-pairs from ^{8}Be-decay is not. This difference is due to the fact that the alpha particles are emitted along paths diverging on opposite sides of the original ^{8}Be trajectory, and therefore both will not always enter the detector. In theory, the simplest way to determine the level of contamination would be to measure the yield, $\frac{d\sigma}{d\Omega}\Delta\Omega$, for several solid angles, ΔΩ, and then extrapolate to ΔΩ=0. A major difficulty with this method is due to the function's non-linearity. If ΔΩ is sufficiently close to zero for a linear extrapolation, the particle yield will be small (for a limited beam time) which would lead to a large statistical

uncertainty in the extrapolated differential cross-section. For that reason, we used a less transparent but more viable method.

Our technique was to parameterize the two unknown spectra, i.e. that of ^{8}Be and the true ^{7}Li, by assuming that the shapes of the kinetic energy distributions are the same for isotopes of a given element, and that there is an overall normalization among them. Thus we expect the true ^{7}Li spectrum (with no contamination from α-pairs) to have the shape of the ^{6}Li spectrum, multiplied by a parameter, m, to be determined. The shape of the ^{8}Be spectrum was assumed to be the same as ^{9}Be with an overall normalization, b, again left as a parameter. The yield of α-pairs is the integral of the ^{8}Be spectrum, weighted by the relative efficiency for detecting each resulting α-pair. This efficiency, ε(E), is a function of the original ^{8}Be energy, E, and the solid angle of the detector, and is given by the following integral:

$$\varepsilon(E) = \frac{2\pi}{\Delta\Omega} \times \int_0^{\theta_0} P(E,\theta) \times \sin(\theta) \times d\theta \qquad (1)$$

where θ is the angle between the original ^{8}Be trajectory and the detector axis, P(E,θ) is the probability that both alpha particles would enter the detector, and θ_0 is the half angle of a detector with solid angle ΔΩ. From the singles data at three solid angles (5, 9 and 22 msr), we obtained three linear equations of the two parameters, m and b, which were then determined to be 1.22±0.10 and 2.0±0.5 respectively, by a least squares fit (see Fig. 1).

Since we are assuming the true ^{7}Li yield is "m" times the ^{6}Li yield, we can correct the previous apparent excited state fraction by the relation:

$$f = f_{obs} \times \frac{Y(^{7}Li_{obs})}{m \times (^{6}Li)} \qquad (2)$$

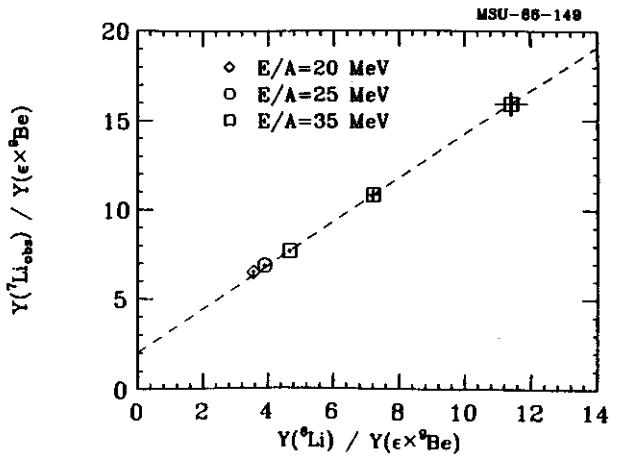

Fig. 1 Parameterization of the ^{7}Li and ^{8}Be yields in terms of the ^{6}Li yield and a model calculation of the contamination from α-pairs, see the text. The fit is to the E/A=35 MeV data.

where $Y(^{7}Li_{obs})$ is the yield of particles identified as ^{7}Li (both ^{7}Li and α-pairs) and Y(^{6}Li) is the yield of ^{6}Li. For the solid angle of ref. 2 (24 msr), we obtained a correction factor of 1.45±0.12. When corrected for contamination from α-pairs, the ^{7}Li fractions are in good agreement with the previously reported values for the ^{7}Be fractions. The extracted temperatures are shown in Fig. 2.

In the second experiment, we extended the measurements of the fraction of particles

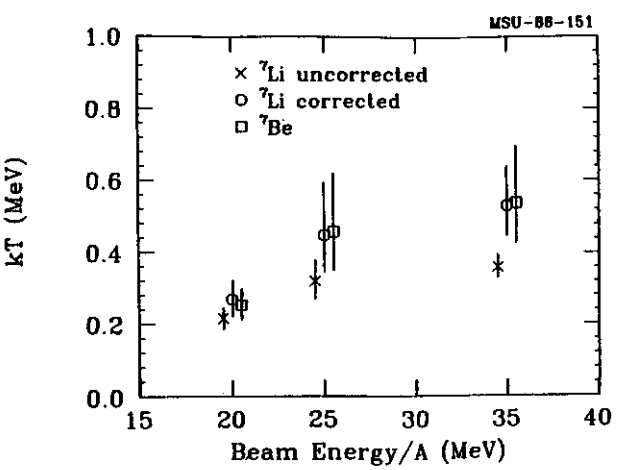

Fig. 2 Temperatures calculated from excited state populations for fragments emitted from the reaction of ^{14}N+Ag versus beam energy.

emitted in their excited state as was described in ref. 2. In addition, we determined the average γ-ray multiplicity, M_γ, and the width of the γ-ray multiplicity distribution, σ, by the method of Ockels.[3] Typical values for E/A=20 MeV are M_γ=18.4±1.8 and σ=9.1±2.5, and for E/A=25 MeV are M_γ=17.0±1.3 and σ=8.8±1.2. Values reported in ref. 2 for E/A=35 MeV are typicaly M_γ=12.3 and σ=7.7±0.9. We did not measure the level of the α-pair contamination of the ^{7}Li particle spectrum at these beam energies, but used m=1.22 as determined from the data at E/A=35 MeV. As shown in Fig. 1, the points from the single solid angle used at E/A=20 MeV and E/A=25 MeV lie along the line portraying the E/A=35 MeV fit, which suggests that the same value for m can be used to determine the actual yield of ^{7}Li fragments and true ^{7}Li fraction in Eq. (2). For these two lower energies, the correction factors (as discussed above) were 1.51±0.13 (for E/A=20 MeV), and 1.46±0.12 (for E/A=25 MeV). Again, the corrected ^{7}Li fractions are much closer than the previous values to those for ^{7}Be. The temperatures extracted from these values are also shown in Fig. 2. As stated earlier, previous temperature measurements of this type have been in serious disagreement with kinetic energy slope parameters determined from a moving source model.[4] The slope parameters obtained for the present data are: 10.±1. for E/A=20 MeV, and 11.±1. for E/A=25 MeV.

We have extracted temperatures from measurements of the excited state populations of ^{7}Li and ^{7}Be from the reaction of ^{14}N with Ag at energies of 280, 350, 490 MeV. Our results show that ^{8}Be significantly contaminates the ^{7}Li spectrum. After correcting the observed ^{7}Li spectrum for this contamination, the excited state populations for ^{7}Li and ^{7}Be are consistent with the same temperature. One would expect this from their similar structure, however the importance of the feeding of these states by the particle decay of higher mass nuclei is very different.[5] Additionally, we have shown (Fig. 2) that the observed excited state population temperatures do not decrease with increasing beam energy. This trend is contrary to two mechanisms previously suggested to explain the apparent low temperature.[5,6] At lower beam energies, we expect less feeding of the ground states of ^{7}Li and ^{7}Be, and hence higher observed excited state populations. Also, it is expected that at E/A=20 MeV the coincident fragment multiplicity will be lower than at E/A=35 MeV, which would result in less cooling via final state interactions[8] at E/A=20 MeV than at E/A=35 MeV. This would predict a decrease in excited state populations with increasing beam energy, which is not seen. We take this as evidence that while both cooling mechanisms discussed in ref. 2 are surely present, it does not appear that they can account for the large discrepancy between the temperatures consistent with the excited state populations and those consistent with the kinetic energy degrees of freedom.

---

a. Present address: Cyclotron Institute, Texas A&M University.

References

1. D. J. Morrissey, W. Benenson, E. Kashy, B. Sherrill, A. D. Panagiotou, R. A. Blue, R. M. Ronningen, J. van der Plicht, and H. Utsunomiya, Phys. Lett. 148B,423(1984).
2. D. J. Morrissey, W. Benenson, E. Kashy, C. Bloch, M. Lowe, R. A. Blue, R. M. Ronningen, B. Sherrill, H. Utsunomiya, and I. Kelson, Phys. Rev. C. 32,877(1985).
3. W. J. Ockels, Z. Phys. A 286,181(1978)
4. B. V. Jacak, G. D. Westfall, C. K. Gelbke, L. H. Harwood, W. G. Lynch, D. K. Scott, H. Stocker, M. B. Tsang, and T. J. M. Symons, Phys. Rev. Lett. 51,1846(1984).
5. H. Stocker, private communication.
6. D. Boal, Phys. Rev. C. 30,749(1984)

THERMAL POPULATION OF NUCLEAR EXCITED STATES

D. J. Morrissey, C. Bloch, W. Benenson, E. Kashy, R. A. Blue,
R. M. Ronningen, and R. Aryaeinejad

Here we report measurements of the population of bound states of ^{7}Be and ^{10}B fragments from the well-studied[1-3] reaction of ^{14}N with ^{12}C. The production of light nuclei in their ground and excited states was studied in the reaction of ^{14}N with a carbon target using beams of 87.5, 101.5, 112, 168, 210, 280 and 350 MeV. Bombarding energies of 87.5 and 101.5 MeV were obtained by degrading a 112 MeV beam from the K500 cyclotron with 6.0 and 12.0 mg/cm^2 aluminum foils, respectively, before the first bending magnet of the beam transport system.

For systems with only <u>one</u> bound excited state (e.g., ^{7}Be) the γ-ray fraction is equal to the fraction of the population initially in the excited state. In general the fraction of the population, f_n, in a given excited state, n, is given by:

$$f_n = \frac{(2j_n+1)\, e^{-\Delta E_n/kT}}{\sum_i (2j_i+1)\, e^{-\Delta E_i/kT}} \qquad (1)$$

where the sum over i in the denominator, usually called the partition function, includes all the states of the system. The γ-ray fraction for these nuclei is not generally equal to the fraction of the population <u>initially</u> in a given state due to γ-ray branching and cascades. The fraction of nuclei in coincidence with a specific γ-ray is rather:

$$f_{E_\gamma} = \frac{\sum_n a_n(E_\gamma)\, (2j_n+1)\, e^{-\Delta E_n/kT}}{\sum_i (2j_i+1)\, e^{-\Delta E_i/kT}} \quad . \qquad (2)$$

Note that the the sum with an index n extends over all higher-lying states that cascade through the state emitting the observed γ-ray and includes the branching ratios, $a_n(E_\gamma)$. Agreement of the population distribution among several pairs of excited states is a good test of thermal equilibrium which does rely on the ground state population. Problems involving preferential feeding of a level by the decay of unbound higher mass nuclei (notably the ground state) will be evident in inconsistencies among the ratios of several levels.

A large amount of data was obtained on the inclusive kinetic energy and angular distributions of reaction products from these reactions and on the coincident γ-ray spectra and multiplicities. The details of the experimental arrangement have been discussed in reference 4. The spectra in coincidence with ^{7}Be fragments contained only the 428 keV γ-ray whereas the ^{10}B coincidence spectra contained the 414, 718 and 1022 keV transitions on very low backgrounds. For example, the γ-ray fractions obtained at 35° (lab) are shown in fig. 1. All the additional measurements were consistent with these results although with poorer statistics.

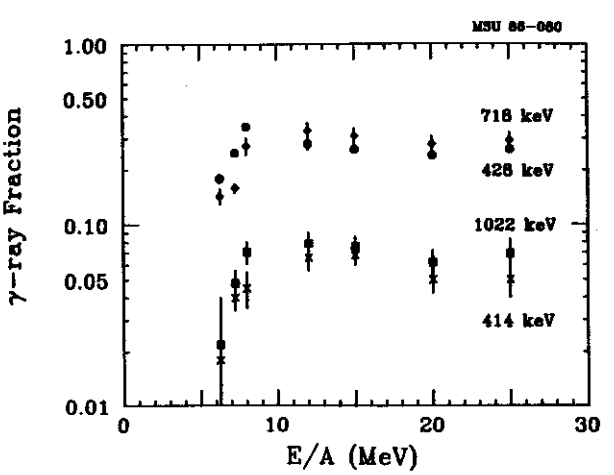

Fig. 1 The measured fractions of ^{7}Be and ^{10}B nuclei (θ_{lab} = 35°) in coincidence with specific γ-ray transitions as a function of the beam E/A. The data points are labeled by transition energy.

In the ^{7}Be case (one observed γ-ray) the temperature was obtained from the ratio of the excited to the total population. The temperature of the source of the ^{10}B fragments (three γ-rays) was obtained by a least-squares fit to three simultaneous equations for the γ-ray fractions. The three equations each contained a sum over feeding states and a single temperature, similar to eq. 2. The results of these determinations are shown in fig. 2 as a function of bombarding energy. Alternatively, the ^{10}B γ-rays can be used to determine the ratios of the populations among the excited states which are also consistent with the temperatures in fig. 2. This indicates that, at least for this case, decay of higher mass nuclei is not an important factor.

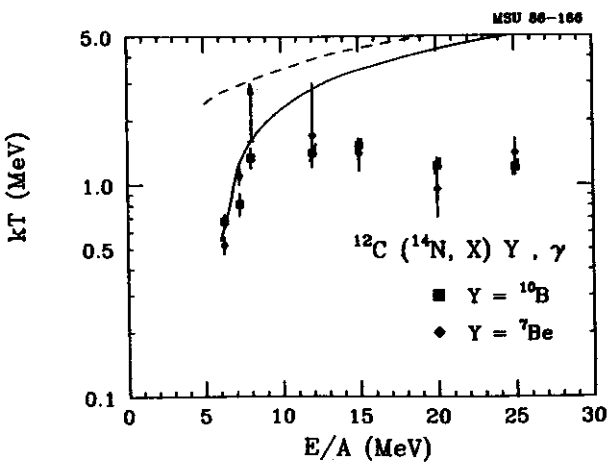

Fig. 2 "Population distribution" temperature of ^{7}Be and ^{10}B fragments from the reaction of ^{14}N + ^{12}C as a function of bombarding energy. The expected temperature after removal of the rotational energy follows the solid curve, see the text. The expected temperature with zero rotational energy is indicated by the dashed curve.

We can make a simple estimate of the variation of the temperature of the compound nucleus, ^{26}Al, with beam energy by relying on previous measurements of this system. In the Fermi gas model the temperature of a compound nucleus is $kT \approx (E_{th}/a)^{1/2}$ where a is the level density parameter. We expect that the excited state populations of these large fragments will reflect the average thermal excitation of the compound nucleus, $\langle E_{th} \rangle$, written as:

$$\langle E_{th} \rangle = E_X - \frac{\langle \ell \rangle^2 \hbar^2}{2\,I} \qquad (3)$$

where E_X is the total excitation energy of the system (equal to the energy in the center of mass plus the ground state Q-value for ^{26}Al). The second term in equation (4) represents the average rotational energy of the system with $\langle \ell \rangle \hbar$ as the average angular momentum and I, as the moment of inertia of the compound nucleus. Reasonable values of the maximum angular momentum (26 ħ) and the rotational constant ($2I/\hbar^2 = 8$ MeV^{-1}) can be obtained from previous studies[1]. Fig. 2 shows the variation of the temperature before subtracting the rotational energy (dashed curve) and that calculated after subtracting the average rotational energy (solid curve). We find that the compound nucleus reaction mechanism begins to fail to describe fragment excited state populations in the same bombarding energy range at which previous measurements have shown a dramatic increase in the yield of direct reactions[1].

References

1. J. Gomez del Campo, et al., Phys. Rev. C29 (1984) 1722, and R.G. Stokstad, et al., Phys. Lett. 70B (1977) 289, and references therein.
2. R.G. Stokstad, et al., Phys. Rev C16 (1977) 2249.
3. R.G. Stokstad, Proc. Intl. Conf. on Reactions Between Complex Nuclei, Nashville, Tennessee, R.L. Robinson, F.K. McGowan, J.B. Ball and J.H. Hamilton, Eds., (North-Holland, Amsterdam, 1974), 1974, Vol. II, p. 327.
4. D.J. Morrissey, et al., Phys. Rev. C32 (1985) 877.

MULTIPARTICLE CORRELATIONS WITH INTERMEDIATE ENERGY HEAVY IONS

Z.M. Koenig, G.D. Westfall, R.S. Tickle[a], G.M. Crawley, D. Fox, R. Fox, B.E. Hasselquist, D. Horn[b], B.V. Jacak, J. Wilczynski, and K. Wilczynska

Fragments emitted from intermediate energy nucleus-nucleus collisions can carry information concerning the details of the reaction mechanisms. By selecting various types of fragments one can categorize the collisions into gentle, grazing reactions or violent, central collisions. Observing large remnants of the projectile at forward angles at beam velocity is a signature of a peripheral collision. Fragments that display a nearly isotropic angular distribution and have energies near the coulomb barrier also arise from peripheral collisions. On the other hand, observing high energy light particles and complex fragments at wide angles is indicative of central collisions. In this experiment gentle, peripheral collisions were selected by observing a projectile-like fragment (PLF) at forward angles and by observing a target-like fragment (TLF) at wide angles. Light particles from these reactions are expected to reflect this event selection using PLFs and TLFs by displaying a lower temperature and asymmetric emission pattern as opposed to light particles from central collisions that have been shown to have relatively high temperatures and isotropic angular distributions in a moving frame.[1]

Light particle (p,d,t,^{3}He,^{4}He) inclusive and coincidence spectra have been measured for the systems 15 and 30 MeV/nucleon C+C and C+Au and for 92 MeV/nucleon Ar+Au. These measurements complement and extend previous measurements of these systems.[2] Light particle spectra were measured at ±45°, ±67.5°, and ±90° in coincidence with projectile-like fragments (PLFs) and target-like fragments (TLFs). The negative angles refer to observations of light particles on the opposite side of the reaction plane. The PLF detectors consisted of multiple element silicon detector telescopes placed at angles outside the grazing angle. For the higher energy measurement two PLF detectors were used as shown in Fig. 1. The TLFs were measured in a Bragg Curve Spectrometer (BCS) at 45° and 90°. The light particles (LP) were detected

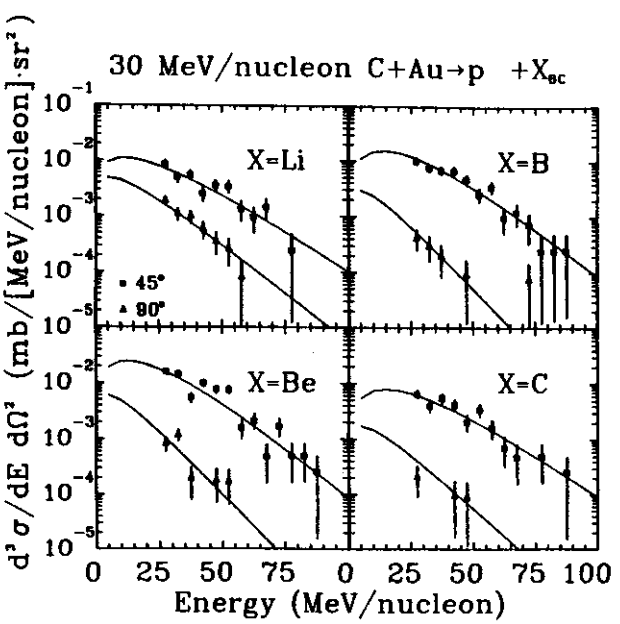

Fig. 1 Protons measured in coincidence with TLFs measured in the Brass curve (BC) counter. The solid line is a moving source fit.

using two sets of CaF_2-plastic scintillator detector telescopes One set of LP detectors was composed of seven CaF_2-plastic telescopes. The second array was made up of six telescopes mounted directly behind the BCS. Data from the 30 MeV/nucleon C+Au will be presented here because it is representative of the other systems studied.

The inclusive light particle spectra were fit with a moving source parameterization where the production cross section Go, source velocity, β, and apparent source temperature, τ, were extracted. these parameters were consistant with previous measurements.[1] The triggered light particle spectra were fit with

the same parameterizations. As an example of triggered light particle spectra, the spectra of protons triggered by TLFs with Z=3 to 6 are shown along with moving source fits in Fig. 1. The parameters extracted from these moving source fits are used to compare triggered light particle spectra to inclusive spectra.

In Fig. 2 such a comparison is made for temperatures extracted using proton spectra from 30 MeV/nucleon C+Au triggered on PLFs at projectile velocity (a), PLFs at intermediate

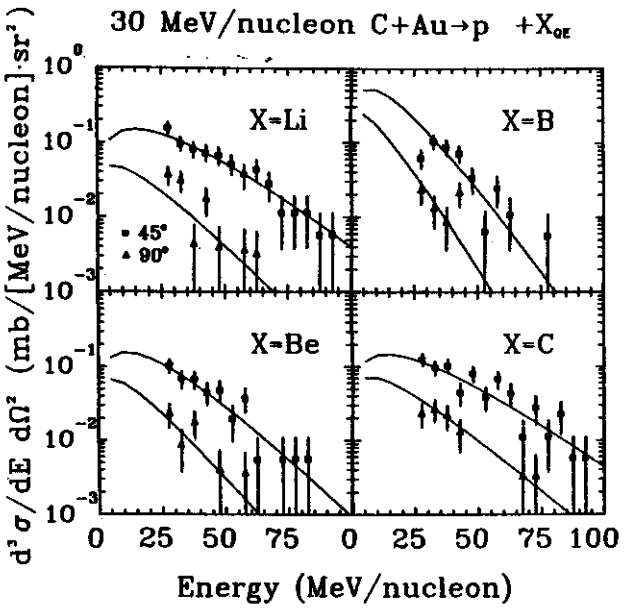

Fig. 2 Protons observed in coincidence with PLFs near projectile velocity. The solid line is a moving source fit.

velocity (b), and TLFs (c). The squares refer to protons observed at the same azimuth as the trigger particle and the triangles refer to protons measured on the opposite side of the reaction plane. There is no significant trend in these comparisons.

Another correlation that can be studied is to study the integrated cross section for emission of light particles in coincidence with PLFs and TLFs on the same side of the reaction plane and of the opposite side. In Fig. 3 the ratio of protons observed on the same side as projectile velocity PLFs, intermediate velocity

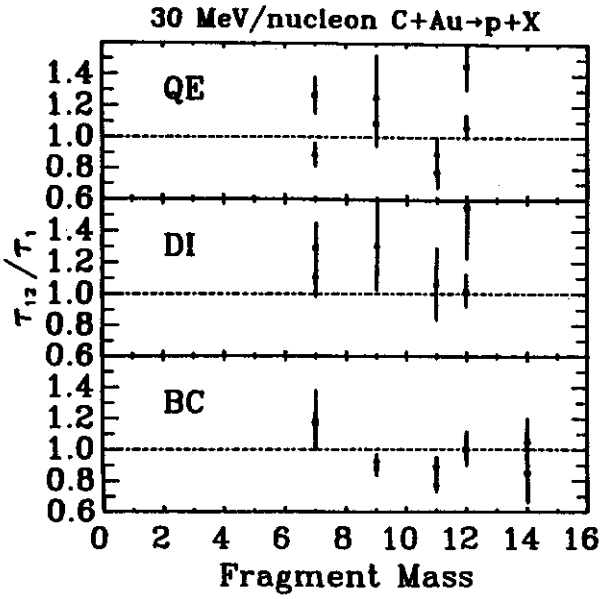

Fig. 3 Ratio of extracted temperatures for protons in coincidence with a) PLFs at projectile velocity (QE), b) PLFs at intermediate velocity (DI), and c) TLFs on the same and opposite side of the reaction plane (BC).

PLFs, and TLFs are shown for 30 MeV/nucleon C+Au. The solid lines represent a calculation incorporating fireball geometry, a thermal distribution, and momentum and energy conservation. If the trigger particles and the observed light particles originate from a common source, then this calculation should account for trivial momentum and energy conservation effects. One can see that the calculation agrees for the two PLF triggers but disagrees for the TLF case. Thus one may conclude that the high energy protons and the TLFs do not originate from the same source.

---

a. University of Michigan, Ann Arbor, Michigan
b. Chalk River, Canada

References

1. B.E. Hasselquist, G.M. Crawley, L.H. Harwood, B.V. Jacak, Z.M. Koenig, G.D. Westfall, J.E. Yurkon, R.S. Tickle, J.P. Dufour, and T.J.M. Symons, Phys. Rev. C32, 145 (1985).

2. B.V. Jacak, G.D. Westfall, C.K. Gelbke, L.H. Harwood, W.G. Lynch, D.K. Scott, H. Stöcker, M.B. Tsang, and T.J.M. Symons, Phys. Rev. Lett. 51, 1846,(1983).

LARGE ANGLE CORRELATIONS IN 40 MEV/NUCLEON $^{12}C+^{12}C$ REACTIONS

D. Fox, D.A. Cebra, G.D. Westfall, J.J. Molitoris, and H. Stöcker

Last year we reported our findings on the ratio of in-plane to out-of-plane p-p correlations for 40 MeV/nucleon C+C[1]. Since then we have published a paper[2] covering the ratios of in-plane to out-of-plane correlations for all pairs of light particles (p, d, t, ^{3}He, and ^{4}He). We have found no peak at energies corresponding to quasielastic nucleon-nucleon scattering for in-plane to out-of-plane ratios in p-p correlations. The angular distribution of these ratios (Fig. 1) shows a very weak peak when compared to similar measurements done at 85[3] and 800[4] MeV/nucleon. As was seen at 85 MeV/nucleon, the correlation between light nuclei increases with increasing mass of the observed particles (Fig. 2).

MSU-86-208

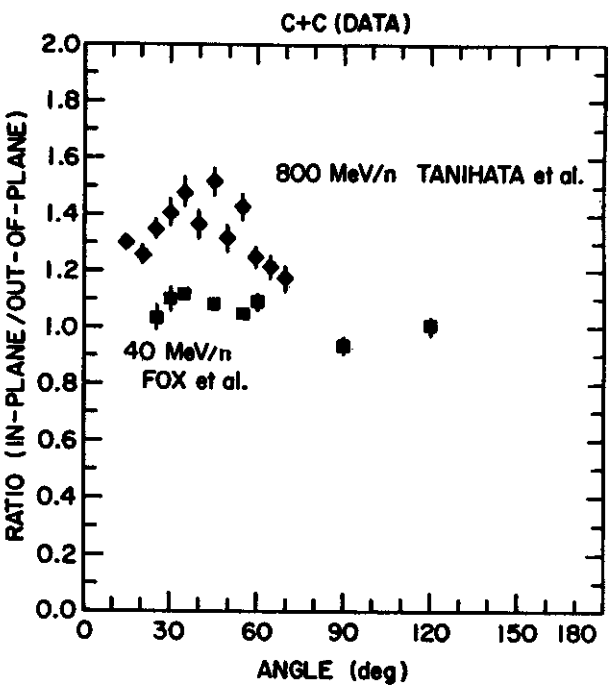

Fig. 1 Angular distribution of the ratio of in- to out-of-plane correlations for 40 (squares) and 800 (diamonds) MeV/nucleon C+C.

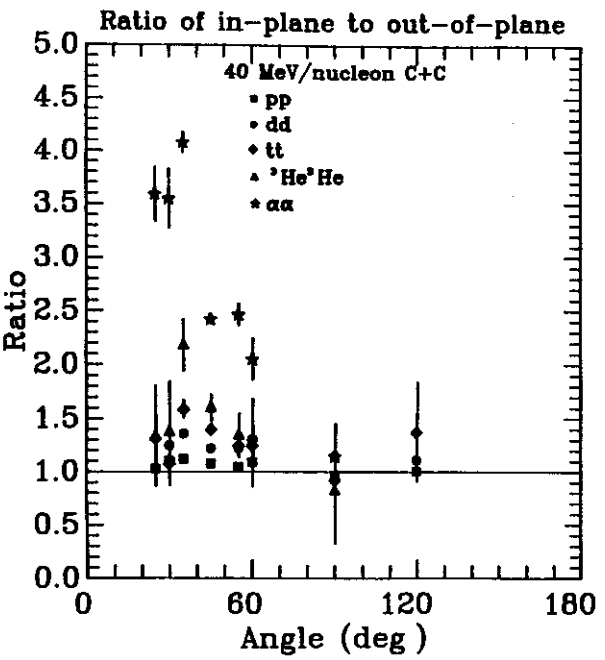

Fig. 2 Angular distribution of the ratio of in- to out-of-plane correlations for p-p, d-d, t-t, ^{3}He-^{3}He, and ^{4}He-^{4}He from 40 MeV/nucleon C+C.

We have attempted to describe these results by two methods, the first is a simple momentum conservation calculation. In this calculation[5] the system is assumed to emit one particle, re-equilibrate and recoil, and emit the second particle. The result is averaged with the case where the second particle is emitted first. The calculation is integrated over impact parameter, with a weight assigned to each impact parameter that is the cross section for observing a nucleon. This weight is a maximum at intermediate values of the impact parameter. This calculation, as shown in Fig. 3, fails to reproduce the observed angular distributions.

We have also carried out Vlasov-Uehling-Uhlenbeck (VUU) calculations for large angle correlations for C+C reactions of 40 and 800 MeV/nucleon. The VUU calculation includes phase

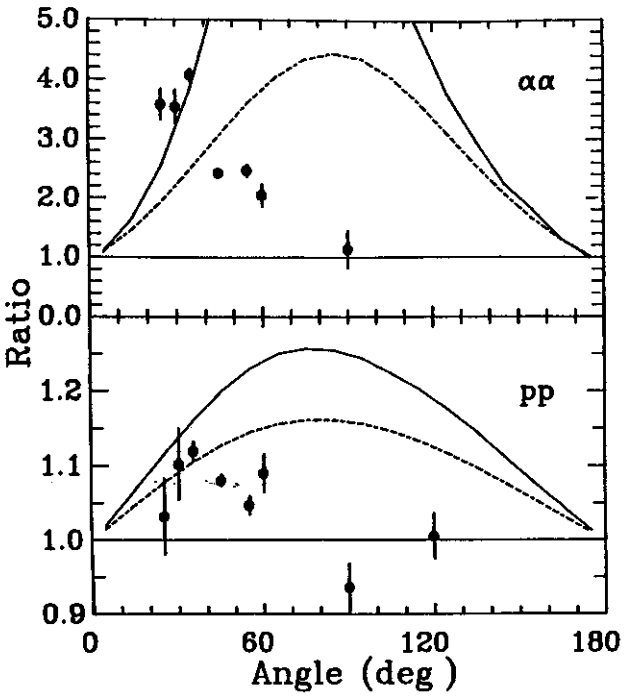

Fig. 3 Angular distribution of the ratio of in- to out-of-plane correlations for p-p and α-α for 40 MeV/nucleon C+C compared with an impact-parameter-averaged momentum conservation calculation (solid lines) and the same calculation carried out assuming an emitting system of 24 nucleons (dashed lines). Note the difference in the ordinate for p-p and α-α correlations.

space Pauli blocking, the nuclear mean field, and two body collisions. The nucleons are then clustered and unstable nuclei are allowed to decay. The calculation, shown in Fig. 4, seems to do a good job of predicting the general trend of the data, although it underestimates the magnitude at 800 MeV.

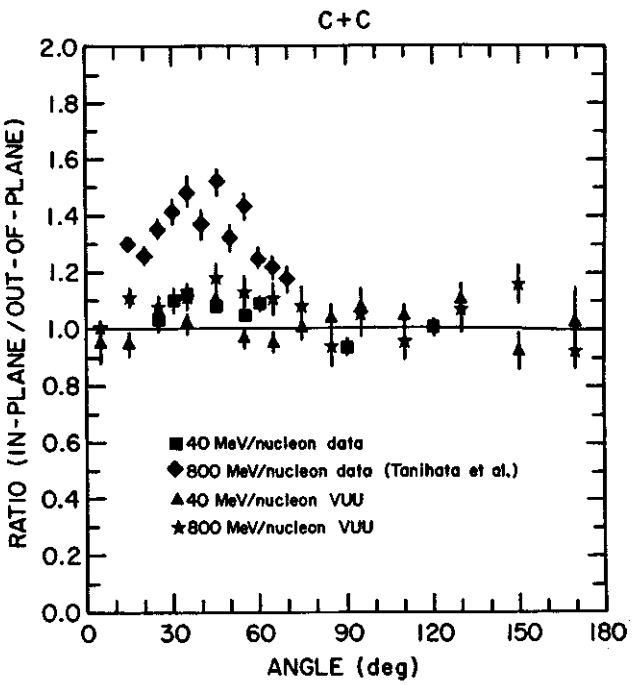

Fig 4. Angular distributions of the ratio of in- to out-of-plane correlations for 40 and 800 MeV/nucleon C+C compared to VUU calculation.

References

1. D. Fox, D.A. Cebra, Z.M. Koenig, J.J. Molitoris, P. Ugorowski, H. Stöcker and G.D. Westfall, Annual Report, Cyclotron Lab, MSU 1983-84, 73 (1985).
2. D. Fox, D.A. Cebra, Z.M. Koenig, P. Ugorowski and G.D. Westfall, Phys. Rev. C
3. P. Kristiansson, L. Carlen, H.-A. Gustafsson, B. Jakobsson, A. Oskarsson, H. Ryde, J.P. Bondorf, O.-B. Nielson, G. Løvhóiden, T.-F. Thorsteinsen, D. Heuer, and H. Nifenecker, Phys. Lett. 155B, 31 (1985).
4. I. Tanihata, M.-C. Lemaire, S. Nagamiys, and S. Schnetzer, Phys. Lett. 97B, 363 (1980).
5. B.E. Hasselquist, G.M. Crawley, L.H. Harwood, B.V. Jacak, Z.M. Koenig, G.D. Westfall, J.E. Yurkon, R.S. Tickle, J.P. Dufour, and T.J.M. Symons, Phys. Rev. C32, 145, (1985).

NEUTRON SPECTRA FROM HIGH ENERGY AU+AU REACTIONS

R. Madey[a], A.R. Baldwin[a], B.D. Anderson[a], J.W. Watson[a], and G.D. Westfall

The study of neutrons emitted from high energy nucleus-nucleus collisions can provide a picture of the reaction undisturbed by coulomb forces. The coulomb force is especially troublesome for the study of nucleons near the target and projectile rapidities. In fact the suppression of forward emission observed in high multiplicity events at low energies (target rapidities) may have been more attributable to coulomb effects than to collective nuclear effects.[1,2]

We have measured double differential cross sections for 390 and 790 MeV/nucleon Au+Au at angles of 0,4,8,15,30,45,90,120, and 160 °. The HISS magnet was used to sweep the beam to ≈15° to allow the measurement of the forward angles. The neutrons were detected using a time-of-flight technique with large solid angle detectors developed by the Kent State group. The centrality of each event was measured using a plastic scintillator downstream of the target placed near the beam-dump that observed the charge of the remaining projectile fragment, if any.

Energy spectra from 0 to 30° are shown in Fig. 1 for 790 MeV/nucleon Au+Au. The most distinguishing feature of these spectra is the large peak in the 0 and 4° spectra at near the beam velocity. In Fig. 2 the 0° spectra are plotted in the rest frame of the projectile. The width of this peak is much narrower than that observed in previous fragmentation experiments where charged fragments were observed. Particles in this region are not due to a simple fragmentation process where energy is shared between the projectile and target with all degrees of freedom being equally probable giving rise to a gaussian momentum distribution but with a much larger width. Possible mechanisms for this narrow distribution are

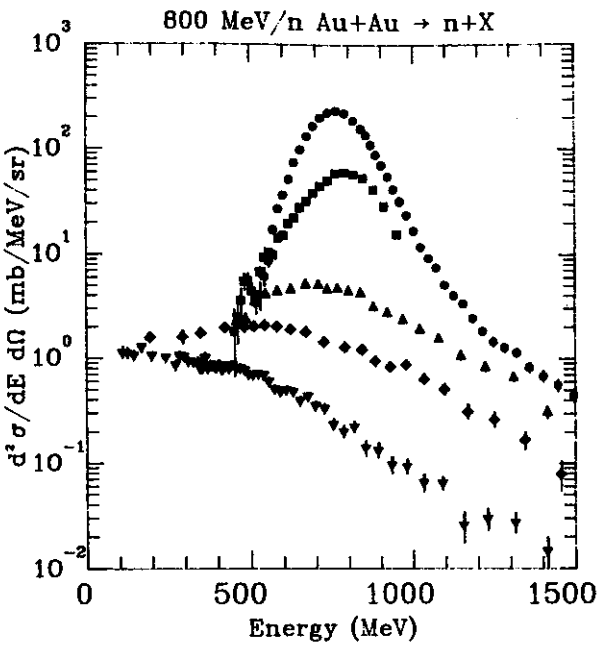

Fig. 1 Energy spectra of neutrons from 800 MeV/nucleon Au+Au at 0,4,8,15 and 30°.

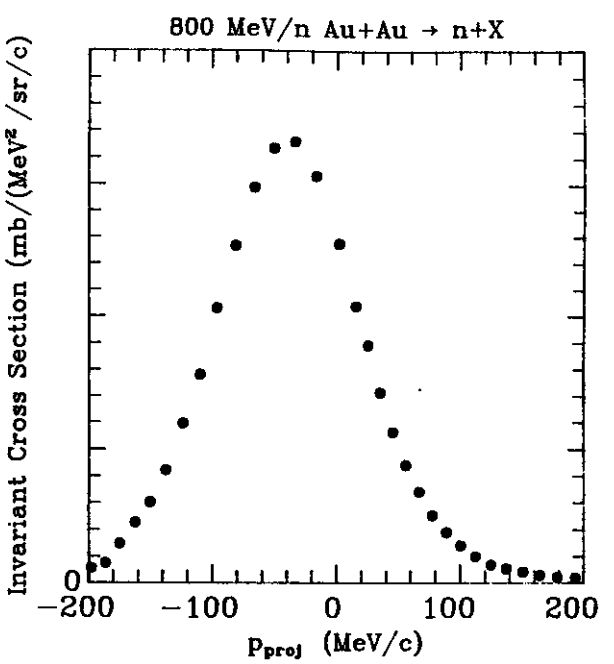

Fig. 2 Momentum spectra at zero degrees in the rest frame of the projectile.

inelastic scattering followed by decay in flight or single nucleon-nucleon direct scattering.

---

a. Kent State University, Kent, Ohio.

References

1. R. Madey, J. Varga, A.R. Baldwin, B.D. Anderson, R.A. Cecil, G. Fai, P.C. Tandy, J.W. Watson, and G.D. Westfall, Phys. Rev. Lett. 55, 1453 (1985).
2. R. Stock, H.H. Gutbrod, W.G. Meyer, A.M. Poskanzer, A. Sandoval, J. Gosset, C.H. King, C. Lukner, N. Van Sen, G.D. Westfall, and K.L. Wolf, Phys. Rev. Lett. 44, 1243 (1980).

EXCLUSIVE FRAGMENTATION STUDIES OF 40 MEV/NUCLEON ^{14}N

D. Horn[a], G.C. Ball[a], R. Bougault[a], D.A. Cebra, D. Fox, E. Hagberg[a], L. Potvin[b], C. Pruneau[c], R. Roy[c], C. St.-Pierre[c], and G.D. Westfall

Inclusive studies of projectile fragmentation[1-6] at beam energies near the Fermi velocity have shown that a transition takes place from low energies (E_{lab} < 10 MeV/nucleon) where narrow momentum distributions are observed to relativistic energies (E_{lab} > 1000 MeV/nucleon) where the momentum widths are significantly wider and become independent of incident energy.[1] These experiments can be extended by measuring most or all of the outgoing projectile fragments which can enable one to differentiate between processes that transfer particles to the target, processes involving inelastic excitation followed by decay in flight, and multiparticle breakup processes.

This experiment is designed to study the exclusive fragmentation of 40 MeV/nucleon ^{14}N incident on a Au target using a 32 element light ion array and two projectile fragment detector telescopes. Each element of the light ion array was composed of a CaF_2-plastic phoswich telescope capable of measuring the energy and particle identification of p,d,t,^{3}He, and ^{4}He fragments. The projectile fragment detectors consisted of two Si-detector telescopes placed at ±12.5°. Coincident light particle spectra were measured at angles ranging from 5 to 25° correlated with PLFs on the same side of the reaction plane and on the opposite side.

A schematic diagram of the experimental arrangement is shown in Fig. 1. The light ion array was mounted on one side of the beam with a PLF telescope mounted in the center of the array. A second PLF telescope was placed at the same polar angle on the opposite side of the scattering chamber.

Preliminary analysis has been carried out. As an example of the type of information one can extract from these measurements, the angular correlation of light particles in coincidence with C fragments, as a function of the angle of the light ion, are shown in Fig. 2. Note that the p-C correlations are peaked on the same side of the reaction plane as the PLF while the α-C correlations are peaked on the opposite side. The p-C system adds up to the original N beam particle which implies that the p-C correlations result from decay in flight while the α-C

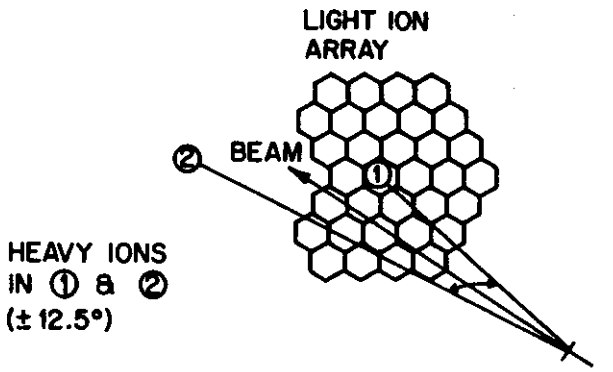

Fig. 1 Schematic diagram of experimental apparatus showing light ion array and two silicon detector telescopes.

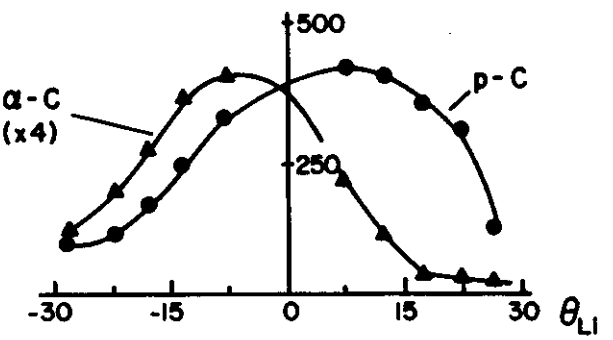

Fig. 2 In-plane correlations of protons and alpha particles with carbon fragments. Negative angles imply the opposite sides of the reaction plane.

correlations must result from more complicated phenomena.

---

a. AECL, Chalk River Nuclear Laboratories, Canada
b. McMaster University, Canada
c. Laval University, Canada

References

1. D.E. Greiner, P.J. Lindstrom, H.H. Heckman, B. Cork, and F.S. Bieser, Phys. Rev. Lett. 35, 152 (1975).
2. C.K. Gelbke, C. Olmer, M. Buenerd, D.L. Hendrie, J. Mahoney, M.C. Mermaz, and D.K. Scott, Phys. Rep. 42, 311 (1978).
3. Y.P. Viyogi, T.J.M. Symons, P. Doll, D.E. Greiner, H.H. Heckman, D.L. Hendrie, P.J. Lindstrom, J. Mahoney, D.K. Scott, H.J. Crawford, K. Van Bibber, G.D. Westfall, H. Wieman, C. MacParland, and C.K. Gelbke, Phys. Rev. Lett. 42, 33 (1979).
4. A. Menchaca-Rocha, M.E. Brandan, M. Buenerd, J. Chauvin, D. Lebrun, P. Martin, P. de Santignon, J.C. Gondrand, I. Dorion, and A. Lounis, Phys. Lett. 131B, 31 (1983).
5. R. Ost et. al., Phys. Rev. C 32, 1927(1985).
6. G. Bizard et. al., Proceedings of Bormio Conference, Jan. 1985.

STUDY OF STATE VARIABLES USING UNSTABLE RESONANCES

D. Fox, D.A. Cebra, J. van der Plicht, R.S. Tickle[a], C. Parks, and G.D. Westfall

The question of whether thermalization occurs in high energy nucleus-nucleus collisions is central to the understanding of the reaction mechanisms dominating these reactions. Evidence arguing for thermalization includes smooth, featureless energy spectra, an apparent common emitting source for all high energy particles, and good agreement between the predictions of statistical models that assume thermalization and production cross sections for light and complex fragments.[1-4] However recent results by Morrissey et. al. argue against thermalization in reactions of 35 MeV/nucleon N+Ag.[5,6] If thermalization had taken place in these reactions, light nuclei would be emitted in excited states and in the ground state with a statistical weight given by the spin of the state. For ^{7}Li the ratio of the cross section for observing the 0.478 MeV state divided by the ground state should be 0.33 for temperatures above a few MeV. The result of Morrissey et. al. gives a ratio of about 0.05 indicating that either a very low temperature is produced or that thermalization is not realized for these fragments. The idea of studying temperatures has been extended by Pochodzalla et. al.[7] using excited nuclei that decay by particle emission rather than by gamma emission for the systems of 35 MeV/nucleon N+Au and 60 MeV/nucleon Ar+Au. These results tend to demonstrate a higher temperature of about 5 MeV independent of the system being studied.

To help unravel these seemingly contradictory results we have measured the production of particle unstable light nuclei from 35 MeV/nucleon N+Ag which is the same system studied by Morrissey et. al.[5,6] These results will complement the existing set of data for ground state and low-lying excited state that decay by gamma emission with a complete set of production cross sections for light nuclei in highly excited states that decay by particle emission. To exclude projectile fragments we measured only angles backward of 45°. To obtain the production cross sections for fragments in excited states we measured a complete angular distributions rather than depending on the shape of the excitation spectra at one angle. State variables such as the temperature or the entropy of the emitting system will be extracted using a complete quantum statistical model developed by Hahn and Stöcker.[8] The production cross section for all observed nuclei, both ground state and excited state, will be compared globally to extract the state variables of the system.

The particle unstable nuclei were detected using an apparatus consisting of an array of sixteen fast/slow plastic scintillator telescopes placed behind a three-plane multi-wire proportional counter (MWPC). The

Fig. 1. Perspective view of the sixteen telescope array.

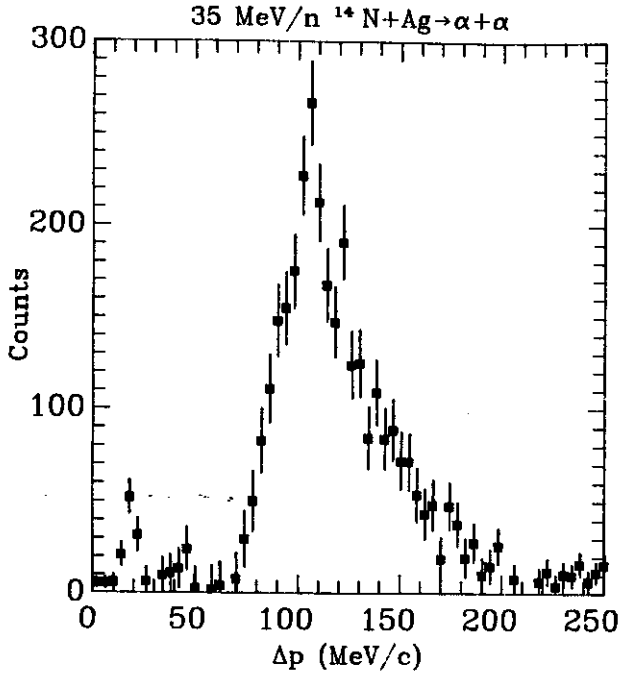

Fig. 2. Two particle correlation functions for α-α plotted as a function of the relative momentum, Δp. The uncorrelated background has been subtracted.

scintillator telescopes provided energy measurement and particle identification for p,d,t,^{3}He, and ^{4}He fragments. A perspective drawing of the array is shown in Fig. 1. By studying various combinations of these nuclei the production of particle unstable states of light nuclei up to ^{8}Be can be studied. The MWPC provided high resolution position measurements for the observed particles which allowed the precise measurement of the relative momenta of the particles that result from the decay of the original excited fragments. The MWPC was capable of dividing up each of the telescopes into 64 sub-areas. This position sensitivity increases greatly the efficiency of the detection system for small relative momenta which can be important for measuring low excitations.

Analysis of these results is still preliminary however in Fig. 2 two particle correlations for α-α is shown. The uncorrilated background has been subtracted. The ground state and firts ixcited state of ^{8}Be are clearly visible.

---

a. University of Michigan, Ann Arbor, Michigan.

References

1. B.V. Jacak, G.D. Westfall, C.K. Gelbke, L.H. Harwood, W.G. Lynch, D.K. Scott, H. Stöcker, M.B. Tsang, and T.J.M. Symons, Phys. Rev. Lett. 51, 1846 (1983).
2. H. Stöcker, G. Buchwald, G. Graebner, P. Subramanian, J.A. Maruhn, W. Greiner, B.V. Jacak, and G.D. Westfall, Nucl. Phys. A400, 63c (1983).
3. A. Mekjian, Phys. Rev. C17, 1051 (1978).
4. J. Gosset, J.I. Kapusta, and G.D. Westfall, Phys. Rev. C18, 844 (1978).
5. D.J. Morrissey, W. Benenson, E. Kashy, B. Sherrill, A.D. Panagiotou, R.A. Blue, R.M. Ronningen, J. van der Plicht, and H. Utsunomiya, Phys. Lett. 148B, (1984).
6. D.J. Morrissey, W. Benenson, E. Kashy, C. Bloch, M. Lowe, R.A. Blue, R.M. Ronningen, B. Sherrill, H. Utsunomiya, and I. Kelson, Phys. Rev. C32, 877 (1985).
7. J. Pochodzalla, W.A. Friedman, C.K. Gelbke, W.G. Lynch, M. Maier, D. Ardouin, H. Delagrange, H. Doubre, C. Grégoire, A. Kyanowski, W. Mittig, A. Péghaire, J. Peter, F. Saint-Laurent, Y.P. Viyogi, B. Zwieglinski, G. Bizard, F. Lefèbvres, B. Tamain, and J. Quèbert, Phys. Rev. Lett. 55, 177 (1985).
8. D. Hahn and H. Stöcker, private communication, 1986.

STUDY OF NON-EQUILIBRIUM LIGHT PARTICLE EMISSION IN 35 MEV/NUCLEON $^{16}O+^{58}NI$

P.L. Gonthier[a], Z.M. Koenig, D.A. Cebra, D. Fox, and G.D. Westfall

The study of pre-equilibrium (non-compound nucleus) light particle emission from low and intermediate energy nucleus-nucleus collisions can provide detailed information concerning the transition from low energy mean field phenomena to high energy nucleon-nucleon dominated interactions. Systematic studies of the O+Ni case have been carried out from 6 to 20 MeV/nucleon.[1-3] These studies were carried out by measuring α particles in coincidence with projectile-like fragments at forward angles. The conclusion from this work at lower energies is that preequilibrium light particles appear to originate either from the target and projectile nuclei themselves or from a hot spot on the target.

The present experiment was designed to study the evolution of the coincident alpha particle emission with increasing energy. The experiment was carried out using a beam of 35 MeV/nucleon ^{16}O from the NSCL K500 Superconducting Cyclotron. One might expect that the high energy phenomenum of an intermediate velocity source would manifest itself at these energies.

In Fig. 1 the evolution of the coincident alpha spectra from $^{16}O+Ni$ from 6 to 20 MeV/nucleon triggered by a projectile-like fragment near the grazing angle is shown as contours of Galilean invariant cross section. At the two lower energies one can clear see the target and projectile sources of the alpha particles. At 20 MeV/nucleon there appears to be a hot spot originating from the target nucleus.

In contrast, similar spectra for 35 MeV/nucleon O+Ni triggered by various projectile-like fragments are shown in Fig. 2. These spectra tend to favor the interpretation that the alpha emission is still largely due to hot spot formation rather than a fully developed intermediate source or fireball.

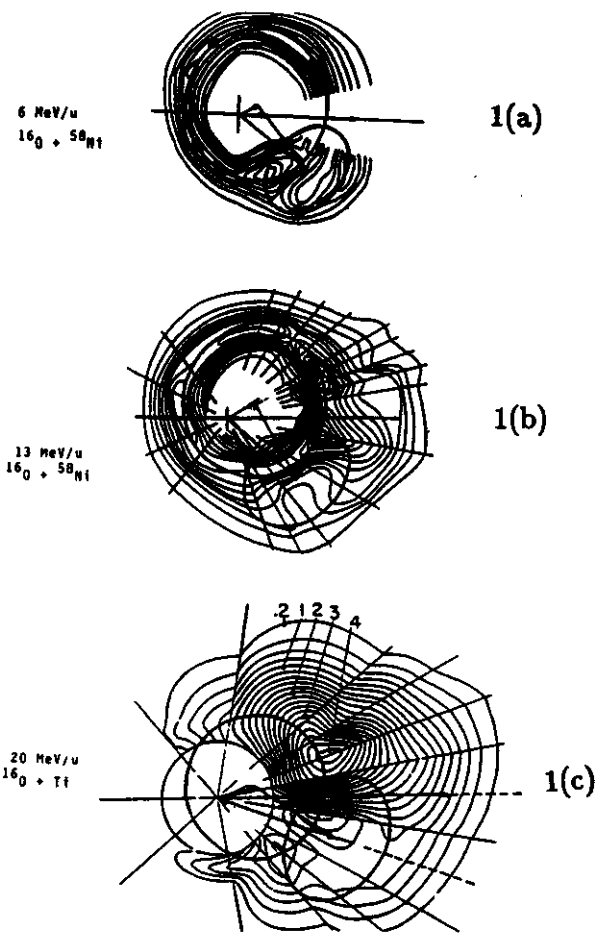

Fig. 1. Experimental velocity plots of α-particles in coincidence with projectile-like fragments. The lines are contours of Galilean invariant cross section. The ellipse and the circle are centered at the average velocity vectors of the projectile-like and target-like fragments.

a. Hope College, Holland, Michigan.

References

1. P. Gonthier et. al., Nucl. Phys. A 411, 289(1983).
2. M.N. Namboodiri et. al., Phys. Rev. C 28, 37c(1983).
3. H. Ho et. al., Phys. Rev. C 27, 584(1983).

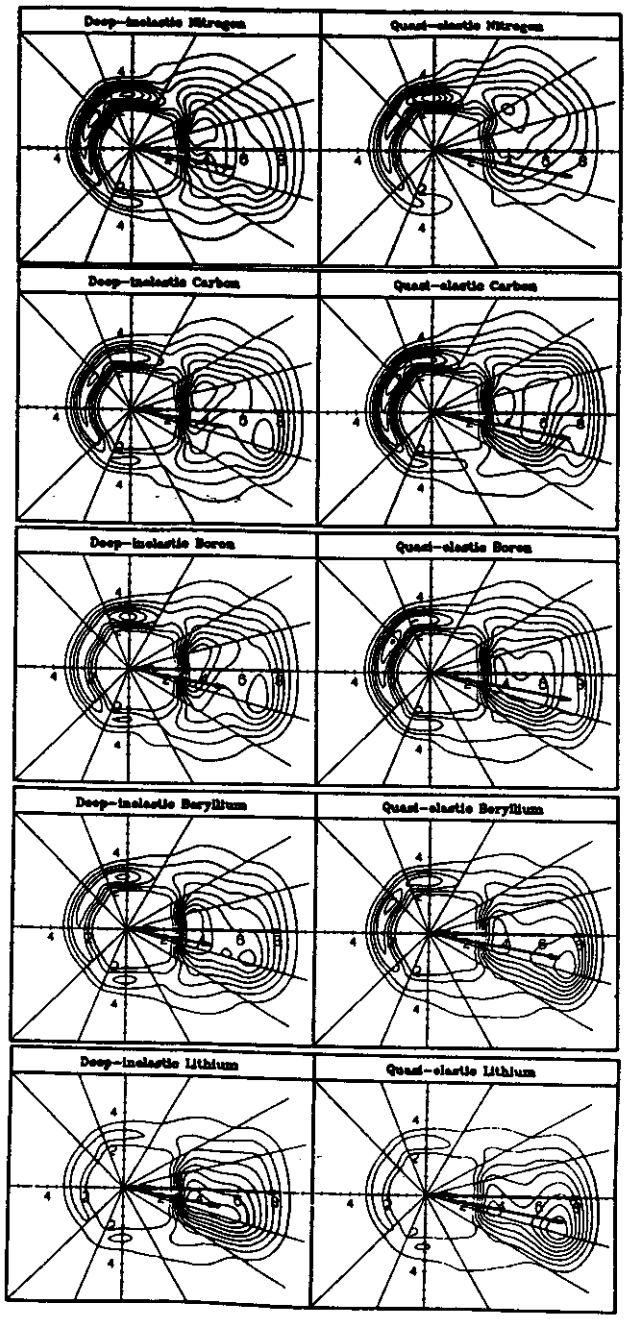

Fig. 2. Experimental velocity plots of α-particles in coincidence with the projectile-like fragments indicated. The lines are contours of Galilean invariant cross section.

FRAGMENTATION STUDIES AT FORWARD ANGLES

S.P. Angius, D. Cebra, G.M. Crawley, D. Fox, R. Ronningen, V. Rotberg, and G. Westfall

Much of the recent work on heavy-ion reactions at energies above 20 MeV/nucleon has focussed on the emission of light particles or has selected high multiplicity events which are thought to arise from central collisions. For more peripheral collisions, on the other hand, the transfer of one or more nucleons from the projectile to the target, and projectile fragmentation have been suggested as possible reaction mechanisms. These processes can in principle be distinguished by their different angular distributions. It is therefore important to be able to measure angular distributions for different fragments down to very forward angles, and to make an accurate identification (Z and M) of the particles observed.

With these motivations, we performed the first of a series of measurements at the S320 spectrograph, using a 35 MeV/nucleon ^{16}O beam on a ^{58}Ni target. Projectile-like fragments were measured at different energy settings, between 2 and 12 degrees. Isotopes of masses between 6 and 19 were separated, and the analysis of the data is in its final stages. Preliminary angular distributions for three different fragments are shown in Fig. 1 for different momentum slices of the spectra (Bρ values). The angles in the plots are measured in the laboratory frame of reference. In general the cross sections appear to decrease smoothly with increasing scattering angle, and the heavier the fragment the steeper is the decrease. However, near the beam rigidity and slightly above the character of the angular distributions changes and the curves show a peak between 3+ and 6+.

For a systematic study of the fragmentation process in this energy range, more measurements are necessary. In the future, we plan to repeat this type of measurement using ^{16}O and ^{18}O beams at energies between 25 and 35 MeV/nucleon, to study the dependence of the reaction mechanisms under investigation on energy and on the Z/N ratio of the projectile.

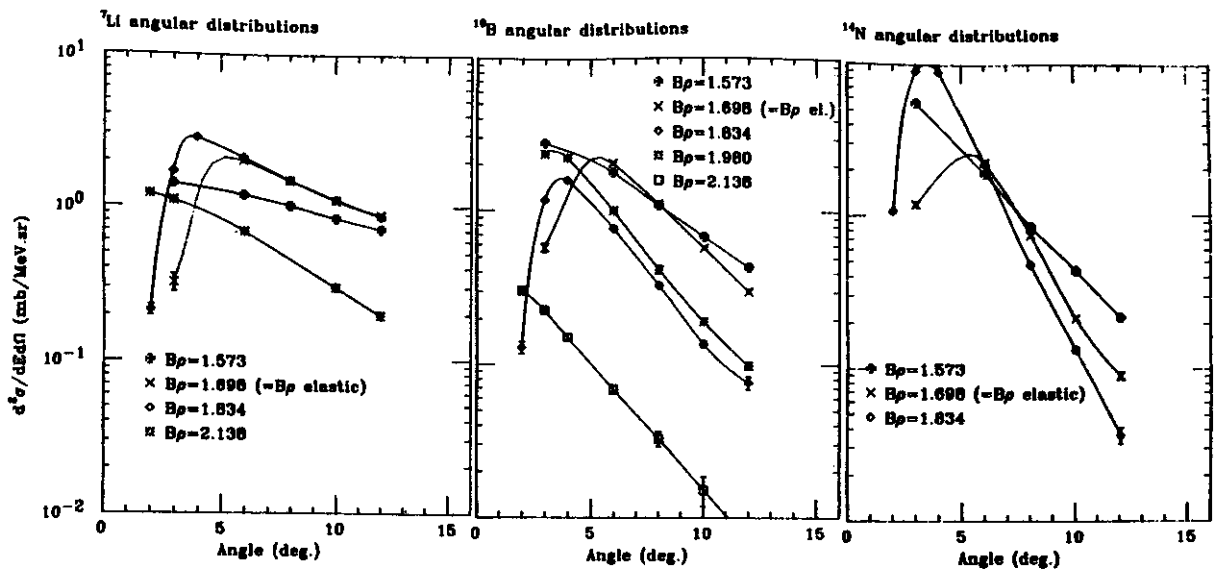

Fig. 1 Preliminary angular distributions for $^{16}O+^{58}Ni$ at 35 MeV/nucl. Data for ^{7}Li, ^{10}B, and ^{14}N are shown, for different rigidities. The lines are drawn through the points to guide the eye.

SOURCE SHAPE PROBING BY BEAM-VELOCITY PIONS

Wm. C. McHarris
in collaboration with the Rasmussen/Crowe Group, Lawrence Berkeley Laboratory

Among the collaborative efforts with the Rasmussen/Crowe Group at Lawrence Berkeley are π^+ and π^- experiments, plus a proposed search for the possible existence of negatively-charged "free pineuts," pions hadronically bound to neutrons. These experiments are based at the LBL Bevalac and are in general more appropriate for LBL reports. However, during the past yearwe have done a considerable amount of calculations on using beam-velocity π^+ as probes for studying transient nuclear shapes, resulting in a paper[1] to be submitted later this year. The following is a summary of this work.

We shall use the Bevalac Beam-30 JANUS spectrometer to measure simultaneously $1\pi^+$ and $2\pi^+$ spectra near beam velocity for ^{139}La on La and on C targets. Our aim is to probe simultaneously the asphericity of the charge distribution by the $1\pi^+$ spectrum and the asphericity of the pion source distribution by the $2\pi^+$ Hanbury-Brown-Twiss correlation. The symmetric and extremely asymmetric bea,-plus-target systems allow the large Coulomb-field corrections to be handled. The possibility of fleeting toroidal or bubble nuclear systems can be probed on a very short time scale by the shape of the π^+ depression near beam velocity.

C.-Y. Wong, in a recent theoretical paper,[2] has revived interest in toroidal and bubble-shaped nuclei by pointing out the altered -- and more favorable -- stability conditions that could exist in heated heavy nuclei. The surface tension of any liquid drop, including nuclei, decreases toward zero as the temperature is raised to the boiling point. Further, the geometrical notions embodied in the abrasion-ablation model suggest that relativistic head-on collisions of a light with a heavy nucleus might punch through to produce a toroid. (Cascade calculations, of course, show much fuzzier complex reaction zones.)

Whether such shapes can survive the evaporation, cooling-down stage is highly unlikely. Nevertheless, the charged pion spectra near beam velocity may give a measure of the shape on a very-short time scale.

There have been a number of theoretical treatments of the Coulomb effects only heavy-ion produced pion spectra, but they have been based generally on two or more charge distributions (spectators and sometimes also at different points in velocity space). Zajc,[3] when working with our group, concluded that the two-pion correlation was not seriously affected by the Coulomb fields of the nuclear pieces, provided the pion spectra were taken in a relatively small solid angle near 90° in the center-of-mass frame of a symmetric target-projectile system. The Coulomb shifts for each of the two pions may be considerable, but the velocity differences as the pions leave the nuclear surface map without much change into the velocity differences in the asymptotic final state. For data gathered over large solid angles, as in streamer-chamber work, and especially for pion momenta taken near 0°, the Coulomb changes in mapping pion momentum differences from initial to final states may be large, notwithstanding the symmetry of the system. Further, the corrections will depend on impact parameter, essentially an unmeasurable quantity.

Thus, we believe that the large Coulomb corrections to the two-pion correlation function can be handled best for heavy nuclei by studying very mass-asymmetric collision systems. Here the Coulomb corrections will be dominated by a single charge center, nearly independent of impact parameter. The ^{139}La + C seems ideally

suited for our first studies, both for the above reasons and because its single-pion spectra have already been studied by the Hashimoto collaboration[4] with the HISS spectrometer, albeit at 800 A·MeV, which is lower than the maximum energy (for La^{48+}) of 1430 A·MeV at which we propose to run. We plan to set the trigger to accept all two-pion events and as large a fraction of one-pion events as the VAX-11/750 Q-system data acquisition allows.

There are a number of open questions concerning Coulomb corrections to two-pion correlation studies. First of all, there are two separate Coulomb effects to be considered. One is the mutual repulsion of the two like-charged pions. This is referred to as the Gamow correction and is easily handled. The second is the interaction of the bulk charge distribution of the colliding heavy-ion system with the pions. The momentum difference of the two pions, as measured in the laboratory, needs to be mapped back into the momentum difference the pions had when leaving the strong-interaction region. Gyulassy was an early advocate of two-pion correlation studies to probe possible coherence of a pion-condensation phase, but he later warned that this second Coulomb correction would be so difficult to handle that any fundamental deductions from the data would be difficult to make.[5] It was in considering this problem that Zajc came to his conclusions that, for the special case of symmetric collision systems and data gathered near 90° in the center-of-mass system, the Coulomb distortions would not be so severe.

Some of us have worried that pion data near beam velocity would have serious Coulomb distortions due to projectile spectator charge. The corrections would depend on impact parameter and thus would be hard to make. The strong beam-velocity π^- peak studied by Sullivan and co-workers[6] in the Rasmussen/Crowe Group via inclusive heavy-ion reactions should confirm this concern. The large-solid-angle streamer-chamber experiments have not been corrected for Coulomb distortions, and members of that group[4] have expressed belief that the beam-velocity π^- peak was over such a small solid angle that the two-pion correlation would not be affected. Humanic[7] introduced velocity shifts on Fe + Fe data near 0° and concluded that the effects were small. Several graduate students have recently redone his analysis, however, and have reopened the question. Nevertheless, we believe that two-pion data taken over a small solid angle lend themselves to relatively straightforward estimates of the Coulomb effects. We are presently working on the calculations for this problem.

We also plan to study the symmetric system, ^{139}La + La. This is a continuation of our studies of the mass dependence of the pion source parameters. The ^{139}La + La system has also been studied by the Hashimoto collaboration[4] at HISS. Our π^+ experiments are needed to complete and complement these others.

The JANUS dipole-dipole spectrometer, coupled to a VAX-11/750 Q-data-acquisition system, will be used to carry out the measurements. This spectrometer provides excellent spatial and momentum resolution (error in target trace-back ≈1 cm, $\Delta P/P < 2\%$) for pions having momenta greater than 150MeV/C; measurements centered at a laboratory pion angle near 0° have $\Delta\Omega \approx 1$ msr. Based on previous experiments, we expect that 120 hours of 3×10^6 particles per pulse of ^{139}La with 1 gm/c^2 targets would allow the acquisition of roughly 50,000 events for each of the two targets proposed. This would allow for a reasonable determination of the pion source parameters for these systems.

References

1. J. O. Rasmussen, Wm. C. McHarris, and C.-Y. Wong, "Nuclear Shape Effects on Heavy-Ion π^+ Spectra near Beam Velocity," to be submitted to Phys. Rev. C.
2. C.-Y. Wong, ORNL, preprint (1985).
3. W. A. Zajc, Ph.D. Thesis, LBL-14864 (1982); W. A. Zajc et al., Phys. Rev. C 29, 2173 (1984).
3. Y. Miake et al., LBL Nuclear Science Division Annual Report, 1983-1984, LBL-18635, p. 101 (1985).
5. M. Gylassy and S. K. Kauffman, Nucl. Phys. A362, 503 (1981).
6. J. P. Sullivan, Ph.D. Thesis, LBL-12546 (1981); J. P. Sulivan et al., Phys. Rev. C 25, 1499 (1982).
7. T. J.Humanic, LBL-19420 (1985).

HIGH ENERGY GAMMA RAY EMISSION IN HEAVY ION COLLISIONS

J. Stevenson, K.B. Beard, W. Benenson, J. Clayton, E. Kashy, A. Lampis,
D.J. Morrissey, M. Samuel, R.J. Smith, A. Tam, J.S. Winfield

We present here the results from the first systematic study of high energy gamma ray emission in intermediate energy heavy ion collisions. Gamma ray energies and angular distributions have been measured for high energy gamma rays (10-120 MeV) from collisions of ^{14}N on Pb, Zn, and C at beam energies of E/A=20, 30, and 40 MeV.

Recent evidence for a surprisingly large yield of high energy gamma rays from intermediate energy heavy ion collisions[1-2] have led to a number of possible explanations. One such model for the process is coherent bremsstrahlung[3-7] in which projectile deceleration in the early stages of the collision generates high energy gamma rays. Such gammas would have a quadrupole angular distribution due to the absence of net current in the center of mass for symmetric nuclear systems, and the characteristic 1/E energy spectrum. Coherent nucleus-nucleus bremsstrahlung should become dominant for heavier systems due to the Z^2 dependence of its gamma ray yield. An alternative approach was to suggest the gamma rays arise from thermal or statistical emission from a hot recoiling nuclear fireball. Here the angular distributions should be near isotropic and the energy spectra exponential.

This latter model seems an unlikely candidate since the system is transparent to gamma rays and the fireball lifetime is likely to be 10^5 times shorter than that needed for gamma ray emission. Detailed gamma ray measurements over a full range of angles, targets and beam energies are needed to distinguish the process responsible for them.

Gamma ray measurements were made with two gamma ray telescopes, each consisting of an active CsI scintillator converter followed by an 8 element Cerenkov detector range stack. Each detector component was viewed by photomultiplier tubes at each end. Gamma ray energies were determined from the electron-positron ranges in the detector. While the Cerenkov detectors are insensitive to most heavy ion collision products, they need to be shielded from the cosmic ray muon background by anticoincidence shields around the detector (reducing the background from .5/sec to 15/hour).

Figure 1 shows the angular distribution of high energy gamma rays for E/A=40 MeV ^{14}N on lead and carbon targets. The angular distributions are shown for gamma ray energy cuts at E=20,40,60, and 80 MeV. As can be seen the angular distributions are slightly forward peaked : $\sigma(30°)/\sigma(150°)$ is around 2.4 for Pb and 3.0 for C targets. These angular distributions are consistent with isotropic emission from a

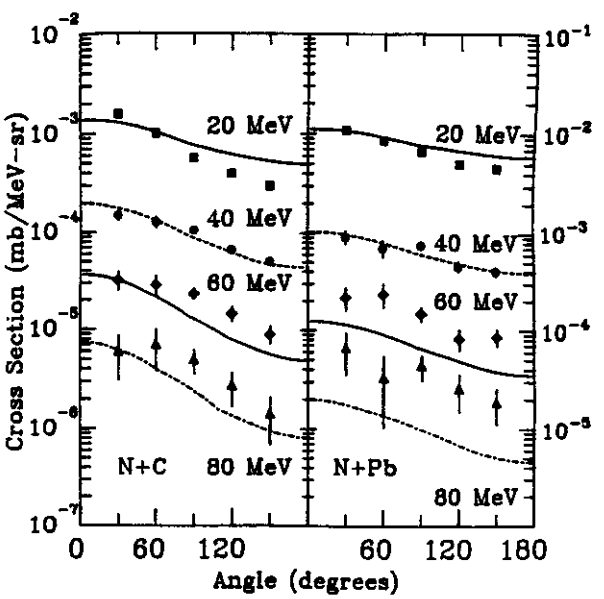

Fig. 1 Angular distribution of high energy gamma rays for E/A=40 MeV ^{14}N+C and Pb.

recoiling source with velocity β_{exp} shown in table 1.

The calculated values are generally intermediate between the nucleus-nucleus center of mass and the nucleon-nucleon center of mass velocities. The calculated curves are based on the nucleon-nucleon bremsstrahlung model described below.

Table 1. Parameters from the best fit to the high energy gamma ray data. Spectra for each target and beam energy were fitted assuming isotropic emission from a recoiling source with velocity β_{Exp} with a gamma ray energy spectrum of the form be $^{-E/\tau}$. For comparison, β^{cm}_{NN} and $\beta^{cm}_{Nuc-Nuc}$ are the nucleon-nucleon and nucleus-nucleus center-of-mass velocities for the projectile-target system.

Target	E/A(MeV)	τ(MeV)	β_{Exp}	β_{NN}	$\beta_{Nuc-Nuc}$
Pb	20.	10.0	0.08	0.104	0.013
Pb	30.	12.0	0.11	0.127	0.016
Pb	40.	14.2	0.10	0.145	0.019
Zn	20.	8.3	0.05	0.104	0.037
Zn	30.	11.8	0.11	0.127	0.045
Zn	40.	13.7	0.10	0.145	0.052
C	20.	7.7	0.08	0.104	0.111
C	30.	11.1	0.10	0.127	0.135
C	40.	13.3	0.12	0.145	0.156

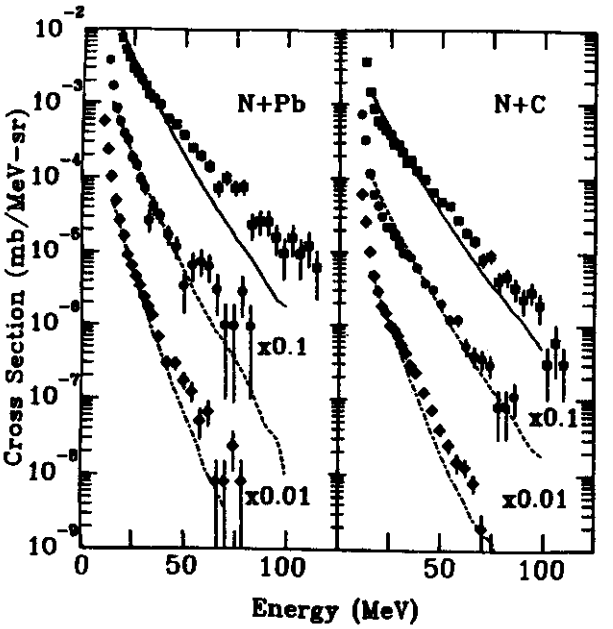

Fig. 2 Gamma ray energy spectra for E/A=40 MeV(square), 30 MeV(circle), and 20 MeV(diamond) ^{14}N+Pb, and C.

Figure 2 shows gamma ray energy spectra at 90 degrees for ^{14}N+Zn at E/A=40, 30, and 20 MeV. The steeply falling low energy parts have a near constant inverse slope ($Ae^{-E/\tau}$) of 2 MeV possibly due to excitation of the giant dipole resonance. More interestingly, the high energy part, above about 30 MeV, is well described as an exponential $Be^{-E/\tau}$. Table 1 gives the best fit values of the inverse slopes. For lead, for example, the high energy part has inverse slopes of 14.2, 12.0, and 10.0 MeV at beam energies of E/A=40,30 and 20 MeV respectively. These slopes appear similar to charged particle energy spectra for similar reactions. The gamma ray spectra show a surprisingly weak beam energy dependence.

The curves in Figures 1 and 2 are based on a model in which gamma rays are bremsstrahlung from collisions of fast neutrons and protons from a thermal source. The yields are calculated in the framework of the nuclear fireball model. For a given fireball size and temperature the bremsstrahlung yield may be calculated per nucleon-nucleon collision in the

isotropic gas. Emission from such a hot isotropic gas predicts an essentially exponential gamma ray energy spectrum with a temperature close to that of the gas.

Similar calculations have been performed by Nifenecker[8] to explain the gamma ray data of Grosse[2].

Our data, for all beam energies and targets, are slightly forward peaked and have exponentially falling energy spectra. The data may be parameterized as isotropic emission from a recoiling source. The data is well reproduced in terms of incoherent nucleon-nucleon bremsstrahlung from this thermal source.

References

1. K. B. Beard, W. Benenson, C. Bloch, E. Kashy, J. Stevenson, D. J. Morrissey, J. Van der Plicht, B. Sherrill, J. S. Winfield, Phys. Rev. C32, 1111 (1985).
2. E. Grosse, International Workshop on Gross Properties of Nulei, Hirschegg, 1985.
3. J. I. Kapusta, Phys. Rev. C15, 1580 (1977).
4. D. Vasak, W. Greiner, B. Müller, Th. Stahl, and M. Uhlig, Nucl. Phys. A428, 291 (1984).
5. Che Ming Ko, G. Bertsch, and j. Aichelin, Phys. Rev. C31, 2324 (1985).
6. W. Bauer, W. Cassing, U. Mosel, M Tohyama, unpublished.
7. U. Mosel, 24th International Winter Meeting on Nuclear Physics, Bormio,Italy (1986).
8. H. Nifenecker, 24th International Winter Meeting on Nuclear Physics, Bormio, Italy (1986).

NEUTRON EMISSION FROM DISCRETE STATES IN HEAVY-ION COLLISIONS

A. Galonsky, G. Caskey,[a] F. Deak,[b] A. Kiss,[b] B.A. Remington,[a] Z. Seres,[c]

A common way of parameterizing particle spectra is to assume thermal evaporation from hot, moving sources and then determine the temperatures and velocities of the sources. However, when a light fragment of the collision particle-decays from a discrete unbound state, we have a moving source of particles of one specific energy. For example, a ^{13}C fragment ejected from the nuclear collision in its excited state at 6.87 MeV decays by emitting a neutron of 1.918 MeV with respect to the ^{13}C fragment. With respect to the laboratory, the neutron energy is determined by vector addition of the two velocities, and the extreme values of neutron energy can by quite far apart, for example, 3.2 and 20.7 MeV if the ^{13}C fragments have 10 MeV per nucleon.

In order to study the role of discrete, particle-unbound states, we measured neutron spectra in coincidence with light fragments resulting from collisions of ^{14}N projectiles at 35 MeV per nucleon with a ^{165}Ho target. The fragments were detected by ΔE-E silicon telescopes, one at an angle of +10° and another at -30° relative to the beam axis. One of the neutron detectors was positioned at +10° and another one at -30° in colinear geometry with the corresponding ΔE-E telescopes.

Figure 1 shows neutron energy spectra in coincidence with boron fragments of 7-14, 14-21, 21-28, and 28-35 MeV per nucleon at 10° and 14-21 MeV per nucleon at 30°. In each spectrum one can see a dominant enhancement at neutron energies equal to the average energy-per-nucleon of the coincident fragment; the yield of the enhancement is about one-half of the total. The inserts in Fig. 1 display the corresponding boron energy distributions at 10° and 30° in coincidence with the neutrons. That the fragment

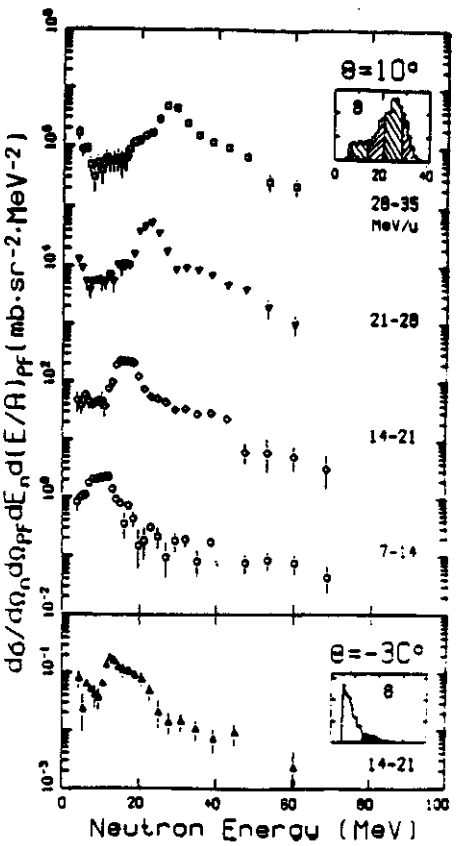

Fig. 1 Neutron energy spectra in coincidence with boron isotopes having energy per nucleon 7-14, 14-21, 21-28 and 28-35 MeV for +10° (upper part) and 14-21 MeV for -30° (lower part). The inserts show the corresponding boron energy distributions.

distributions are clearly very different for the two cases, suggests different reaction mechanisms for 10° and 30°. Nevertheless, the enhancements dominate the neutron energy spectra at both angles. Similar structures, but with different widths and strengths, can be seen in neutron energy spectra coincident with reaction fragments of other light elements such as Li, Be, and C.

These enhancements, always correlated with

the velocity of the fragment, suggest that the neutron spectra should be plotted as a function of the relative velocity between neutron and fragment. Such relative velocity spectra are shown in Fig. 2 for both fragments and neutrons detected at 10°. The parent nuclei are ^{8}Li, ^{12}B, and ^{13}C. In each coincident event the velocity of the fragment was calculated from its measured kinetic energy after establishing its isotopic identity, and the velocity of the neutron was derived from its flight time.

Each relative velocity spectrum is dominated by structure caused by the decay of a particle-unstable nucleus. This structure is also observed at 30°. We have uniquely identified the discrete transitions responsible for the major peaks. The relevant parameters of those transitions are listed in Table I. For ^{11}B, where the decay energies are only 19 keV, there is a single peak centered at zero relative velocity--a simple case of kinematic focusing. But for ^{7}Li, where the decay energy is 222 keV, there is a pair of peaks centered about zero relative velocity. In this case the neutron detector solid angle is not big enough to capture all of the neutrons emitted from a fragment headed towards the detector. Instead, we get a forward peak ($v_f - v_n < 0$) and a backward peak.

The same is true for ^{12}C, but there are four prominent peaks corresponding to two transitions. The peaks at ±20 mm/ns in Fig. 2 arise from decay of the first unbound state of ^{13}C augmented by decays from a triplet of states

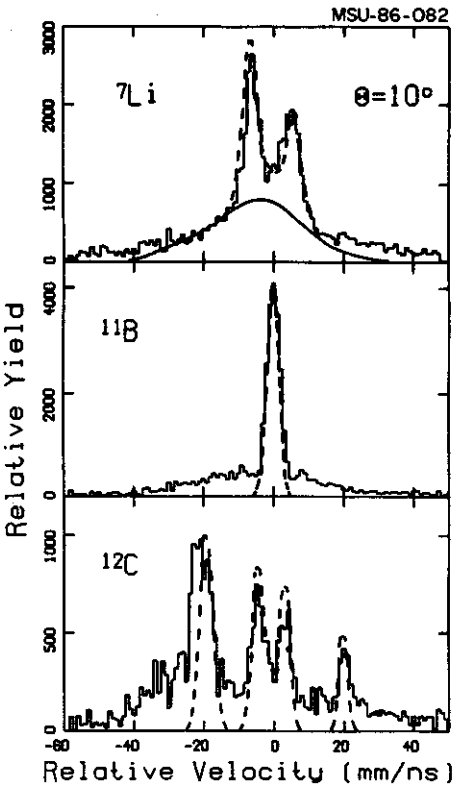

Fig. 2. Coincident fragment-neutron relative velocity spectra for ^{7}Li, ^{11}B and ^{12}C at +10°. The abcissa is fragment velocity minus neutron velocity. Dashed lines are results of Monte Carlo simulations of discrete neutron decays. For ^{7}Li there is also a simulation (solid line) of thermal emission of neutrons.

0.7 MeV higher. Here, the neutron energy is so high that we cannot resolve the individual states, and there is a sizeable difference in the solid angles for accepting forward and backward neutrons. The peaks at ±5 mm/ns correspond to decay from a more highly excited state, at 9.50 MeV, but to the 4.44-MeV state of

Table I. Parameters of the levels in the neutron decays associated with the peaks in Fig. 2.

Detected Fragment	Parent State Nuclide	E_x(MeV)	Γ(keV)	Daughter E_x(MeV)	Decay E decay (MeV)	Rel.Vel. (mm/ns)
^{7}Li	^{8}Li	2.255	33	0	0.222	7.0
^{11}B	^{12}B	3.389	3.1	0	0.019	1.9
^{12}C	^{13}C	6.864	6	0	1.918	20
^{12}C	^{13}C	9.500	5	4.439	0.114	5.0

^{12}C rather than to the ground state. The solid angle for detecting the 4.44-MeV branch is much greater than for detecting the ground-state branch.

The actual shape of a line (or pair of lines) depends on many parameters of the experiment, such as the 3-dimensional finite geometry of the fragment and neutron detectors, the angular and energy distributions of the fragments, the experimental time resolutions of the fragment and neutron detectors, the recoil of the fragment from the decay of the parent, the pulse-height thresholds of the detectors, the energy dependence of the neutron detection efficiency, and the width and decay energy of the parent state. Estimating where necessary, we put these quantities into a Monte Carlo code for each of the transitions in Fig. 2. Normalizing each transition to the data, we obtained the results given by the dashed lines in the figure. The simulations do reproduce the most important features of the experimental spectra. For the lines at ±20 mm/ns in the ^{12}C spectrum the computation included only the first unbound state; the triplet above it accounts for the broadening of these lines.

Since discrete lines do not account for the entire spectrum in any case, we used the Monte Carlo code for ^{7}Li at 10° to determine whether a thermal spectrum could account for the continuum under the lines. The solid line in the top part of Fig. 2 is the result for an assumed source temperature of 2.5 MeV. The distribution of source velocities was that obtained from the measured spectrum of ^{7}Li fragments. The thermal contribution is about equal to that of the single discrete line. For the other isotopes in Fig. 2 the thermal part is relatively smaller. At 30°, where central collisions dominate, discrete emission is equally important. This means that even in inclusive measurements not all of a spectrum has a thermal origin, and thermal parameters derived neglecting this fact are somewhat in error. The same is true of proton spectra.

Where more than one discrete state can be discerned in a relative velocity spectrum, it is interesting to determine the relative populations of the states. If these excited nuclei are boiled out of hot nuclear matter in thermal equilibrium, their populations are determined only by a Boltzmann factor that depends on the spins of the states and the temperature of the hot nuclear matter. Conversely, a measurement of the relative populations of two states of known spins determines the temperature. This idea has been used by Morrissey, et al.,[11] to analyze the gamma decays of excited ^{7}Li, ^{8}Li and ^{7}Be nuclei. Unexpectedly, the temperature determined from the relative populations of particle-stable excited states was much lower (≈ 0.5 MeV) than the temperature determined by the slopes of the fragment energy spectra.

From the data in Fig. 2 it is obvious that we can determine a temperature with respect to excited ^{13}C nuclei. The preliminary result is around 1.0 to 1.5 MeV. It should be remembered that these data are for fragments and neutrons emitted at 10°, an angle close to the grazing angle. The assumption of thermal equilibrium may not be valid at this angle. At 30°, where central collisions may dominate, we are analyzing data which are colinear, but of very low statistical accuracy.

---

a. LeCroy Corp.
b. Eötvös University, Budapest
c. Rose-Hulman Institute of Technology
d. Central Research Institute, Budapest

References:

1. D.J. Morrissey, W. Benenson, E. Kashy, C. Bloch, M. Lowe, R.A. Blue, R.M. Ronningen, B. Sherrill, H. Utsunomiya and I. Kelson, Phys. Rev. C 32,877(1985).

REACTION MECHANISMS OF HEAVY-ION COLLISIONS STUDIED VIA NEUTRON EMISSION

A. Galonsky, G. Caskey[a], F. Deak[b], C.K. Gelbke[e], J. Kasagi[c], A. Kiss[b], J.J. Kolata[d], B.A. Remington[e], Z. Seres[f], and M.B. Tsang,

From neutron spectra measured in coincidence with light fragments, we can obtain information concerning the dynamic as well as the statistical aspects of heavy ion reactions. We have measured neutron spectra in coincidence with light fragments from the reactions of ^{14}N with Ho, Ni, and C at E/A = 35 MeV.

When a neutron was in coincidence with a fragment, the neutron energy was determined from the time difference between the two particles plus the time of flight of the fragment.

Fragments were detected at six angles between 7° and 30°. The energy spectra of boron fragments from the reaction of ^{14}N with Ho are shown in Fig. 1. The character of the spectrum changes drastically from 7° and 10°, where a quasi-elastic peak dominates, to 30°, where there is only an exponential decrease. The spectra of other fragments--lithium, berylium, and carbon--have features similar to those of the boron spectra.

From a peripheral collision we might expect to see neutrons from a surface hot spot whose decay might then create a left-right asymmetry of the emitted neutrons. Figure 2 shows a neutron velocity scatter plot for coincident high energy boron fragments detected at 10°. The arrow in the figure indicates the average velocity vector of the boron fragments. There are more high velocity neutrons at middle angles (70° and 110°) on the side of the beam opposite that of the detected boron,[1] than on the same side. Since the boron fragments are close to the grazing angle, presumably undergoing positive-angle scattering, neutrons from a stationary surface hot spot would be shielded by the target and would produce the reverse asymmetry. What is required is a dynamic effect

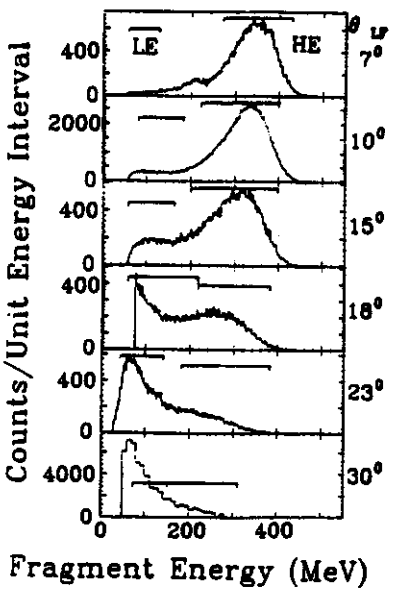

Fig. 1 Spectra of boron fragments from the Ho target at angles of 7° to 30°. The low-energy (LE) and high-energy (HE) gates used to produce coincident neutron spectra are indicated.

wherein the source acquires transverse momentum, perhaps balancing some of the transverse momentum of the boron fragment.

Other aspects of the data may be seen in the neutron multiplicity spectra of Fig. 3 where the neutrons are in coincidence with lithium fragments of energies 14 to 28 MeV/u at 10°. The two topmost spectra are for ±10°; the lower ones are for successively larger angles. We focus on three features of the data. 1) At the lowest energies the cross section decreases at about the same rate for all angles; even the absolute values are constant to within a factor of two. 2) The high energy neutrons are very forward peaked. 3) The spectra at ±10° are approximately equal below 15 MeV and above 50 MeV, but between 15 and 50 MeV the +10° spectrum is much higher than the -10° spectrum. Spectra

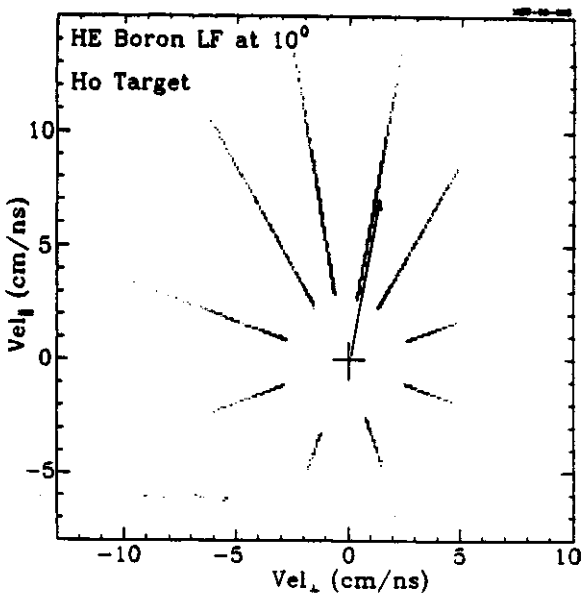

Fig. 2 Velocity scatter plot for neutrons detected at ±10°, ±30°, ±70°, ±110°, and ±160°. The neutrons are in coincidence with quasi-elastic boron fragments at +10°, that is, at 10° to the right.

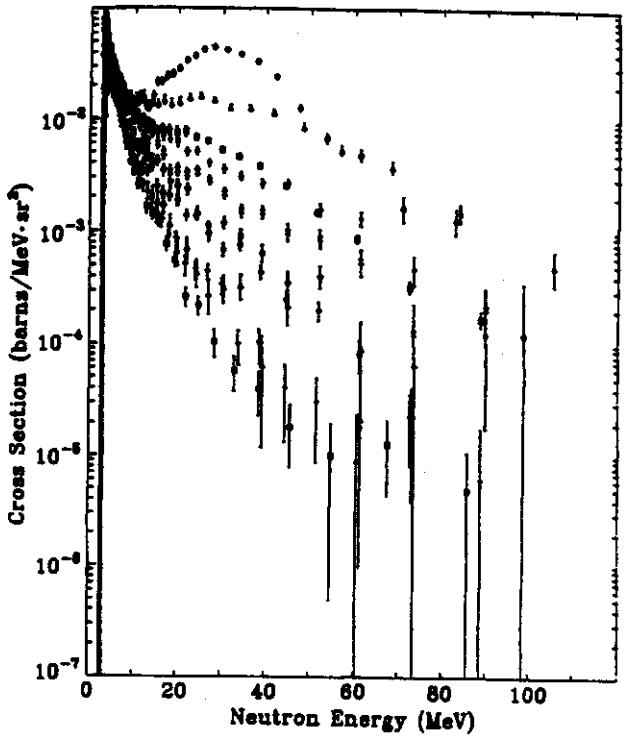

Fig. 3 Neutron energy spectra at angles ranging from 10° (+10° topmost) to 110°. The neutrons are gated by lithium fragments at +10° having E/A = 14-28 MeV.

gated by other fragments (Be, B, or C) at 10°, whether of high energy or low energy, exhibit similar features. Enhancement of the neutron cross section at +10° arises from kinematic focusing of the neutrons emitted in sequential decay of the excited parent fragments, as discussed elsewhere in this report.

We have fitted the neutron spectra with two moving, thermal sources--a slowly-moving, target-like source (TLS) and an intermediate-rapidity source (IRS). Those spectra containing significant contributions from fragment sequential decay were not included in the fits. In general, the two-source model fits all the data except the contribution from excited fragments.

In the fitting procedure each source has four parameters to be determined--a strength, a temperature, a direction, and a speed. The TLS is responsible for the almost-isotropic, low-energy neutrons. The temperature is found to be independent of the angle and of the species of the coincident fragment and depends only slightly on the loss of kinetic energy and on the identity of the target nucleus. The temperature is 2-3 MeV when the target is Ho and about 3-4 MeV when the target is Ni.

Assuming a given mass for the source, the strength, or multiplicity, of a thermal source depends only on its temperature. We would therefore expect there to be no dependence of multiplicity upon fragment angle. When we look at the multiplicities, however, (Fig. 4) we see that they increase with angle. The reason is that we measure an "associated" multiplicity, a multiplicity per detected fragment. The true multiplicity of the source is higher. Particularly at small angles there are processes, such as projectile fragmentation, that produce a fragment without a neutron-emitting TLS partner. Will the curves level off at some fragment angle and give us the true multiplicity? Only future experiments will tell. In the meantime we have resorted to

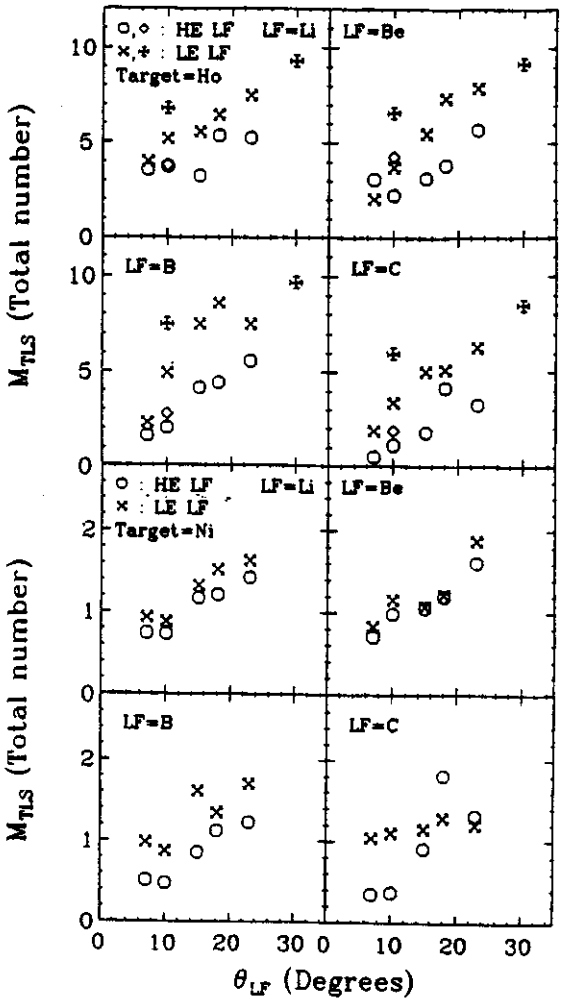

Fig. 4 Plot of M_{TLS}, total associated multiplicity, versus fragment angle for the Ho target (top four) and Ni target (bottom four). Each quadrant represents a different fragment. The diamond and cross plotting symbols correspond to an independent set of data and analysis. Open symbols correspond to high-energy (HE) fragments and closed symbols to low-energy (LE) fragments. (Note the differences in scale between the Ho and the Ni values.)

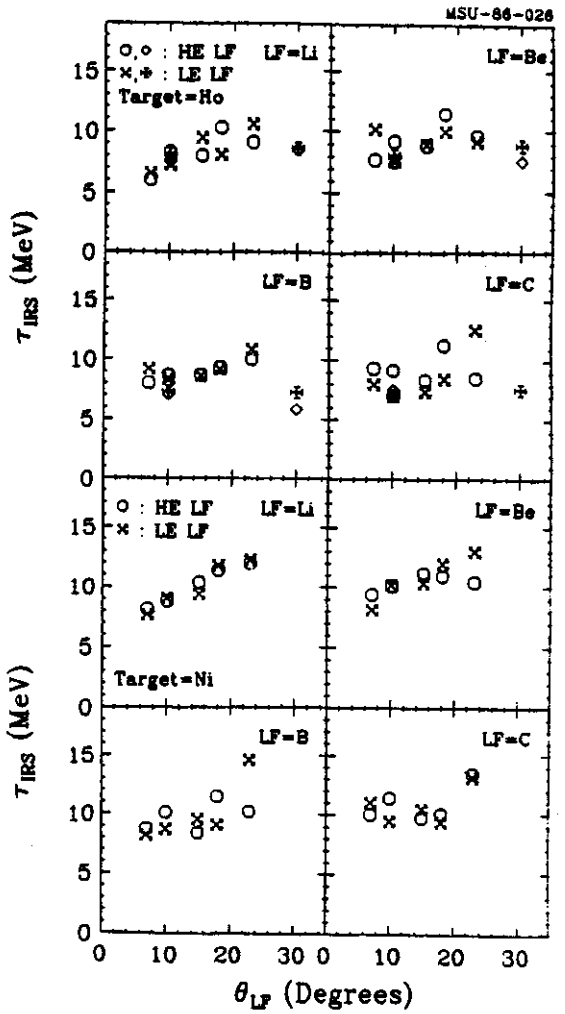

Fig. 5 IRS temperature parameter, τ_{IRS}, versus fragment angle. Symbols and format are the same as for Fig. 4.

calculation, using the compound-nucleus code CASCADE,[2] to estimate neutron multiplicity. The results, 12 for Ho and 2.3 for Ni, are consistent with our observations in that they are greater than our associated multiplicities.

The other source, the IRS, moves very rapidly (at about half the projectile velocity) and its temperature is higher than the temperature of the TLS. The combination of high velocity and high temperature enables it to produce the forward-peaked, high-energy neutrons. A similar fast, hot source has been used rather successfully to fit the high-energy portions of inclusive charged particle spectra.[3] With a LE gate on the coincident fragment this source moves at 0°, but with a HE gate the IRS balances the transverse momentum of the quasi-elastic fragment by moving to the side opposite the fragment, thus producing the observed neutron asymmetry.

The values of temperature and velocity, (actually E/A, which ∝ velocity-squared) derived from fitting the gated neutron spectra, are given in Figs. 5 and 6, respectively. It is a

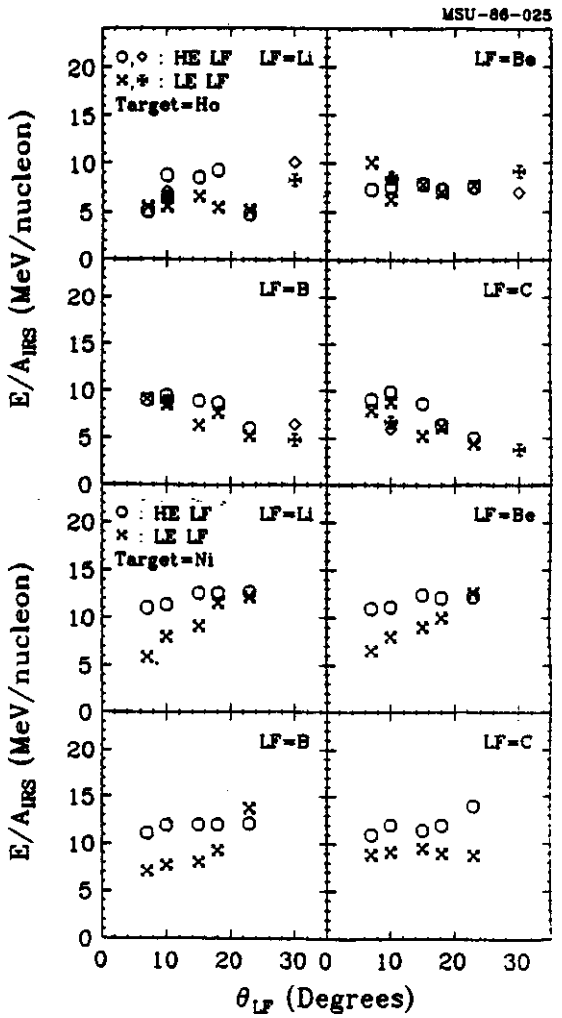

Fig. 6 IRS energy/nucleon, E/A_{IRS}, versus fragment angle. Symbols and format are the same as for Fig. 4.

striking feature of these plots that no clear, systematic trends are observed for either the temperature or the velocity of the IRS as a function of the species, the energy, or the angle of the coincident fragment. It is as if the properties of the IRS--at least when it emits neutrons--were independent of how or when the fragment was produced. Perhaps the IRS emits neutrons at a very early stage of the interaction, before the final "fate" of the projectile has been determined. In peripheral collisions the projectile may break up downstream from the target nucleus,[4] hence decoupling the detected fragment from those neutrons emitted early in the collision. In more central collisions perhaps the fragment itself is emitted from the IRS, but at a later time, after it has cooled and grown from the accretion of target nucleons.[5] Then once again the source of the fragment would have no memory of the early neutron emission.

Although the IRS is hotter than the TLS, its associated multiplicity is lower. The IRS emits only 1-2 neutrons per coincident fragment compared with 5-10 (Fig. 4) from the TLS. This must mean that the IRS is much smaller. In fact, since our fitting gave us the magnitude and direction of the IRS velocity, we determined its mass from momentum balance against the fragment in the peripheral collisions, with the result $A_{IRS} \leq 10\text{-}15$.

---

a. LeCroy Corp.
b. Eötvös University, Budapest, Hungary
c. Tokyo Inst. Technology
d. Notre Dame
e. Hulman Institute of Technology
f. Central Research Laboratory, Budapest, Hungary

References:

1. G. Caskey, A. Galonsky, B.A. Remington, M.B. Tsang, C.K. Gelbke, A. Kiss, F. Deak, Z. Seres, J.J. Kolata, J. Hinnefeld, and J. Kasagi, Phys. Rev. C 31,1597(1985).
2. F. Pühlhofer, Nucl. Phys. A280,267(1977).
3. B.V. Jacak, G.D. Westfall, C.K. Gelbke, L.H. Harwood, W.G. Lynch, D.K. Scott, H. Stöcker, M.B. Tsang and T.J.M. Symons. Phys. Rev. Lett. 51, 1846(1983).
4. M.J. Murphy, S. Gil, M. Harakeh, A. Ray, A. Seamster, R. Vandenbosch, and T. Awes, Phys. Rev. Lett. 53,1543(1984).
5. D.J. Fields, W.F. Lynch C.B. Chitwood, C.K. Gelbke, M.b. Tsang, H. Utsunomiya and J. Aichelin, Phys. Rev. C 30,1912(1984).

CONTRIBUTION OF PROJECTILE BREAKUP TO "BEAM-VELOCITY" FRAGMENTS FROM REACTIONS OF ^{22}NE AT 428 MEV

H. Utsunomiya[a], D.J. Morrissey, L.H. Harwood, E.C. Deci[b], and R.A. Blue

We have made measurements of the double differential cross sections of projectile-like fragments (PLF's) from reactions induced by ^{22}Ne projectiles at 428 MeV. The PLF's were observed at near the classical grazing angle with four targets, ^{26}Al, ^{93}Nb, ^{165}Ho, and ^{197}Au. The experiment was carried out with a 428 MeV ^{22}Ne beam from the K500 cyclotron. The PLF's were detected in a ΔE/E silicon telescope that was able to completely resolve isotopes in the range from ^{10}B to ^{23}Na. The solid angle of the detector was limited to 0.73 msr in order to minimize the effects of kinematic broading.

The cross sections for production of three isotopes [^{21}F, ^{20}F and ^{18}O] showed a strong increase with increasing target mass. However, for the remaining fragments, the isotopic distribution was found to be nearly the same for all four targets. Fig. 1 shows the spectra obtained for various isotopes at or very near the classical grazing angle for each target. The columns of figs. 1(a) and (b) show the dependence of the ^{19}F and ^{16}O kinetic energy spectra on target mass. Fig. 1(c) shows the energy spectra of various PLF's observed with a single target, ^{165}Ho. One can see that the low energy components, which make the apparent widths of the peaks broad, increase rapidly with decreasing target mass. Thus the empirical method of extracting a "width parameter" for the momentum distribution[1] by fitting the high energy edge with a Gaussian function is very sensitive to the lower limit of the fitting region. The solid curves in Fig. 1 represent calculations with the extended-Serber model[2,3] which were individually normalized to the peak yields. We estimated the Coulomb energies needed in for the calculation with a interaction radius of 1.5 fm. The calculations were quite

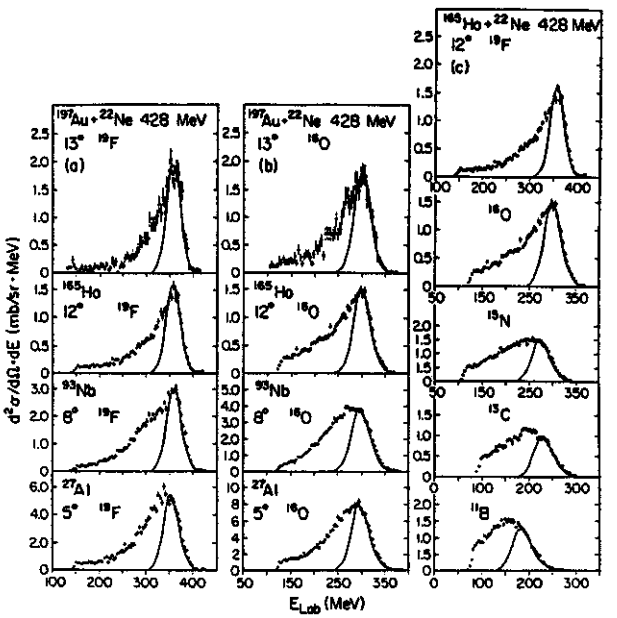

Fig. 1. Energy spectra of the indicated fragment from various targets, (a) and (b), or a series of fragments from one target, (c) measured at or very near the classical grazing angle.

insensitive to this parameter, for example the lower value of 1.2 fm decreases the width of the calculated FWHM of the distribution by only 1 to 4 percent. However, the model includes an energy shift of approximately 10 MeV (representative of dissipated energy) that was adjusted to obtain the curves in fig. 1.

One of the great advantages of the extended Serber model is its ability to predict angular distributions. Fig. 2, for example, shows the measured angular distributions of ^{19}F, ^{16}O and ^{15}N (at the peak of the kinetic energy distribution) for the gold target. The solid curves show the results of an optimized calculation in which the deflection angle was "tuned" to give the best fit (changing from 10° to 9° to 8° for the respective isotopes). The dashed curves show the results obtained with a

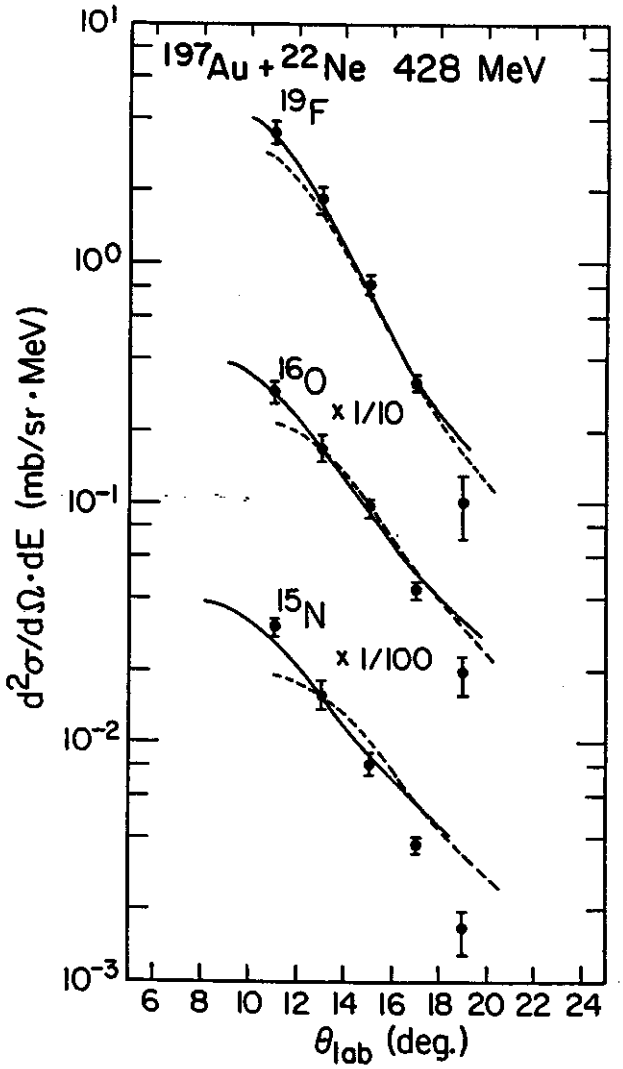

Fig. 2. Angular distributions of the indicated fragments obtained with a gold target. The curves represent the extended Serber model calculations.

constant deflection angle, 11°, slightly smaller than the grazing angle of 12°. Both calculations were normalized to the data at 13°.

Overall, the gross features of the energy spectra and angular distributions of PLF's observed from the reaction of ^{22}Ne at E/A = 20 MeV with various targets can be reasonably well described by the extended-Serber model. This model has two adjustable parameters, a kinetic energy shift or dissipation energy and a deflection angle. Our data indicates that the deflection angle can be taken to be nearly equal to the classical grazing angle and thus only the small shift energy needs to be fitted to the data.

---

a. Texas A&M University, College Station, TX.
b. Alma College, Alma, MI.

References

1. Ch. Egalhaaf, et al., Phys. Rev. Lett. 46, 813 (1981).
2. H. Utsunomiya, Phys. Rev. C32, 849 (1985).
3. R. Serber, Phys. Rev. 72, 1008 (1947).

MASS AND ISOBARIC YIELDS FROM HEAVY ION REACTIONS BY ACTIVATION TECHNIQUES

S.Y. Cho,[a] Y.H. Chung,[a] M. Bronikowski,[a] N.T. Porile,[a] D.J. Morrissey

The interaction of intermediate energy ^{12}C and ^{14}N ions with copper and silver is being investigated by means of activation techniques. The experiments involve measurements of the cross sections and recoil ranges of diverse radionuclides formed in the interaction. The cross sections can be used to obtain the isobaric yield and mass yield distributions and the recoil ranges give the value of the average momentum transfer.

We have to date performed irradiations with 25 and 35 MeV/A ^{12}C ions and with 40 MeV/A ^{14}N ions. The cross sections for the formation of some 30 nuclides from copper have been obtained at each energy. The results were converted to total isobaric cross sections by means of an iterative charge distribution analysis.[1] Figure 1 shows the resulting mass yield distribution obtained at each energy. Several trends may be noted. First, the cross sections for the formation of products in the vicinity of the target are relatively large at 25/A MeV but are much lower at the higher energies. The formation of these products presumably results from complete or incomplete fusion, or from deep inelastic processes, and the contribution of these mechanisms appears to decrease significantly between 25/A MeV and 35/A MeV. The fractional momentum transfer obtainable from the recoil data should allow us to obtain more precise information on the mechanism by which these products are formed.

The evolution of the mass yield curve with increasing energy has some interesting features. The location of the peak in the distribution shifts from A≈60 to A≈55 between 25/A and 40/A MeV. At the same time, the region of exponentially decreasing corss sections, which extends from just below this peak down to A≈35, can be characterized by a gradually decreasing

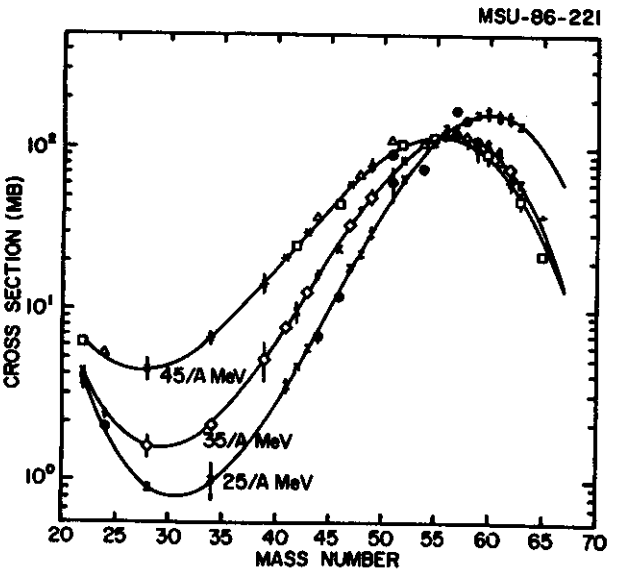

Fig. 1 Mass yield distributions for the interaction of copper with 25/A MeV ^{12}C, 35/A ^{12}C, and 40/A ^{14}N ions. The points are based on experimentally measured cross sections which were corrected for the unmeasured yields at the respective mass numbers on the basis of a charge distribution analysis.[1] The different symbols indicate the fraction of the isobaric yield represented by the experimental data: Δ, +, 4, >50%, □, x, X̄, 20-50%, *, , Z <20%. The curve is the result of a 4-parameter fit to the data.[1]

slope. The slope of this exponential is a measure of the temperature of the excited target remnant and the data show that this temperature increases with the projectile energy.

Below A≈35, the curves go through a broad minimum and then increase at the lowest mass numbers, showing the increasing probability for the formation of intermediate mass fragments. High yields in this mass region are particularly evident at 40/A MeV. Since these data were obtained with ^{14}N rather than with ^{12}C projectiles, it remains to be determined whether this effect can be ascribed to the increase in available energy or to the identity of the projectile.

a. Purdue University, W. Lafayette, IN.

References

1. N.T. Porile, G.D. Cole, and C.R. Rudy, Phys. Rev. C19, 2288 (1979).